Politecnico di Milano
School of Industrial and Information Engineering
Master of Science in Mathematical Engineering

Master Thesis in Computational Science and Engineering

A posteriori analysis of topological model reduction error, with application to mass transport in microcirculation

Advisor:
Prof. Paolo ZUNINO

Co-Advisor:
Dr. Federica LAURINO

Stefano BRAMBILLA
Matr. 853558

Academic Year 2017-2018

To Eleonora,
the only exception

Abstract

Topological model reduction can decrease the high computational costs of simulations in many multiscale systems, especially applied to biology and geology, where small inclusions embedded in a 3D continuum can be described as one-dimensional (1D) concentrated sources. However, concentrated sources lead to singular solutions that still require computationally expensive graded meshes, due to the ill-posedness of restriction operators applied on manifolds with co-dimension larger than one. We apply topological model reduction to coupled transport problems applied to the microcirculation. In this framework, the *a posteriori* analysis of the error due to this model reduction is still unexplored. We propose a Dual-Weighted Residual estimator for the modeling error. The use of this technique is a first step for an adaptive method, able to optimally refine the grid where the error is larger. We build a suitable solver based on the C++ finite element library *GetFEM++*, able to simulate the transport of particles in a capillary network embedded in a permeable biological tissue, and afterwards compute the suitable estimators for the modeling error. The solver may be a valid support in the computational analysis of physical phenomena related to microcirculation, with possible applications to drug delivery for cancer treatment or to lymphatic clearance of the brain in neurodegenerative diseases.

Sommario

L'applicazione di tecniche di riduzione di modello permette di ridurre gli alti costi computazionali delle simulazioni in problemi multi-scala, specialmente applicati alla biologia e alla geologia, dove piccole inclusioni all'interno di un mezzo continuo 3D possono essere descritte come sorgenti concentrate unidimensionali (1D). Purtroppo, usando sorgenti concentrate si ottengono soluzioni singolari che richiedono l'utilizzo di mesh computazionalmente molto costose, poichè gli operatori di restrizione applicati a varietà con co-dimensione maggiore di uno non sono ben definiti. Applichiamo tecniche di riduzione di modello a problemi accoppiati di trasporto nella microcircolazione. In questo contesto, l'analisi *a posteriori* dell'errore commesso nella riduzione di modello è ancora inesplorata. Proponiamo quindi uno stimatore di tipo Dual-Weighted Residual per l'errore di modello. L'uso di questa tecnica è un primo passo per costruire un metodo adattivo, capace di raffinare in maniera ottima la griglia laddove l'errore è maggiore. Costruiamo un risolutore numerico basato sulla libreria per elementi finiti *GetFEM++*, scritta in C++, capace di simulare il trasporto di particelle in una rete di capillari all'interno di un tessuto biologico permeabile, e successivamente di calcolare degli stimatori dell'errore di modello. Questo risolutore potrà essere un valido supporto per l'analisi computazionale dei fenomeni fisici legati alla microcircolazione, con possibili applicazioni al trasporto di farmaci per il trattamento di tumori o al drenaggio linfatico del cervello in malattie neurodegenerative.

Contents

Introduction **1**

1 A mathematical model for coupled 3D-1D mass transport system **4**
- 1.1 Dimension analysis 6
- 1.2 Boundary and initial conditions 8
- 1.3 Weak formulation 9
  - 1.3.1 Weak formulation for the tissue problem 9
  - 1.3.2 Weak formulation for the vessel problem 10
- 1.4 Numerical Approximation 12
- 1.5 Algebraic formulation 14
  - 1.5.1 Coupling terms 15
- 1.6 Numerical Results 17
  - 1.6.1 Uncoupled 1D and 3D test 17
  - 1.6.2 Coupled 3D-1D problem on a single branch 21
  - 1.6.3 Test on a single bifurcation 23
  - 1.6.4 Coupled 3D-1D problem on a complex network 29

2 Numerical approximation and a-priori error analysis **33**
- 2.1 Setting 33
  - 2.1.1 Geometry 33
  - 2.1.2 Reference problem 35
  - 2.1.3 Topological model reduction of the problem on Σ 36
  - 2.1.4 Topological model reduction of the problem on $\Omega_\oplus$ 37
  - 2.1.5 Extension of the 1D problem to a metric graph 38
  - 2.1.6 Coupled problems with hybrid dimensionality 40
- 2.2 Well-posedness analysis 41
  - 2.2.1 Additional regularity of the solution of the problem in Ω . . 45
  - 2.2.2 Finite element approximation 49

3 Model error analysis **52**
3.1 Theory of dual-based estimator of modeling error 52
3.1.1 Approximate error representation formula 54
3.2 Modeling error analysis 56
3.2.1 Useful results 57
3.2.2 Analysis of modeling error of the one dimensional problem (Assumption A1) 59
3.2.3 Analysis of modeling error relative to the domain (Assumption A2) 62
3.2.4 Analysis of modeling error relative to the transmission conditions (Assumption A3) 65
3.2.5 Conclusions 68

4 Numerical tests **70**
4.1 Estimators 70
4.1.1 Localization of the estimator 71
4.1.2 Derivation of $\eta^{(i)}$ 72
4.2 Scenario A 75
4.2.1 Validation: null terms 76
4.3 Scenario B 78
4.4 Scenario C 81
4.5 Scenario D 83
4.6 Scenario E 86
4.7 Discussion of the results 93

Conclusion and future perspectives **98**

Appendix **100**

A C++ Code **101**
A.1 Design of the code 101
A.2 Assembling routines 106
A.3 The library `transport3d1d` 115
A.4 Doxygen documentation 116

Bibliography **118**

List of Figures

1.1 3D and 1D Manifolds 4
1.2 Vessel discretization for interpolation and average operators. 16
1.3 Uncoupled problem 1.19 on a single branch network. 18
1.4 Uncoupled problem 1.23 on $\Omega = (0,1)^3$ 20
1.5 Coupled problem on single unitary branch 22
1.6 Uncoupled problem on a simple bifurcation. 25
1.7 Coupled problem on a bifurcation Λ with physiological parameters . 29
1.8 Complex network with physiological parameters 31

2.1 Visualization of the quasi-uniform mesh used for the convergence test, the exact solution u_e and the numerical solution u_h. 51

4.1 Scenario A: Primal reduced coupled problem 76
4.2 Scenario A: Validation of null terms (1) 77
4.3 Scenario A: Validation of null terms (2) 77
4.4 Scenario A: Validation of null terms (3) 78
4.5 Scenario A: Residuals 79
4.6 Scenario A: Weights 79
4.7 Scenario A: Estimators 80
4.8 Scenario A: Global estimators 81
4.9 Scenario B: Estimators 82
4.10 Scenario B: Global estimators 83
4.11 Scenario B: $l^{(1)}$ 84
4.12 Scenario C: Estimators 85
4.13 Scenario C: Global estimators 86
4.14 Scenario C: $l^{(1)}$ 87
4.15 Scenario D: Different grids 88
4.16 Scenario D: Residuals 88
4.17 Scenario D: Weights 89
4.18 Scenario D: Estimators 90
4.19 Scenario D: Global estimators 91

4.20 Scenario E: Residuals 91
4.21 Scenario E: Weights 92
4.22 Scenario E: Estimators 92
4.23 Scenario E: Global estimators 93

List of Tables

1.1 Mass balance at the junction (uncoupled) 26
1.2 Physiological parameters 28
1.3 Mass balance at the junction (coupled) 30

2.1 Convergence of the discretization error 51

4.1 Parameters of the numerical simulation for modeling error 71
4.2 Results of Estimators 94

Introduction

The final goal of the thesis is to simulate the transport of particles in the capillary network and the drug delivery in the interstitial tissue. In the last decades, the study of complex diseases such as cancer [25] and neurological diseases [36] indicates the need for combining the efforts of quantitative sciences and medicine, as in the Computer Aided Clinical Trials (CACT) [53]. We aim to develop new techniques to overcome some of the limitations in the simulations of multiscale, multiphysics, multimodel systems, which are among the grand challenges in Computational Science and Engineering. In this context, the application of topological or geometrical model reduction techniques plays an essential role, exploiting the multiscale nature that characterizes all the biological systems and using the interactions among results obtained at different time- and space-scales. For example, small inclusions of a continuum can be described as zero-dimensional (0D) or one-dimensional (1D) concentrated sources in order to reduce the computational cost of simulations. Many problems in this area are not well investigated yet, such as the coupling of three-dimensional (3D) continua with embedded (1D) networks, although it arises in applications of paramount importance such as microcirculation, flow through perforated media, and many others, both in biological and geological systems.

In particular, models involving the cardiovascular system are usually very expensive, due to the complexity of the equations governing the hemodynamics and to the large number of vessels composing the circulatory system. Therefore, many adhoc reduction techniques have been proposed [45, 19, 20, 21], exploiting the large aspect ratio of the vessel in order to approximate the fluid dynamics in the vessel and the fluid exchange from one capillary to the surrounding tissue. Subsequently, other non-specific approaches have been developed, casting the microcirculation problem into a new unified framework to formulate and approximate coupled partial differential equations (PDEs) on manifolds with heterogeneous dimensionality. This approach was originally proposed in [12, 14, 13], but also employed in [34, 52], extending the reduction of fluid dynamics equations to other PDEs. This field has recently attracted the attention of several researchers from the perspective of theory and applications. The main computational barrier consists in the ill-posedness of restriction operators (such as the trace operator) applied on manifolds with co-dimension larger than one. Therefore it requires particular attention to prove existence of a solution in the weak sense. From the point of view of numerical approximation and analysis of such problems, we mention [5, 6, 26, 27, 28, 30, 31, 40]. More precisely, in [5, 26, 27] optimal a-priori error estimates for the finite element approximation of elliptic equations in with Dirac sources are addressed. The solution of 1D differential equations embedded in 2D is studied in [30], recently extended to 3D-1D in [31]. The consistent derivation of numerical approximations schemes for PDEs in mixed dimension is addressed in [6], while [40] focuses on the approximation of 3D-1D coupled problems with mixed finite elements. This approach has already been applied in many fields, such as drug delivery [11, 29, 54], cancer treatment [10, 37, 38], nephrology [43], neurology [35, 51] but also geology [18].

Within this general framework, the specific objective of this work is to contribute to the theory of these model reduction techniques with an *a posteriori* analysis of the error. The use of topological reduction is validated thanks to the *a priori* results, but the state of art lacks of any quantitative consideration of the modeling error. In fact, the direct connection between the modeling error and the dimension of the inclusion has been previously addressed in [28]; however, the results concern non fully-computable L^2-norm estimates of the error. We move from this approach, and we introduce the Dual-Weighted Residual (DWR) *a posteriori* estimates: this technique allows to compute some user-defined functional of the error through the solution of an ad-hoc dual problem. It generally consists in three steps: *(i)* compute a proper residual of the weak primal formulation; *(ii)* compute some weights deriving from the dual solution; *(iii)* multiply the residuals by the weights. The DWR method has been extensively studied in the last decades for what concerns the discretization error [15, 3, 46, 1], but it has been also applied to the modeling error [7]. The estimator computed in this way is particularly useful since it allows to see the localization of the error. In the framework of problems dependent on the topological shape, such as the ones related to small inclusions in a continuum, it is important to know how the error is distributed in the domain. This information allow us to investigate the suitability of the model reduction and perform mesh adaptation: therefore, we can refine the mesh grid where the modeling error is larger.

The outline of the thesis is as follows. Chapter 1 contains a multiscale PDE model of transport of particles and fluid exchange between microcirculation and tissue interstitium, with special attention to the 3D-1D reduction of the vessels. The model describes all the principal component of the motion from a physiological point of view: diffusion through the vessel and the tissue, advection in the blood stream, mass exchange through the capillary walls, consumption and production due to metabolic response, absorption of mass due to the lymphatic system. We develop a new C++ solver able to simulate the mass exchange between an arbitrarily complex microvascular network and a generic biological tissue. This Chapter provides some simulations that validate the code and explore the effect of some terms of the equations. Unfortunately, the complete physiological equations are not the right framework to develop a rigorous theory for the well-posedness of the coupled PDEs and for the modeling error estimators. In fact, there is not enough research to rigorously study the advection and reaction terms yet. Therefore in Chapter 2 we consider a specific case, precisely a generic elliptic coupled problem on a network completely embedded in a 3D domain, and we provide an accurate derivation of the reduced 3D-1D problem from the reference 3D-3D one. We perform this reduction through three specific assumptions, namely: *(i)* the unknown of the network problem depends only on the axial coordinate; *(ii)* the 3D domain include both the region around the inclusion and the inclusion itself; *(iii)* we neglect the fluctuations of the 3D unknown on the interface between the domains. We then analyse the well-posedness of the reduced problem and the convergence of the numerical error of its discrete formulation. In Chapter 3 we review the theory of the DWR methods applied to the modeling error [7] and then we apply it to the error arising from each of the three assumptions. We also prove some stability results in order to guarantee the quality of the computed estimators. Finally, Chapter 4 contains the definitions of the fully-computable localized estimators of the modeling error, and the results obtained numerically with our solver.

Chapter 1

A mathematical model for coupled 3D-1D mass transport system

We present a mathematical model for mass transport for a capillary network immersed in a permeable biological tissue. The domain of our model is a subspace of $\mathbb{R}^3$ composed by two parts, namely Ω_t and Ω_v, the interstitial tissue and the vessel bed respectively. We assume that the capillaries can be described as cylindrical vessels, with Γ defined as the outer surface of Ω_v and Λ as the one-dimensional manifold representing the centerline of the capillary network. The vessel radius R may change in the network.

The physical quantity of interest is the concentration of transported solutes $c\,(x,t)$. In particular, we denote $c_v\,(x,t)$ the concentration in the domain Λ, and $c_t\,(x,t)$ the concentration in the domain Ω_t.
To model drug transport we assume that the molecules are advected by the fluid and diffuse in all the domain. Furthermore, chemical species can be metabolized

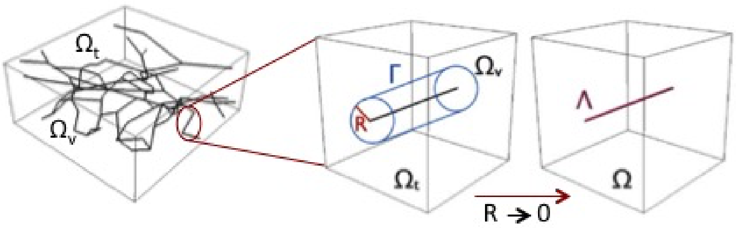

Figure 1.1: On the left, microvasculature within a tissue interstitium; in the center, the interstitial tissue slab with one embedded capillary; on the right, the reduction from 3D to 1D description of the capillary vessel.

by the cells in the interstitial tissue. We assume that the capillary walls behave as semipermeable membranes: there is both a leakage of fluid and a selective filtration of molecules in the vessel walls. We also consider the lymphatic system, which absorbs the fluid in excess due to capillary leakage. We assume the volumetric flow rate to be proportional to the pressure difference between the interstitium and the lymphatic system.

Therefore, we model transport by means of advection-diffusion equations in the network, and by means of advection-diffusion-reaction equations in the volume.

$$\begin{aligned} \frac{\partial c_t}{\partial t} + \nabla \cdot (c_t \boldsymbol{u_t} - D_t \nabla c_t) + m c_t + L_P^{LF} \frac{S}{V} (p_t - p_L)\, c_t = f_c \delta_\Lambda \qquad & \text{on } \Omega \times (0,T)\,, \\ \frac{\partial c_v}{\partial t} + \frac{\partial}{\partial s} \left((\boldsymbol{u_v} \cdot \boldsymbol{\lambda})\, c_v - D_v \frac{\partial c_v}{\partial s} \right) = -\frac{1}{\pi R^2} f_c \quad & \text{on } \Lambda \times (0,T)\,, \end{aligned} \tag{1.1}$$

where D_t and D_v are the molecular diffusivities, in the tissue and in the vessels, respectively, assumed to be constant in each region. The metabolization rate m can be modeled as a function of concentration values, but we consider it constant at this stage.
In the lymphatic drainage term, L_P^{LF} is the idraulic permeability of the lymphatic wall, the ratio $\frac{S}{V}$ is the surface area of lymphatic vessels per unit volume of tissue and p_L is the hydrostatic pressure within the lymphatic channels.
The function $f_c = f_c\left(\overline{p}_t, p_v, \overline{c}_t, c_v\right)$ represents the mass flux per unit length of capillary vessels, between the capillary bed and the interstitial tissue. This function is written according to the Kedem-Katchalsky equations, which describes the behaviour of a selective semipermeable membrane. This reads as:

$$f_c = 2\pi R \left[L_p (1-\sigma) \left[(p_v - \overline{p}_t) - \sigma (\pi_v - \overline{\pi}_t) \right] \left[w \overline{c}_t + (1-w) c_v \right] + P(c_v - \overline{c_t}) \right] \tag{1.2}$$

on $\Lambda \times (0,T)$, where L_P is the hydraulic permeability of the vessel wall, σ is the osmotic reflection coefficient, σ is the sieving coefficient, $p_v - \overline{p}_t$ is the pressure drop between vessels and tissue, $\pi_v - \overline{\pi}_t$ is the oncotic pressure jump; finally, $0 < w < 1$ is a weight depending on the Péclet number of the solute transport through the wall, usually set $w = \frac{1}{2}$, and P is the permeability of the vessel wall with respect to solutes. We recall that we defined Λ as the one-dimensional manifold representing the centerline of the capillary network, as in Figure 1.1; it would then be inappropriate to use the pointwise c_t on Λ in order to compute the coupling term. In fact, we employ the average value of concentration over the cylindrical surface of the real domain of the capillary vessel, Γ. We introduce the average value of a field g:

$$\overline{g}\,(s) := \frac{1}{2\pi R} \int_0^{2\pi} g\,(s,\theta)\, R d\theta. \tag{1.3}$$

We apply the average operator to every quantity of interest in the mass flux $f_c\left(\overline{p}_t, p_v, \overline{c}_t, c_v\right)$ which is defined on the volume Ω_t, namely c_t, p_t and π_t.

We finally model the advection and pressure fields to be the solutions of the equations for the fluid dynamics of the blood. We consider the tissue an isotropic porous medium and the blood flow in the vessels to be steady and incompressible: then, the advection field is described by Darcy's law in the interstitial volume and by Poiseuille's flow in the microcirculation. Then, the velocity fields $\boldsymbol{u_t}$ and $\boldsymbol{u_v}$, and the hydrostatic pressures p_t and p_v satisfy the following equations:

$$
\begin{aligned}
-\nabla \cdot \left(\frac{k}{\mu}\nabla p_t\right) + L_P^{LF}\frac{S}{V}\left(p_t - p_L\right) - f_b\left(\overline{p}_t, p_v\right)\delta_\Lambda =& 0 && \text{in } \Omega \times (0,T)\,,\\
\boldsymbol{u_t} =& -\frac{k}{\mu}\nabla p_t && \text{in } \Omega \times (0,T)\,,\\
-\frac{\pi R^4}{8\mu}\frac{\partial^2 p_v}{\partial s^2} + f_b\left(\overline{p}_t, p_v\right) =& 0 && \text{on } \Lambda \times (0,T)\,,\\
\boldsymbol{u_v} =& -\frac{R^2}{8\mu}\frac{\partial p_v}{\partial s}\boldsymbol{\lambda} && \text{on } \Lambda \times (0,T)\,,
\end{aligned}
\tag{1.4}
$$

where k is the hydraulic permeability of the interstitial volume, μ is the blood viscosity and the function $f_b\left(\overline{p}_t, p_v\right)\delta_\Lambda$ denotes the fluid flux leaking from the capillaries to the interstitial volume, defined as:

$$
f_b\left(\overline{p_t}, p_v\right) : \; = 2\pi R L_p\left(\left(p_v - \overline{p}_t\right) - \sigma\left(\pi_v - \overline{\pi}_t\right)\right) \quad \Lambda \times (0,T)\,. \tag{1.5}
$$

1.1 Dimension analysis

In this section we want to perform a dimension analysis in order to study the relative impact of the different mechanics, namely the molecular diffusion, advection, consumption and leakage. The physical variables on which our analysis will depend are length, velocity, pressure and concentration; the characteristic length is the average spacing between capillary vessels d, the characteristic velocity is the average velocity in the capillary bed U, the characteristic pressure is the average pressure in the interstitial space ΔP, and the characteristic concentration is the maximum value C_{max} of concentration of that chemical species we can find in an healthy organism. The adimensional parameters follow:

$R' = \dfrac{R}{d}$	non-dimensional radius,
$A_t = \dfrac{D_t}{dU}$	inverse of Péclett number in the interstitium,
$A_v = \dfrac{D_v}{dU}$	inverse of Péclet number in the blood stream,
$D_\alpha = m\dfrac{d}{U}$	Damkohler number,
$Q = L_P \dfrac{\Delta P}{U}$	hydraulic conductivity of the capillary walls,
$Q^{PL} = L_P^{LF} \dfrac{S}{V} \dfrac{d\Delta P}{U}$	hydraulic conductivity of the lymphatic walls,
$\Upsilon = \dfrac{P}{U}$	magnitude of leakage from the capillary bed,
$\kappa_t = \dfrac{k}{\mu} \dfrac{\Delta P}{Ud}$	hydraulic conductivity of the tissue,
$\kappa_v = \dfrac{\pi R'^4}{8\mu} \dfrac{d\Delta P}{U}$	hydraulic conductivity of the capillary bed.

-

Using these parameters, the equations (1.1), (1.2) and (1.4) read as follows:

$$\begin{aligned} \frac{\partial c_t}{\partial t} + \nabla \cdot \left(c_t \boldsymbol{u_t} - A_t \nabla c_t\right) + D_\alpha c_t + Q_{PL} \left(p_t - p_L\right) c_t = f_c \delta_\Lambda \qquad & \text{in } \Omega \times (0,T)\,, \\ \frac{\partial c_v}{\partial t} + \frac{\partial}{\partial s}\left(u_v c_v - A_v \frac{\partial c_v}{\partial s}\right) = -\frac{1}{\pi R^2} f_c \quad & \text{on } \Lambda \times (0,T)\,, \end{aligned} \tag{1.6}$$

$$f_c = 2\pi R' \left[Q\left(1-\sigma\right)\left[\left(p_v - \overline{p}_t\right) - \sigma\left(\pi_v - \overline{\pi}_t\right)\right]\left[w\overline{c}_t + (1-w)c_v\right] + \Upsilon(c_v - \overline{c}_t)\right] \tag{1.7}$$

$$\begin{aligned} \nabla \cdot \boldsymbol{u_t} + Q_{PL}\left(p_t - p_L\right) - Q\left(p_v - \overline{p}_t\right)\delta_\Lambda =& 0 \quad \text{in } \Omega \times (0,T)\,, \\ \frac{1}{\kappa_t}\boldsymbol{u_t} + \nabla p_t =& 0 \quad \text{in } \Omega \times (0,T)\,, \\ \frac{\partial u_v}{\partial s} + \frac{1}{\pi R'^2} Q\left(p_t - \overline{p}_t\right) =& 0 \quad \text{on } \Lambda \times (0,T)\,, \\ \frac{\pi R'^2}{\kappa_v} u_v + \frac{\partial p_v}{\partial s} =& 0 \quad \text{on } \Lambda \times (0,T)\,. \end{aligned} \tag{1.8}$$

For semplicity, the variables for concentration, velocity and pressure have maintained the same symbol after the re-scaling for C_{max}, U and ΔP respectively. However, note that the transport equations are linear in the variables c_t and c_v, so the adimensionalization of this quantities does not affect the equations.

Besides, we used the notation $u_v = (\boldsymbol{u_v} \cdot \lambda)$ for the velocity in the one dimensional vessels.

1.2 Boundary and initial conditions

In order to guarantee the uniqueness of the solution of the dimensionless problem, we need to specify some boundary conditions on $\partial\Omega$ and $\partial\Lambda$, and an initial condition for $t = 0$. The choice of the following boundary conditions depends on both the variational formulation and the available data. In fact, we must impose essential and natural conditions over the boundary integrals derived from integrations by parts.

The boundary of the vessel network is the set of the capillary extrema; we distinguish these points between inflow and outflow extrema, respectively the points with velocity inward-pointing and outward-pointing; we define these sets $\partial\Lambda \equiv \Lambda^{IN} \cup \Lambda^{OUT}$. We claim to be a constant concentration of the chemical species on the inflow boundary; this condition is linked to a constant injection of the solute in the network. On the outflow boundary, the particles are free to leave the system: a homogeneous Neumann boundary condition correctly models this phenomenon. The conditions are:

$$\begin{aligned} c_v &= c_{in} && \text{on } \partial\Lambda^{IN} \times (0,T)\,, \\ \frac{\partial c_v}{\partial s} &= 0 && \text{on } \partial\Lambda^{OUT} \times (0,T)\,. \end{aligned}$$

At the boundary of the volume Ω, we have flow of fluid with particles; the quantity of solution exchanged with the exterior depends on the concentration of the solution itself. We model this condition with a Robin condition:

$$-A_t \nabla c_t \cdot \boldsymbol{n} = \beta_t \left(c_t - c_{out}\right) \qquad \text{on } \partial\Omega \times (0,T)\,.$$

Remark 1.2.1. We described the physical boundary condition that we need to close the problem; nevertheless, we develop a more general framework for boundary conditions, considering all the different cases. Therefore, from now on we will use this boundary conditions:

$$\begin{aligned}
c_v &= c_{in} && \text{on } \partial\Lambda^{IN} \times (0,T)\,,\\
-A_v \frac{\partial c_v}{\partial s} &= \beta_v \left(c_v - c_{0,v}\right) && \text{on } \partial\Lambda^{OUT} \times (0,T)\,,\\
c_t &= c_{ext} && \text{on } \partial\Omega^{DIR} \times (0,T)\,,\\
-A_t \nabla c_t \cdot \boldsymbol{n} &= \beta_t \left(c_t - c_{0,t}\right) && \text{on } \partial\Omega^{MIX} \times (0,T)\,.
\end{aligned}$$

The choice of the parameters defines all the standard boundary conditions, namely Dirichlet, Neumann and Robin conditions.

Finally, we recall that our problem is time-dependent, so we must impose an initial condition over all domain:

$$\begin{aligned}
c_t\,(t=0) &= c_{in,t} && \text{on } \Omega,\\
c_v\,(t=0) &= c_{in,v} && \text{on } \Lambda.
\end{aligned}$$

1.3 Weak formulation

The coupled problem we want to solve has no explicit analytical solution, so we must solve it numerically, through finite element methods; therefore we must write the variational form. In particular, in this section we will propose a *dual mixed* weak formulation of both the tissue and vessel problems.

1.3.1 Weak formulation for the tissue problem

To obtain a variational formulation of the particle transport problem in the interstitial tissue, the test space for the concentration is

$$Q_t := H^1_{0,\partial\Omega^{DIR}}\left(\Omega\right).$$

Let us proceed multiplying (1.6)(a) with a sufficiently smooth function q_t and integrating over Ω:

$$\begin{aligned}
&\int_\Omega \frac{\partial c_t}{\partial t} q_t \, d\Omega + \int_\Omega \nabla\cdot\left(c_t \mathbf{u}_t - A_t \nabla c_t\right) q_t \, d\Omega + \int_\Omega D_\alpha c_t q_t \, d\Omega + \int_\Omega Q^{PL}\left(p_t - p_L\right) c_t q_t \, d\Omega\\
&- \int_\Omega 2\pi R' \left\{(1-\sigma)\, Q \left[(p_v - \bar{p}_t) - \sigma\left(\pi_v - \bar{\pi}_t\right)\right] w - \Upsilon\right\} \delta_\Lambda \bar{c}_t q_t \, d\Omega\\
= &+ \int_\Omega 2\pi R' \left\{(1-\sigma)\, Q \left[(p_v - \bar{p}_t) - \sigma\left(\pi_v - \bar{\pi}_t\right)\right](1-w) + \Upsilon\right\} \delta_\Lambda c_v q_t \, d\Omega.
\end{aligned}$$

We apply the Green's theorem and the boundary condition to the diffusion term:

$$\int_\Omega \nabla\cdot(-A_t\nabla c_t)\,q_t\,d\Omega = \int_\Omega A_t\nabla c_t\cdot\nabla q_t\,d\Omega - \int_{\partial\Omega} A_t q_t\nabla c_t\cdot\boldsymbol{n}\,d\sigma$$
$$= \int_\Omega A_t\nabla c_t\cdot\nabla q_t\,d\Omega - \int_{\partial\Omega^{DIR}} A_t q_t\nabla c_t\cdot\boldsymbol{n}\,d\sigma + \int_{\partial\Omega^{MIX}} \beta_t c_t q_t\,d\sigma - \int_{\partial\Omega^{MIX}} \beta_t c_{0,t} q_t\,d\sigma$$

We re-write the advection term in non-conservative form:

$$\int_\Omega \nabla\left(\mathbf{u_t}c_t\right)q_t\,d\Omega = \int_\Omega \mathbf{u_t}\cdot\nabla c_t q_t\,d\Omega + \int_\Omega \nabla\cdot\mathbf{u_t}c_t q_t\,d\Omega \tag{1.9}$$

Finally, we substitute these two results into this equation:

$$\begin{aligned}
&\int_\Omega \frac{\partial c_t}{\partial t}q_t\,d\Omega + \int_\Omega A_t\nabla c_t\cdot\nabla q_t\,d\Omega + \int_{\partial\Omega^{MIX}}\beta_t c_t q_t\,d\sigma - \int_{\partial\Omega^{MIX}}\beta_t c_{0,t}q_t\,d\sigma\\
&+\int_\Omega \mathbf{u_t}\cdot\nabla c_t q_t\,d\Omega + \int_\Omega \nabla\cdot\mathbf{u_t}c_t q_t\,d\Omega + \int_\Omega D_\alpha c_t q_t\,d\Omega + \int_\Omega Q^{PL}\left(p_t - p_L\right)c_t q_t\,d\Omega\\
&-\int_\Omega 2\pi R'\left\{(1-\sigma)\,Q\left[(p_v-\bar{p}_t)-\sigma\left(\pi_v-\bar{\pi}_t\right)\right]w-\Upsilon\right\}\delta_\Lambda\bar{c}_t q_t\,d\Omega\\
&=+\int_\Omega 2\pi R'\left\{(1-\sigma)\,Q\left[(p_v-\bar{p}_t)-\sigma\left(\pi_v-\bar{\pi}_t\right)\right](1-w)+\Upsilon\right\}\delta_\Lambda c_v q_t\,d\Omega.
\end{aligned}\tag{1.10}$$

$\forall q_t \in H^1_{0,\partial\Omega^{DIR}}(\Omega)$.

Notice that the boundary term on the Dirichlet boundary vanishes, thanks to the choice of the space of the test functions: the Dirichlet boundary condition will be enforced in an essential way, directly on the matrix.

1.3.2 Weak formulation for the vessel problem

Accounting the vessel problem, the test space for the concentration is:

$$Q_v := H^1_{0,\partial\Lambda^{IN}}\left(\Lambda\right).$$

We approach the weak formulation in a standard way, by means of multiplying equation (1.6)(b) by a test function q_v and integrating over Λ:

$$\begin{aligned}
&\int_\Lambda \frac{\partial c_v}{\partial t}q_v\,ds + \int_\Lambda \frac{\partial}{\partial s}\left(u_v c_v - A_v\frac{\partial c_v}{\partial s}\right)q_v\,ds\\
&+\int_\Lambda \frac{2}{R'}\left\{(1-\sigma)\,Q\left[(p_v-\bar{p}_t)-\sigma\left(\pi_v-\bar{\pi}_t\right)\right](1-w)+\Upsilon\right\}c_v q_v\,ds =\\
&=-\int_\Lambda \frac{2}{R'}\left\{(1-\sigma)\,Q\left[(p_v-\bar{p}_t)-\sigma\left(\pi_v-\bar{\pi}_t\right)\right]w-\Upsilon\right\}\bar{c}_t q_v\,ds.
\end{aligned}$$

At this point, it is not possible to simply integrate by parts, because of the presence of multiple junctions. To tackle this issue, must divide the integral over the whole network between each branch; in order to handle the terms at the junctions, we write the mass balance at each junctions, that is:

$$\sum_{i\in P_j^{out}} \pi R_i'^2 \left(-A_v \frac{\partial c_v}{\partial s} + u_v c_v\right)\Bigg|_{\Lambda_i^+} = \sum_{i\in P_j^{in}} \pi R_i'^2 \left(-A_v \frac{\partial c_v}{\partial s} + u_v c_v\right)\Bigg|_{\Lambda_i^-} \quad \forall j \in \mathcal{J}, \tag{1.11}$$

where $\mathcal{J}$ is the set of all the junctions, $\mathcal{P}_j^{out}$ and $\mathcal{P}_j^{in}$ is the set of the indexes of the branches exiting and entering the junction j, Λ_i^+ and Λ_i^- denote the inflow and outflow extrema of branch Λ_i. Notice that, for the choice of the functional space, c_v must be continuous in every point; in addition, the conservation of local flow rate in every vessel junctions must hold. For this reasons, the mass balance of the advective fluxes holds separately from the mass balance of the diffusive fluxes:

$$\sum_{i\in P_j^{out}} \pi R_i'^2 u_v c_v\big|_{\Lambda_i^+} = \sum_{i\in P_j^{in}} \pi R_i'^2 u_v c_v\big|_{\Lambda_i^-} \qquad \forall j \in \mathcal{J}, \tag{1.12}$$

$$\sum_{i\in P_j^{out}} \pi R_i'^2 A_v \frac{\partial c_v}{\partial s}\bigg|_{\Lambda_i^+} = \sum_{i\in P_j^{in}} \pi R_i'^2 A_v \frac{\partial c_v}{\partial s}\bigg|_{\Lambda_i^-} \qquad \forall j \in \mathcal{J}. \tag{1.13}$$

For this reason, before we integrate by parts, we multiply the equation by a factor $\pi R'^2$; in this way, the diffusive and advective term are correctly scaled by the cross section area. We can now apply the Green's theorem to the diffusive term:

$$\begin{aligned}
\int_\Lambda \frac{\partial}{\partial s}\left(-\pi R'^2 A_v \frac{\partial c_v}{\partial s}\right) q_v d\Lambda &= \sum_i^N \int_{\Lambda_i} \frac{\partial}{\partial s}\left(-\pi R_i'^2 A_v \frac{\partial c_v}{\partial s}\right) q_v d\Lambda \\
&= \sum_i^N \left\{ \int_{\Lambda_i} \pi R_i'^2 A_v \frac{\partial c_v}{\partial s}\frac{\partial q_v}{\partial s} d\Lambda + \left[-\pi R_i'^2 A_v \frac{\partial c_v}{\partial s} q_v\right]_{\Lambda_i^-}^{\Lambda_i^+} \right\} \\
&= \int_\Lambda \pi R'^2 A_v \frac{\partial c_v}{\partial s}\frac{\partial q_v}{\partial s} d\Lambda + \sum_i^N \left[-\pi R_i'^2 A_v \frac{\partial c_v}{\partial s} q_v\right]_{\Lambda_i^-}^{\Lambda_i^+}.
\end{aligned}$$

The extrema terms can be distinguished in boundary terms and junction terms; thanks to the compatibility condition of the diffusive mass balance, the junction terms vanish. Finally the diffusive term reads as:

$$\begin{aligned}
\int_\Lambda \frac{\partial}{\partial s}\left(-\pi R'^2 A_v \frac{\partial c_v}{\partial s}\right) q_v d\Lambda = &\int_\Lambda \pi R'^2 A_v \frac{\partial}{\partial s} c_v \frac{\partial}{\partial s} q_v \, d\Lambda - [\pi R'^2 A_v \frac{\partial}{\partial s} c_v q_v]_{\partial\Lambda^{IN}} \\
&+ [\pi R'^2 \beta_v c_v q_v]_{\partial\Lambda^{OUT}} - [\pi R'^2 \beta_v c_{0,v} q_v]_{\partial\Lambda^{OUT}}.
\end{aligned}$$

As done in the tissue terms, we write in a non conservative form the advection term:

$$\int_\Lambda \pi R'^2 \frac{\partial}{\partial s}\left(u_v c_v\right) q_v \, ds = \int_\Lambda \pi R'^2 u_v \frac{\partial c_v}{\partial s} q_v \, ds + \int_\Lambda \pi R'^2 \frac{\partial u_v}{\partial s} c_v q_v \, ds \tag{1.14}$$

Globally, combining the previous results, the weak formulation for the vessel problem is

$$\begin{aligned} &\int_\Lambda \pi R'^2 \frac{\partial c_v}{\partial t} q_v \, ds + \int_\Lambda \pi R'^2 A_v \frac{\partial}{\partial s} c_v \frac{\partial}{\partial s} q_v \, d\Lambda + [\pi R'^2 \beta_v (c_v - c_{0,v}) q_v]_{\partial\Lambda^{OUT}} \\ &+ \int_\Lambda \pi R'^2 u_v \frac{\partial c_v}{\partial s} q_v \, ds + \int_\Lambda \pi R'^2 \frac{\partial u_v}{\partial s} c_v q_v \, ds \\ &+ \int_\Lambda 2\pi R' \left\{ (1-\sigma)\, Q \left[(p_v - \bar{p}_t) - \sigma\left(\pi_v - \bar{\pi}_t\right)\right](1-w) + \Upsilon \right\} c_v q_v \, ds \\ =& -\int_\Lambda 2\pi R' \left\{ (1-\sigma)\, Q \left[(p_v - \bar{p}_t) - \sigma\left(\pi_v - \bar{\pi}_t\right)\right] w - \Upsilon \right\} \bar{c}_t q_v \, ds. \end{aligned} \tag{1.15}$$

Therefore, the whole problem is: find $c_t \in Q_t \times (0, T)$ and $c_v \in Q_v \times (0, T)$ such that

$$\begin{cases} & \left(\frac{\partial c_t}{\partial t}, q_t\right)_\Omega + \left(A_t \nabla c_t, \nabla q_t\right)_\Omega + \left(\mathbf{u}_t \cdot \nabla c_t, q_t\right)_\Omega + \left(\nabla \cdot \mathbf{u}_t c_t, q_t\right)_\Omega \\ + & \left(Q^{LF}\left(p_t - p_L\right) c_t, b_t\right)_\Omega + \left(D_\alpha c_t, q_t\right)_\Omega + \left(\beta_c c_t, q_t\right)_{\partial\Omega} \\ - & \left(2\pi R' \left\{(1-\sigma)\, Q\left[(p_v - \bar{p}_t) - \sigma\left(\pi_v - \bar{\pi}_t\right)\right] w - \Upsilon\right\} \bar{c}_t, q_t\right)_\Lambda + \\ - & \left(2\pi R' \left\{(1-\sigma)\, Q\left[(p_v - \bar{p}_t) - \sigma\left(\pi_v - \bar{\pi}_t\right)\right](1-w) + \Upsilon\right\} c_v, q_t\right)_\Lambda \\ = & -\left(\beta c_{0,t} q_t\right)_{\partial\Omega^{MIX}} \qquad \forall q_t \in Q_t, \\ & \left(\pi R'^2 \frac{\partial c_v}{\partial t}, q_v\right)_\Lambda + \left(\pi R'^2 u_v \frac{\partial c_v}{\partial s}, q_v\right)_\Lambda + \left(\pi R'^2 \frac{\partial u_v}{\partial s} c_v, q_v\right)_\Lambda + \\ + & \left(\pi R'^2 A_v \frac{\partial c_v}{\partial s}, \frac{\partial q_v}{\partial s}\right)_\Lambda + [\pi R'^2 \beta_v c_v q_v]_{\partial\Lambda^{OUT}} \\ + & \left(2\pi R' \left\{(1-\sigma)\, Q\left[(p_v - \bar{p}_t) - \sigma\left(\pi_v - \bar{\pi}_t\right)\right](1-w) + \Upsilon\right\} c_v, q_v\right)_\Lambda + \\ + & \left(2\pi R' \left\{(1-\sigma)\, Q\left[(p_v - \bar{p}_t) - \sigma\left(\pi_v - \bar{\pi}_t\right)\right] w - \Upsilon\right\} \bar{c}_t, q_v\right)_\Lambda \\ = & -[\pi R'^2 \beta_v c_{0,v} q_v]_{\partial\Lambda^{OUT}} \qquad \forall q_v \in Q_v, \end{cases} \tag{1.16}$$

with $c_t(t = 0) = 0$ and $c_v(t = 0) = 0$.

1.4 Numerical Approximation

We proceed with the description of finite element implementation of our problem. First of all, we will discretize the domains Ω and Λ; next, we will define the discrete functional spaces for our solutions; finally, we will derive the Galerkin formulation for problem (1.16).

Our formulation let us discretize independently the partitions Ω and Λ.

In order to discretize the domain for the tissue interstitium problem, we introduce an admissible triangulation $\mathcal{T}_t^h$ of $\bar{\Omega}$, i.e.

$$\bar{\Omega} = \bigcup_{K \in \mathcal{T}_t^h} K,$$

which satisfies the usual conditions of a conforming triangulation of Ω, while we are implicitly assuming that Ω is a polygonal domain. With a standard notation, $h = \max_{K \in \mathcal{T}_t^h} h_K$, where h_K is the diameter of the element K. The solutions of (1.16)(a) are approximated using continuous piecewise-polynomial finite elements for the concentration. More precisely, we have

$$X_k^h := \left\{ v_h \in C^0\left(\bar{\Omega}\right) \text{ s.t. } v_h|_K \in P_k(K) \quad \forall K \in \mathcal{T}_t^h \right\}$$

for every integer $k \geq 0$, where P_k indicates the standard space of polynomials of degree $\leq k$ in the variables $\mathbf{x} = (x_1, \ldots, x_d)$.

Concerning the capillary network problem, we adopt the same splitting of the domain described at the continuous level, denoted by

$$\Lambda_h = \bigcup_{i=1}^{N} \Lambda_i^h,$$

where Λ_i^h is a partition of the one-dimensional manifold Λ_i made by segments S. For the concentration, we define the finite element space over the whole network Λ_h as

$$Y_k^h(\Lambda) := \left\{ w_h \in C^0\left(\bar{\Lambda}\right) \text{ s.t. } w_h|_S \in P_k(S) \quad \forall S \in \Lambda_h \right\},$$

for every integer $k \geq 0$.

The discrete formulation arising from (1.16) is easily obtained by projecting the equations on the discrete spaces

$$Q_t^h = X_k^h(\Omega) \quad \text{and} \quad Q_v^h = Y_k^h(\Lambda)$$

for $k \geq 0$ and adding the subscript h to each variable (c_t^h and c_v^h).

The space discretization must be complemented with the time advancing scheme. Let us subdivide the time interval $[0, T]$ in N time steps of size $\Delta t > 0$, so that $t^n = n\Delta t$, with $n = 0, \ldots, N-1$. The equations have been solved with the backward Euler finite difference scheme:

$$\frac{\partial y}{\partial t} = f(y) \quad \Rightarrow \quad \frac{y^{n+1} - y^n}{\Delta t} = f\left(y^{n+1}\right).$$

Let us denote with $c_t^{h,n}$ and $c_v^{h,n}$, the numerical approximation of $c_t^h\left(t^n\right)$ and $c_v^h\left(t^n\right)$, respectively, therefore the fully discrete formulation of problem (1.16) reads as follows:

$\forall\, n = 0, \ldots, N-1$, to find $c_t^{h,n+1} \in Q_t^h$ and $c_v^{h,n+1} \in Q_v^h$ such that

$$\left\{\begin{array}{rl}
 & \frac{1}{\Delta t}\left(c_t^{h,n+1}, q_t^h\right)_\Omega + \left(A_t \nabla c_t^{h,n+1}, \nabla q_t^h\right)_\Omega + \left(\left[D_\alpha + Q^{PL}\left(p_t - p_L\right)\right] c_t^{h,n+1}, q_t^h\right)_\Omega \\
+ & \left(\mathbf{u}_t^h \cdot \nabla c_t^{h,n+1}, q_t^h\right)_\Omega + \left(\nabla \cdot \mathbf{u}_t^h c_t^{h,n+1}, q_t^h\right)_\Omega + \left(\beta_t c_t^{h,n+1}, q_t^h\right)_{\partial\Omega^{MIX}} \\
- & \left(2\pi R' \left\{(1-\sigma) Q\left[\left(p_v^h - \bar{p}_t^h\right) - \sigma\left(\pi_v^h - \bar{\pi}_t^h\right)\right] w - \Upsilon\right\} \bar{c}_t^{h,n+1}, \bar{q}_t^h\right)_\Lambda \\
- & \left(2\pi R' \left\{(1-\sigma) Q\left[\left(p_v^h - \bar{p}_t^h\right) - \sigma\left(\pi_v^h - \bar{\pi}_t^h\right)\right] (1-w) + \Upsilon\right\} c_v^{h,n+1}, \bar{q}_t^h\right)_\Lambda \\
= & \frac{1}{\Delta t}\left(c_t^{h,n}, q_t^h\right)_\Omega - \left(\beta c_{0,t} q_t^h\right)_{\partial\Omega^{MIX}} \qquad \forall q_t^h \in Q_t^h, \\
 & \frac{1}{\Delta t}\left(\pi R'^2 c_v^{h,n+1}, q_v^h\right)_\Lambda + \left(\pi R'^2 A_v \frac{\partial c_v^{h,n+1}}{\partial s}, \frac{\partial q_v^h}{\partial s}\right)_\Lambda + \left(\pi R'^2 u_v^h \frac{\partial c_v^{h,n+1}}{\partial s}, q_v^h\right)_\Lambda \\
+ & \left(\pi R'^2 \frac{\partial u_v^h}{\partial s} c_v^{h,n+1}, q_v^h\right)_\Lambda + \left[\pi R'^2 \beta_v c_v^{h,n+1} q_v^h\right]_{\partial\Lambda^{OUT}} \\
+ & \left(2\pi R' \left\{(1-\sigma) Q\left[\left(p_v^h - \bar{p}_t^h\right) - \sigma\left(\pi_v^h - \bar{\pi}_t^h\right)\right] (1-w) + \Upsilon\right\} c_v^{h,n+1}, q_v^h\right)_\Lambda \\
+ & \left(2\pi R' \left\{(1-\sigma) Q\left[\left(p_v^h - \bar{p}_t^h\right) - \sigma\left(\pi_v^h - \bar{\pi}_t^h\right)\right] (-w) - \Upsilon\right\} \bar{c}_t^{h,n+1}, q_v^h\right)_\Lambda \\
= & \frac{1}{\Delta t}\left(\pi R'^2 c_v^{h,n}, q_v^h\right)_\Lambda - \left[\pi R'^2 \beta_v c_{0,v} q_v^h\right]_{\partial\Lambda^{OUT}} \qquad \forall q_v^h \in Q_v^h.
\end{array}\right. \tag{1.17}$$

with $c_t^{h,0} = 0$ and $c_v^{h,0} = 0$.

1.5 Algebraic formulation

We aim at studying the algebraic counterpart of the discrete problem (1.17). The number of degrees of freedom of the discrete spaces are defined as

$$N_t^h := dim\left(Q_t^h\right) \quad \text{and} \quad N_v^h := dim\left(Q_v^h\right),$$

Let us introduce the finite element basis for Q_t^h and Q_v^h: $\{\varphi_t^i\}_{i=1}^{N_t^h}$ and $\{\varphi_v^i\}_{i=1}^{N_v^h}$, respectively. These two sets are completely independent, since the 3D and 1D meshes do not conform. Let $\mathbf{C}_t^n = \left\{C_t^{j,n}\right\}_{j=1}^{N_t^h}$, $\mathbf{C}_v^n = \{C_v^{j,n}\}_{j=1}^{N_v^h}$ be the degrees of freedom of the finite element approximation, using the finite element basis it is possible to set:

$$c_t^{h,n}\left(\mathbf{x}\right) = \sum_{j=1}^{N_t^h} C_t^{j,n} \varphi_t^j\left(\mathbf{x}\right),\ \forall \mathbf{x} \in \Omega \quad \text{and} \quad c_v^{h,n}\left(s\right) = \sum_{j=1}^{N_v^h} C_v^{j,n} \varphi_v^j\left(s\right),\ \forall s \in \Lambda.$$

Exploiting the linear combinations in the discrete weak form and the linearity of the inner products, the fully discrete form (1.17) of the model leads to the linear system

$$\begin{bmatrix} \frac{1}{\Delta t}\mathbb{M}_t + \mathbb{A}_t + \mathbb{B}_{tt} & \mathbb{B}_{tv} \\ \mathbb{B}_{vt} & \frac{1}{\Delta t}\mathbb{M}_v + \mathbb{A}_v + \mathbb{B}_{vv} \end{bmatrix} \begin{bmatrix} \mathbf{C}_t^{n+1} \\ \mathbf{C}_v^{n+1} \end{bmatrix} = \begin{bmatrix} \frac{1}{\Delta t}\mathbb{M}_t\mathbf{C}_t^n + \mathbb{F}_t \\ \frac{1}{\Delta t}\mathbb{M}_v\mathbf{C}_v^n + \mathbb{F}_v \end{bmatrix}. \tag{1.18}$$

Submatrices and subvectors in (1.18) are defined as follows:

$$\begin{aligned}
[\mathbb{M}_t]_{i,j} &:= \left(\varphi_t^j, \varphi_t^i\right)_\Omega , \\
[\mathbb{A}_t]_{i,j} &:= \left(A_t \nabla\varphi_t^j, \nabla\varphi_t^i\right)_\Omega + \left(\mathbf{u}_t^h \cdot \nabla\varphi_t^j, \varphi_t^i\right)_\Omega + \left(\nabla \cdot \mathbf{u}_t^h \varphi_t^j, \varphi_t^i\right)_\Omega \\
&\quad + \left(\left[D_\alpha + Q^{PL}\left(p_t - p_L\right)\right] \varphi_t^j, \varphi_t^i\right)_\Omega + \left(\beta_t \varphi_t^j, \varphi_t^i\right)_{\partial\Omega^{MIX}} , \\
[\mathbb{M}_v]_{i,j} &:= \left(\pi R'^2 \varphi_v^j, \varphi_v^i\right)_\Lambda , \\
[\mathbb{A}_v]_{i,j} &:= \left(\pi R'^2 A_v \frac{\partial\varphi_v^j}{\partial s}, \frac{\partial\varphi_v^i}{\partial s}\right)_\Lambda + \left(\pi R'^2 u_v^h \frac{\partial\varphi_v^j}{\partial s}, \varphi_v^i\right)_\Lambda + \left(\pi R'^2 \frac{\partial u_v^h}{\partial s} \varphi_v^j, \varphi_v^i\right)_\Lambda \\
&\quad + [\pi R'^2 \beta_v \varphi_v^j \varphi_v^i]_{\partial\Lambda^{OUT}}, \\
[\mathbb{B}_{tt}]_{i,j} &:= \left(-2\pi R' \left\{(1-\sigma) Q \left[\left(p_v^h - \bar{p}_t^h\right) - \sigma\left(\pi_v^h - \bar{\pi}_t^h\right)\right] w - \Upsilon\right\} \bar{\varphi}_t^j, \bar{\varphi}_t^i\right)_\Lambda , \\
[\mathbb{B}_{tv}]_{i,j} &:= \left(-2\pi R' \left\{(1-\sigma) Q \left[\left(p_v^h - \bar{p}_t^h\right) - \sigma\left(\pi_v^h - \bar{\pi}_t^h\right)\right] (1-w) + \Upsilon\right\} \varphi_v^j, \bar{\varphi}_t^i\right)_\Lambda , \\
[\mathbb{B}_{vt}]_{i,j} &:= \left(2\pi R' \left\{(1-\sigma) Q \left[\left(p_v^h - \bar{p}_t^h\right) - \sigma\left(\pi_v^h - \bar{\pi}_t^h\right)\right] w - \Upsilon\right\} \bar{\varphi}_t^j, \varphi_v^i\right)_\Lambda , \\
[\mathbb{B}_{vv}]_{i,j} &:= \left(2\pi R' \left\{(1-\sigma) Q \left[\left(p_v^h - \bar{p}_t^h\right) - \sigma\left(\pi_v^h - \bar{\pi}_t^h\right)\right] (1-w) + \Upsilon\right\} \varphi_v^j, \varphi_v^i\right)_\Lambda , \\
[\mathbb{F}_t]_{i,} &:= -\left(\beta_t c_{0,t} \varphi_t^i\right)_{\partial\Omega^{MIX}} , \\
[\mathbb{F}_v]_{i,} &:= -\left(\pi R'^2 \beta_v c_{0,v} \varphi_v^i\right)_{\partial\Lambda^{OUT}} ,
\end{aligned}$$

where the *bar* operator corresponds to the average operator as in (1.3). In particular, it holds

$$\begin{aligned}
&\mathbb{M}_t \in \mathbb{R}^{N_t^h \times N_t^h}, \quad \mathbb{A}_t \in \mathbb{R}^{N_t^h \times N_t^h}, \quad \mathbb{B}_{tt} \in \mathbb{R}^{N_t^h \times N_t^h}, \quad \mathbb{B}_{tv} \in \mathbb{R}^{N_t^h \times N_v^h}, \quad \mathbb{F}_t \in \mathbb{R}^{N_t^h}, \\
&\mathbb{M}_v \in \mathbb{R}^{N_v^h \times N_v^h}, \quad \mathbb{A}_v \in \mathbb{R}^{N_v^h \times N_v^h}, \quad \mathbb{B}_{vv} \in \mathbb{R}^{N_v^h \times N_v^h}, \quad \mathbb{B}_{vt} \in \mathbb{R}^{N_v^h \times N_t^h}. \quad \mathbb{F}_v \in \mathbb{R}^{N_v^h}
\end{aligned}$$

1.5.1 Coupling terms

Concerning the implementation of the exchange matrices $\mathbb{B}_{tt}$, $\mathbb{B}_{tv}$ and $\mathbb{B}_{vt}$, it is necessary to introduce a discrete average operator $\bar{\pi}_{vt} : Q_t^h \to Q_v^h$ that extracts the mean value of a generic basis function of Q_t^h and a discrete interpolation operator $\pi_{tv} : Q_v^h \to Q_t^h$ that returns the value of a basis function of Q_t^h in correspondence of nodes of Q_v^h.

For every node $s_k \in \Lambda_h$, we let $\mathcal{T}_\gamma\left(s_k\right)$ be the discretization of the perimeter of the vessel $\gamma\left(s_k\right)$, assuming that $\gamma\left(s_k\right)$ is a circle of radius R defined on the

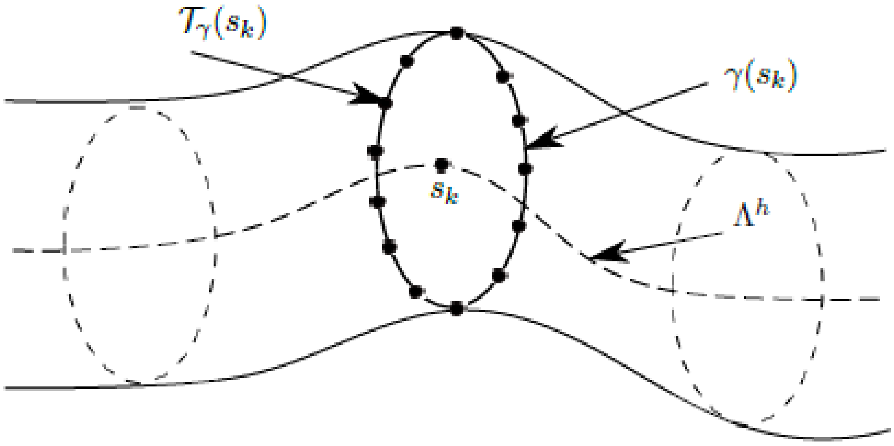

Figure 1.2: Illustration of the vessel with its centerline Λ_h, a cross section, its perimeter $\gamma(s_k)$ and its discretization $\mathcal{T}_\gamma(s_k)$ used for the definition of the operators $\bar{\pi}_{vt}$ and π_{tv}.

orthogonal plane to Λ_h at point s_k (see Figure 1.2). The set of points of $\mathcal{T}_\gamma(s_k)$ is used to interpolate the basis function φ_t^i. The average operator $\bar{\pi}_{vt}$ is defined in such a way that $\bar{q}_t = \bar{\pi}_{vt} q_t$ and each row of the corresponding matrix $\bar{\Pi}_{vt} \in \mathbb{R}^{N_v^h \times N_t^h}$ is defined as

$$\bar{\Pi}_{vt}\big|_k = \mathbf{w}^T(s_k)\,\Pi_\gamma(s_k) \qquad k = 1,\ldots,N_v^h,$$

where $\mathbf{w}$ is the vector of weights of the quadrature formula for the approximation of $\bar{q}_t(s) = \frac{1}{2\pi R'}\int_0^{2\pi} q_t(s,\theta)\,R'd\theta$ in the nodes belonging to $\mathcal{T}_\gamma(s_k)$ and $\Pi_\gamma(s_k)$ is the local interpolation matrix that returns the values of each test function φ_t^i on the set of points belonging to $\mathcal{T}_\gamma(s_k)$. Omitting the parameters, it is possible to analyze the structure of the exchange matrices. Therefore, thanks to these operators, the exchange matrices are implemented as

$$\begin{aligned}
&\mathbb{B}_{vv} \propto \mathbb{M}_{vv}\\
&\mathbb{B}_{tt} \propto \bar{\Pi}_{vt}^T \mathbb{M}_{vv} \bar{\Pi}_{vt}\\
&\mathbb{B}_{tv} \propto \bar{\Pi}_{vt}^T \mathbb{M}_{vv}\\
&\mathbb{B}_{vt} \propto \mathbb{M}_{vv} \bar{\Pi}_{vt}.
\end{aligned}$$

1.6 Numerical Results

We develop a C++ code which provides a solution for the model described in Chapter 1. The code will be discussed in Appendix A; in this section we show the numerical results which validate the code and show some of the applications.

Firstly we will present benchmarks on very simple networks, where we have the exact solution or, at least, we can predict the trend of the solution; in addition, we will not use physiological parameters.

Subsequently, we will test a more complex network with physiological parameters.

1.6.1 Uncoupled 1D and 3D test

Let us first consider an uncoupled problem, to validate separately the equations in the tissue and in the network. To achieve this framework, we set $Q = 0$ and $\Upsilon = 0$, that means the capillary walls are impermeable to both fluid and particles.

Stand-alone vessel network problem

Given the uncoupled framework, in a network made of a single unitary branch, $\Lambda = [0\,,\,1]$ the equation on vessels become a standard one-dimensional advection-diffusion problem. Assigning Dirichlet conditions on the boundary, we have:

$$\begin{cases} \frac{\partial}{\partial t} c_v(s,t) - A_v \frac{\partial^2}{\partial s^2} c_v(s,t) + u_v \frac{\partial}{\partial s} c_v(s,t) = 0 & s \in (0,1)\,, t > 0, \\ c_v(0,t) = 1, \qquad c_v(1,t) = 0, \qquad c_v\,(s,0) = 0, & s \in (0,1)\,, t > 0, \end{cases} \tag{1.19}$$

Under the hypothesis of a constant advection field, the stationary problem has an easy exact solution, that is:

$$c_v^{ex}(s) = \frac{\exp\left(\frac{u_v}{A_v}\right) - \exp\left(\frac{u_v}{A_v} s\right)}{\exp\left(\frac{u_v}{A_v}\right) - 1}. \tag{1.20}$$

We then proceed to test some numerical simulation on the exact solution: as shown in Figure 1.3, the results fit the theoretical expectations.

Remark 1.6.1. The advection field is computed by imposing Dirichlet conditions on the pressure at the extrema of the vessel. In the uncoupled case, the pressure is linear and the velocity, proportional to the first derivative of pressure, is constant.

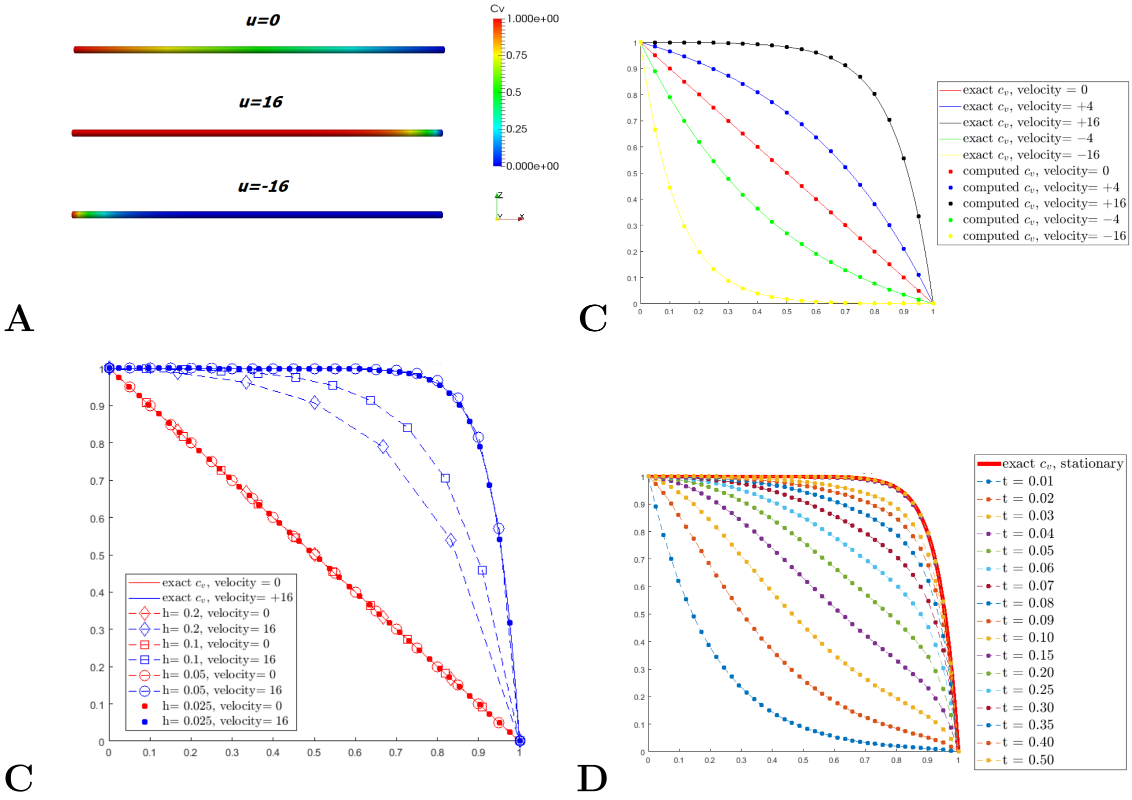

Figure 1.3: Uncoupled problem 1.19 on a single branch network. In all the simulations $A_t = 1$, $R' = 1$. In panels A and B, Λ is discretized with 21 equally distribuited nodes. Panel A shows concentration profiles on the branch for different velocities. Panel B shows concentration profiles on the branch for different velocities, compared to the exact solution. In this simulations Péclet number ranges between 0 and 0.8. Panel C shows how the mesh size affect the simulation in case of large Péclet. We compare the numerical approximations with $u_v = 0$ and $u_v = 16$ for different discretizations; notice that in the second case, with $h_v \in \{0.2, 0.1, 0.05, 0.025\}$, Péclet take values $\mathcal{P}e_v = \{3.2, 1.6, 0.8, 0.4\}$. For Péclet larger than 1, artificial diffusivity is added to stabilize the solution, therefore the numerical data fit the exact solution only for small enough h_v. Panel D shows a time-dependent solution converging to the stationary solution after a few time-steps. In this simulation: $u_v = 16$ and $h_v = 0.025$.

Setting p_{in} and p_{out} the Dirichlet conditions of pressure of inlet and outlet, exact pressure and velocity is:

$$
\begin{aligned}
p_v^{ex}(s) &= \quad p_{in} + (p_{out} - p_{in})\, s && s \in (0,1)\,, && (1.21)\\
u_v^{ex}(s) &= -\tfrac{\kappa_v}{\pi R'^2}\tfrac{\partial p_v}{\partial s} = \tfrac{\kappa_v}{\pi R'^2}\left(p_{in} - p_{out}\right) && s \in (0,1)\,. && (1.22)
\end{aligned}
$$

The numerical tests in this section are made with unitary parameters, $\kappa_v = 1$ and $R' = 1$; therefore the velocity in the branch is easily computed as $u_v^{ex}(s) = \pi^{-1}\left(p_{in} - p_{out}\right)$.

Remark 1.6.2. The well-known theory of advection-diffusion warns us of the risks of an advection dominated setting. For this reason, the code computes Péclet number in both tissue and vessels before solve the linear system; in case of Péclet number larger than 1, in order to avoid instability, we add artificial diffusion, namely $A_v^* = (1 + \mathcal{P}e_v)\, A_v$ for vessels and $A_t^* = (1 + \mathcal{P}e_t)\, A_t$, where the Péclet numbers are defined as $\mathcal{P}e_v = A_v^{-1} h_v \max(u_v)$ and $\mathcal{P}e_t = A_t^{-1} h_t \max(|\boldsymbol{u_t}|)$.

This stabilization method has many drawbacks, such as an excessive diffusion in the solution, but, on the other hand, it has a very simple implementation. In the future, one could try to implement a stronger stabilization method, like streamline diffusion or SUPG. Nevertheless, this seems not to be a priority, since in physiological simulations (see Section 1.8) the diffusion is usually dominating advection.

Stand-alone tissue problem

We study the uncoupled tissue problem on $\Omega = (0,1)^3$, which becomes an advection-diffusion-reaction problem:

$$
\frac{\partial}{\partial t} c_t + \nabla \cdot (c_t \boldsymbol{u_t} - A_t \nabla c_t) + D_\alpha c_t = 0 \qquad \text{on } \Omega,\ t > 0. \tag{1.23}
$$

In this case, we just want to confront qualitatively some numerical simulations with different advection fields. Therefore, we test a tissue slab with fixed concentration on two parallel faces, in order to see how particles diffuse in the domain; the particles can filtrate through the other four faces. We give appropriate boundary conditions, namely Dirichlet and Robin conditions, and an initial condition:

$$
\begin{cases}
c_t(x,\, y,\, z,\, t) = 1 & \text{on } x = 0,\ y \in [0,1]\,,\ z \in [0,1]\,,\ t > 0,\\
c_t(x,\, y,\, z,\, t) = 0 & \text{on } x = 1,\ y \in [0,1]\,,\ z \in [0,1]\,,\ t > 0,\\
-A_t \nabla c_t(x,\, y,\, z,\, t) \cdot \boldsymbol{n} = \beta_c c_t & \text{on } x \in [0,1]\,,\ y \in \{0,1\}\,,\ z \in \{0,1\}\ t > 0,\\
c_t(x,\, y,\, z,\, t) = 0 & \text{on } x \in [0,1],\ y \in [0,1],\ z \in [0,1],\ t = 0.
\end{cases} \tag{1.24}
$$

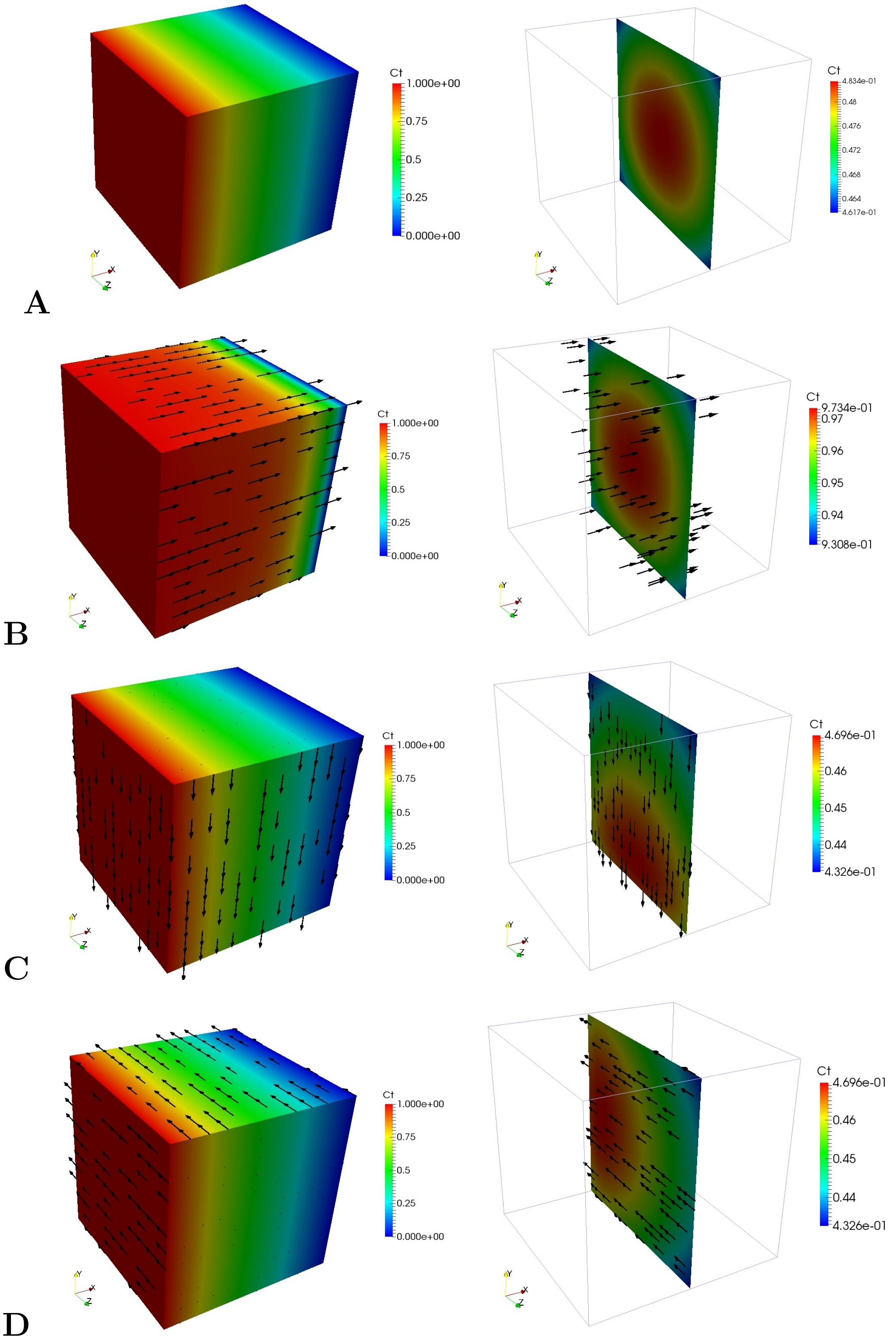

Figure 1.4: Uncoupled problem 1.23 on $\Omega = (0,1)^3$, discretized with 21 points on each direction. In every panel, the figure on the left shows the concentration in all the domain; the figure on the right shows the concentration on the y-z plane $x = 0.5$. Panel A has $u = 0$ (only diffusion). Panel B has $\boldsymbol{u} = 8\boldsymbol{i}$. Panel C has $\boldsymbol{u} = -8\boldsymbol{j}$. Panel D has $\boldsymbol{u} = -8\boldsymbol{k}$.

In this test, we want to focus on the effect of the advection with respect to the diffusion; therefore, we set $D_\alpha = 0$ and look at stationary solutions with $\mathcal{P}e < 1$. We performed four tests: $\boldsymbol{u_t} = 0$, $\boldsymbol{u_t} = 8\boldsymbol{i}$, $\boldsymbol{u_t} = -8\boldsymbol{j}$, and $\boldsymbol{u_t} = -8\boldsymbol{k}$. We see that in the first case, which has no advection, the concentration decrease linearly on the x axis, between the two Dirichlet conditions $c_t = 1$ and $c_t = 0$; besides, we can see that in an arbitrary y-z plane, more particles are in the center of the domain, as they exit at the borders because of the Robin conditions. On the other hand, when there is a velocity field directed along the x axis, particles diffuse faster in this direction, and the Dirichlet condition $c_t = 1$ spread in a larger part of the domain. Finally, the advection fields directed along the y and z axis, give a concentration which diffuse linearly in the x-axis, but in the y-z slices particles are no longer in the center, but move according the advection field.

Remark 1.6.3. The advection field is computed numerically using opportune conditions. In fact, in this case the fluid equations are:

$$\begin{cases} \frac{1}{\kappa_t}\boldsymbol{u_t} + \nabla p_t = 0 & \text{in } \Omega, \\ \nabla \cdot \boldsymbol{u_t} = 0 & \text{in } \Omega. \end{cases} \tag{1.25}$$

If we give Dirichlet conditions on pressure on two parallel faces, and homogeneous Neumann contidions on velocity on the remaining four faces of the domain, the fluid behaves as in a pipe: We find a linear pressure profile and constant velocity (depending on the gradient of pressure). For example, let us suppose we give Dirichlet conditions on the faces with normal directed as the x-axis, exact pressure and velocity are:

$$p_t^{ex}(x,\, y,\, z) = \quad p_{in} + (p_{out} - p_{in})\, x \qquad \text{in } \Omega, \tag{1.26}$$

$$u_t^{ex}(x,\, y,\, z) = \quad -\kappa_t \nabla p_t = \kappa_t\, (p_{in} - p_{out})\, \boldsymbol{i} \qquad \text{in } \Omega. \tag{1.27}$$

In our tests, $\kappa_t = 1$, therefore the module of the advection field is equal to the pressure jump.

1.6.2 Coupled 3D-1D problem on a single branch

We want to test the coupling terms between one-dimensional network and the three-dimensional tissue. We consider the case of the single unitary vessel immersed in a unitary cube of interstitial tissue. Unfortunately, we don't have any analytical solution for this case, so we simplify the model in order to see the effect of the exchange of mass: we set $A_t = 1$, $A_v = 1$,$\boldsymbol{u_t} = 0$, $u_v = 0$ and $D_\alpha = 0$. As described in 1.7, the exchange term is made of two parts: one depending on oncotic pressure and the other caused by the vessel permeability to the particles. For this test case, we decided to model an equilibrium case, where pressure jump

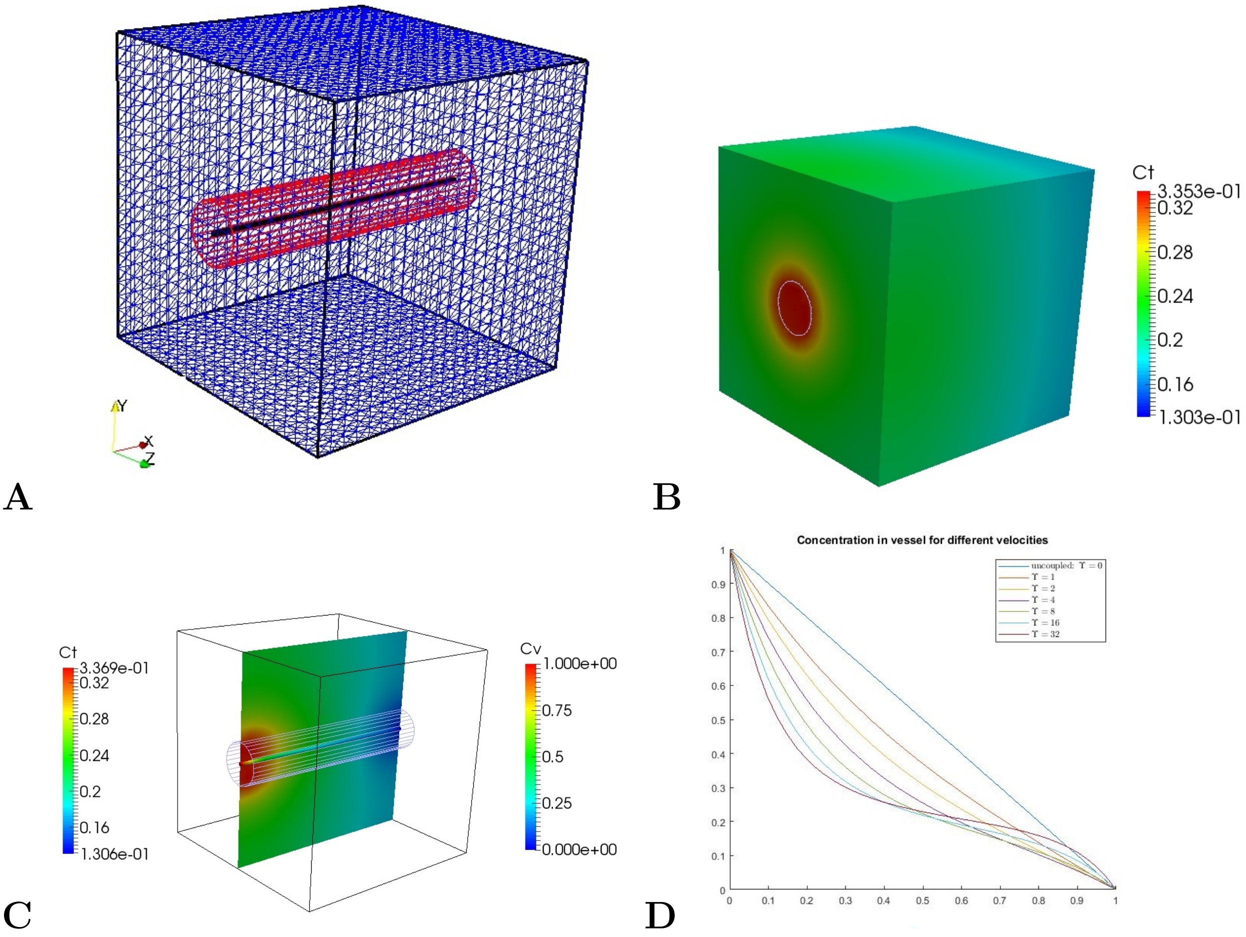

Figure 1.5: Coupled problem 1.6 on single unitary branch Λ discretized with 41 points; tissue domain $\Omega = (0,1)^3$ has 21 points in each directions. The radius of the vessel is $R' = 0.1$. Panel A shows the mesh we used for the simulations. Besides the 3D and the 1D mesh, the real vessel is plotted in red. Panel B shows the concentration c_t in the domain. Panel C shows concentration c_t on the plane $z = 0.5$, c_v in the vessel, and the real vessel. Panel D plots the concentration c_v along the branch, for different value of Υ, ranging from $\Upsilon = 0$ to $\Upsilon = 32$.

of blood between vessel and tissue is equal to the oncotic pressure jump; this is achieved by setting $Q = 0$, $\Upsilon = 4$, and therefore we only show the effects of the permeability.

We used a discretization of 21 points for the single branch Λ and a regular mesh with $h = 0.05$ (21 points for each side of the cube Ω), as shown in Fig. 1.5. The boundary conditions are Dirichlet in the vessel ($c_v = 1$ in inlet and $c_v = 0$ in outlet), while there are Neumann conditions in all the tissue faces, that is: $-\nabla c_t \cdot \boldsymbol{n} = \beta_t c_t$ with $\beta_t = 0.1$. A stationary solution is computed. The figure shows how the concentration diffuses from the vessel to the surrounding tissue. As told before, we don't have any exact solution for this problem, but the plot represents the expected solution.

To investigate further the effect of permability we show the plot of c_v in the single branch for different values of permeability, namely $\Upsilon = \{0, 1, 2, 4, 8, 16, 32\}$. We see that the Dirichlet condition still holds for all the case. For $\Upsilon = 0$ we find the linear solution of the uncoupled benchmark; increasing the leakage of particles, the mass in the center of the vessel decreases. It is interesting to note the for high values of permeability, there is a point in which the exchange of mass is balanced by the diffusivity in the tissue: since the leakage of particles depends on the concentration jump on the vessel wall, if permeability and diffusivity are sufficiently high, concentration in tissue surrounding the outlet exchanges back particles in the vessel; this phenomenon results in the inflection point and in the super-linear plot for $\Upsilon \geq 16$.

1.6.3 Test on a single bifurcation

We now verify the code with a slightly more complex one-dimensional domain, that is a single bifurcation. This network is made by the junction of three capillaries with same length; we will call the bifurcation Λ and the branches Λ_0, Λ_1 andΛ_2. We set the first branch, Λ_0, from $x_A = (0, 0.5, 0.5)$ to $x_M = (0.58, 0.5, 0.5)$, to be an inlet capillary; Λ_1 and Λ_2, from x_M to $x_B = (1, 0.9, 0.5)$ and $x_C = (1, 0.1, 0.5)$ respectively, will be the outlet vessels. We discretize each branch with 21 equidistant points; the interstitial tissue Ω is modeled again as a unitary cube, discretized in a uniform mesh of tetrahedra with 15 points on each side.

For this geometrical setting, neither the uncoupled nor the coupled problem have an exact solution. We provide some tests for this two cases in order to see if the code behaves according to our predictions. Precisely, we will pay attention to the junction point x_M and to the behaviour in asymmetrical conditions.

The junction point is crucial in order to see if the mass balance is respected: for the sake of clarity, we write again the equation of the mass fluxes(1.11):

$$\sum_{i\in P_j^{out}} \pi R_i'^2 \left(-A_v \frac{\partial c_v}{\partial s} + u_v c_v\right)\bigg|_{\Lambda_i^+} = \sum_{i\in P_j^{in}} \pi R_i'^2 \left(-A_v \frac{\partial c_v}{\partial s} + u_v c_v\right)\bigg|_{\Lambda_i^-} \qquad \forall j \in \mathcal{J}. \tag{1.28}$$

In our simple case, the sum of the fluxes in branches Λ_1 and Λ_2 at the junction point must be equal to the flux in branch Λ_0 in x_M. Notice that we also proved, with (1.12) and (1.13), that the diffusive and advective fluxes must hold separately.

Remark 1.6.4. The following simulations will have radius constant in each branch but variable on different branches. This is physiologically correct: it is unlikely that the two daughter vessels and the parent vessel have the same radius. The radii of the daughter branches are calculated on the basis of the Murray's Law, that is $R_0^3 = R_1^3 + R_2^3$. This relation derives from the minimization of the cost of the transport, that is the sum of the power required for transport itself and the power required to maintain the transport medium. This law is observed in respiratory and vascular systems of animals, and has many applications in bio-engineering. This model is not sensitive to the angle of the daughter branches.

In the following sections, we will study the uncoupled case and successively the coupled case. We will initially study symmetric problems, with $R_1' = R_2' = R_0'\sqrt[3]{1/2}$ and the same boundary conditions on both outlets. Next, we will see the behaviour of the simulation with $R_1' \neq R_2'$ and with different boundary conditions in the outlets.

Uncoupled problem on the single bifurcation network

Using the geometrical setting above described, we study the transport of particles in the bifurcation when there is no exchange of mass through the wall. Therefore, we set $Q = 0$, $\Upsilon = 0$ and $A_v = 1$, and solve only the equation in the network. We set Dirichlet conditions on the network: $c_v = 1$ at the inlet and $c_v = 0$ at the outlet. We then run three simulation with different advection fields and different value for the radii, as shown in Fig. (1.6) and in Tab. (1.1). The following test will be diffusion-dominated, so there will no need to stabilize; the Péclet number in the network, under the advection field of the first test, is $\mathcal{P}e = 0.3331$.

In the panel A of Fig. (1.6) we see the discrete solution of a symmetric bifurcation. The advection field is computed by imposing the Dirichlet conditions $p_v = 0.1\pi$ on the inlet and $p_v = 0$ on the two outlets; the radii of the outlet branches are the same and follow the Murray's Law: $R_0' = 0.1$ and $R_1' = R_2' = 0.793$. Therefore the velocities in branches Λ_1 and Λ_2 are equal. The plots show that effectively the particles are equally distribuited in the two outlet branches.

In panel B, we change the boundary conditions on pressure, in order to change the advection field: $p_v|_{x_A} = 0.1\pi$, $p_v|_{x_B} = 0.2$ and $p_v|_{x_C} = 0$. Under these

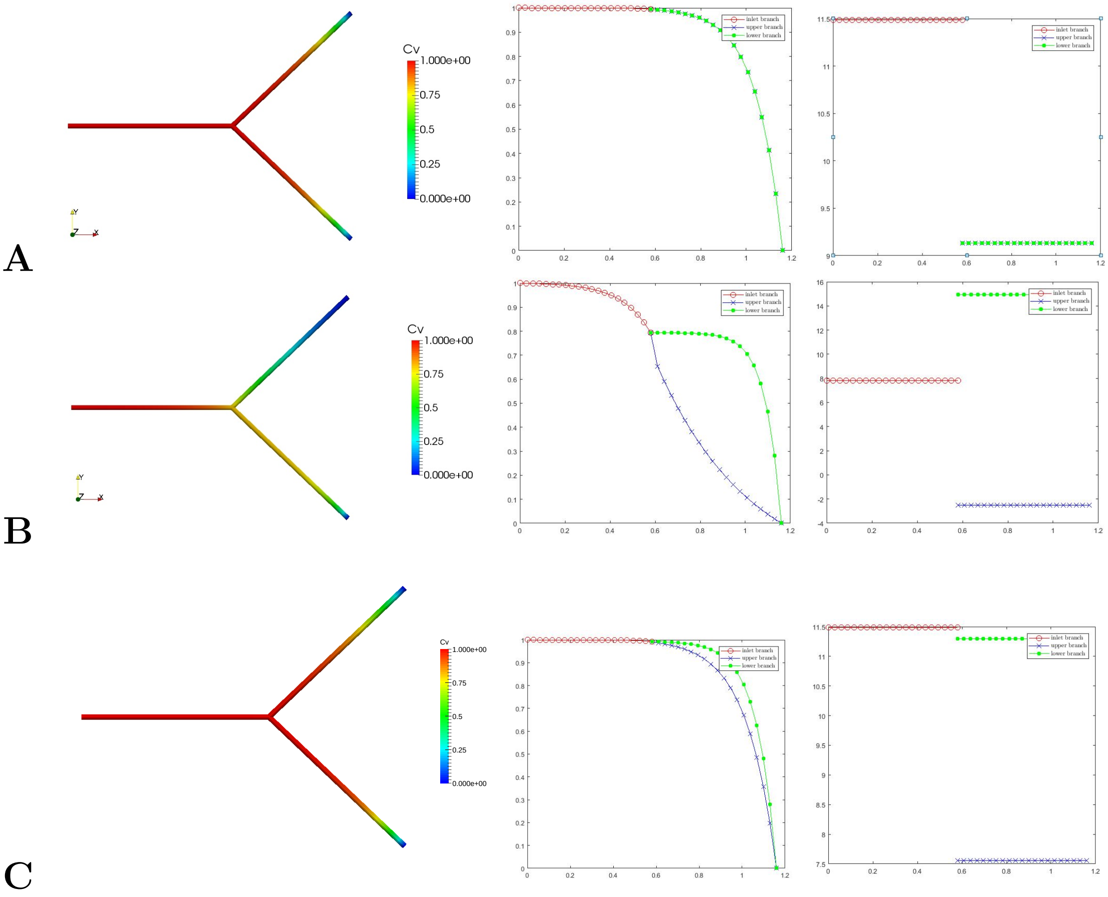

Figure 1.6: Uncoupled($Q = 0, \Upsilon = 0$) problem on a simple bifurcation. For every panel, we show the concentration in the bifurcation Λ(left), the plot of c_v for every branch (center) and the plot of u_v for every branch (right). The boundary condition on the transport problem is $c_v = 1$ in the inlet and $c_v = 0$ in both outlets, in each panel. In panel A, the radii in the branches are $R'_0 = 0.1$, $R'_1 = R'_2 = 0.793$; the boundary condition on the pressure-velocity problem are Dirichlet condition $p_v = 0.1\pi$ in the inlet and $p_v = 0$ in both outlets. In panel B, the radii in the branches are $R'_0 = 0.1$, $R'_1 = R'_2 = 0.793$; the boundary condition on the pressure-velocity problem are Dirichlet condition $p_v = 0.1\pi$ in the inlet, $p_v = 0.2$ in the upper branch and $p_v = 0$ in the lower branch. In panel C, the radii in the branches are $R'_0 = 0.1$, $R'_1 = 0.872$, $R'_2 = 0.713$; the boundary condition on the pressure-velocity problem are Dirichlet condition $p_v = 0.1\pi$ in the inlet and $p_v = 0$ in both outlets.

A

	BC on p_v	BC on c_v	Radius	Diffusive flux	Advective flux
Λ_0 (Inlet)	$p_v = 0.1\pi$	$c_v = 1$	0.1	-1.499700e-03	3.591721e-01
Λ_1 (Outlet)	$p_v = 0$	$c_v = 0$	0.0793	-1.008313e-03	1.795861e-01
Λ_2 (Outlet)	$p_v = 0$	$c_v = 0$	0.0793	-1.008309e-03	1.795860e-01
$\sum_{\Lambda_i}$				-5.169232e-04	1.880776e-11

B

	BC on p_v	BC on c_v	Radius	Diffusive flux	Advective flux
Λ_0 (Inlet)	$p_v = 0.1\pi$	$c_v = 1$	0.1	-4.603712e-02	1.952491e-01
Λ_1 (Outlet)	$p_v = 0.2$	$c_v = 0$	0.0793	-4.943547e-02	-3.923221e-02
Λ_2 (Outlet)	$p_v = 0$	$c_v = 0$	0.0793	-4.457923e-05	2.344813e-01
$\sum_{\Lambda_i}$				-3.442929e-03	2.456449e-11

C

	BC on p_v	BC on c_v	Radius	Diffusive flux	Advective flux
Λ_0 (Inlet)	$p_v = 0.1\pi$	$c_v = 1$	0.1	-2.117772e-03	3.584519e-01
Λ_1 (Outlet)	$p_v = 0$	$c_v = 0$	0.0872	-2.503887e-03	1.792260e-01
Λ_2 (Outlet)	$p_v = 0$	$c_v = 0$	0.0713	-2.881484e-04	1.792259e-01
$\sum_{\Lambda_i}$				-6.742632e-04	1.876815e-11

Table 1.1: Boundary conditions of the test cases on the uncoupled bifurcation, and mass balance at the junction. In each table, we have: the list of the branches (first column), the value of the Dirichlet conditions on the pressure (second column), the value of the Dirichlet conditions on the concentration (third column), the radius in the branch (fourth column), the diffusive flux $\pi R_i'^2 A_v \frac{\partial c_v}{\partial s}$ at the junction (fifth column) and the advective flux $\pi R_i'^2 u_v c_v$ at the junction (sixth column). The last row of each table give the mass balance in the junction due to diffusive and advective fluxes, respectively. Table A refers to the simulation with the same Dirichlet condition on pressure on the two outlets, and same radius in the outlet branches. Table B refers to the simulation where the Dirichlet condition on pressure is different on the two outlets. Table C refers to the simulation where the radii in the outlet branches are different.

conditions, the velocity in the upper branch Λ_1 is negative, that means that the fluid is actually entering from this branch and not exiting; we see that this affects the concentration of particles, that is larger in the lower branch Λ_2.

In panel C, we change the value of the radii: we increase $R'_1$by 10% and reduce R'_2 according the Murray's Law: $R'_0 = 0.1$, $R'_1 = 0.872$ and $R'_2 = 0.713$. The velocity u_v is therefore slightly larger in the smaller branches, and this advection field brings slightly more mass in Λ_2.

We now check the mass balance at the junction: the values are reported in Tab.(1.1). We see that in all the cases the advective flux is correctly balanced with a high precision; this means that the conservation in the local flow rate is well imposed, and that the continuity of c_v is respected at the junction, as we could see in the previous plots. On the other hand, the diffusive flux is correctly balanced but with small precision: in the tests we presented, and in all the other simulations we computed, the sum of the fluxes is usually a order 10^{-1} smaller than the higher of the diffusive fluxes, instead of being close to zero. This small precision may be due to different factors: this mass balance is weakly enforced on the junction points, from the integration by parts, in (1.15); maybe changing the formulation more accurate results can be achieved. Besides, the diffusive flux depend on the first derivative of c_v: we recall that we use piecewise linear finite element, and therefore the first derivative of c_v is piecewise constant. Higher order of finite elements may result in higher accuracy in mass balance.

Coupled 3D-1D problem with a single bifurcation

We now test the bifurcation with the coupled model, and see the effect of permeability with multiple branches. We use the same geometrical framework described above, but we now start using the physiological parameters from Tab. (1.2), taken from [9, 44]; under these settings, we still have a diffusion-dominated problem, as the Péclet numbers are $\mathcal{P}e_v = 8.586e-02$ and $\mathcal{P}e_t = 4.417e-05$. We set Dirichlet conditions on the network: $c_v = 1$ at the inlet and $c_v = 0$ at the outlet; we set mixed conditions on the faces of the 3D domain, $-A_t\nabla c_t = 0.1c_t$. As done before, we test a symmetric and an asymmetric framework, as shown in Fig. (1.7).

In the panel A of Fig. (1.7) we see the discrete solution of a symmetric bifurcation. The advection field is computed by imposing the Dirichlet conditions $p_v = 32$ on the inlet and $p_v = 28.5$ on the two outlets; the radii of the outlet branches are the same and follow the Murray's Law: $R'_0 = 10^{-5}$ and $R'_1 = R'_2 = 7.93 \cdot 10^{-6}$. Therefore the velocities in branches Λ_1 and Λ_2 are equal. The plots show that effectively the particles are equally distribuited in the two outlet branches. The particles in the tissue are distribuited along the whole bifurcation; we notice that the highest concentration in tissue is around the junction. This can be explained by the fact that only source of c_t is the permeability of the network, which is de-

SYMBOL	PARAMETER	UNIT	VALUE
d	characteristic length	m	1×10^{-4}
D	characteristic length of the domain	m	1×10^{-4}
R	average radius	m	4×10^{-6}
K	tissue hydraulic conductivity	m^2	1×10^{-18}
μ_t	interstitial fluid viscosity	cP	1.2
μ_v	blood viscosity	cP	9.33 (Pries Formula)
L_p	wall hydraulic conductivity	$m^2 s\, kg^{-1}$	1×10^{-12}
ΔP	characteristic pressure	Pa	133.32
U	characteristic velocity	$m\, s^{-1}$	1×10^{-3}
$\delta\pi$	oncotic pressure gradient	$mmHg$	25
σ	reflection coefficient	$[-]$	0.95
$L_p^{LF}\frac{S}{V}$	lymphatic wall hydraulic conductivity	$m^2 s\, kg^{-1}$	0
D_t	diffusivity in the tissue	cm^2/s	1.35×10^{-5}
D_v	diffusivity in the vessels	cm^2/s	5×10^{-3}
P	permeability of the vessel wall	cm/s	3.5×10^{-3}
m	metabolic rate	$1/s$	8.0645

SYMBOL	PARAMETER	UNIT	VALUE
δp	hydrostatic pressure drop	$mmHg$	3.5
p_0	far field pressure	$mmHg$	-1
β_t	boundary conductivity	m/s	10^{-2}
β_v	boundary permeability	m/s	10^{-2}
c_{in}	concentration at inlet	$\#/m^3$	1
c_{out}	concentration at outlets	$\#/m^3$	0

Table 1.2: Physiological parameters from [9, 44] . First table contains parameters for the equations and the dimension analysis. Second table contains parameters for boundary conditions.

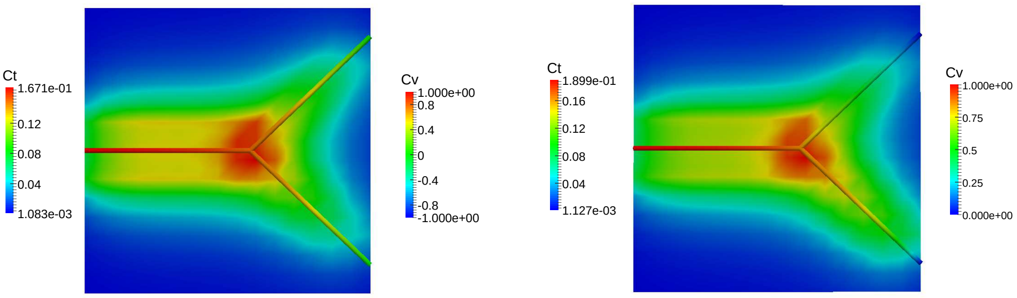

Figure 1.7: Coupled problem on a bifurcation Λ with physiological parameters from table 1.2. The plot show the bifurcation Λ and the tissue Ω cut in half by a x-y plane. On the left, a symmetric junction; the radii are $R'_0 = 0.1$, $R'_1 = R'_2 = 0.793$; the Dirichlet conditions on pressure are $p_v = 32$ in inlet and $p_v = 28.5$ in both outlets. On the right, an asymmetric junction; the radii are $R'_0 = 0.1$, $R'_1 = R'_2 = 0.793$; the Dirichlet conditions on pressure are $p_v = 32$ in inlet, $p_v = 28.5$ in the upper outlet and $p_v = 23$ in the lower outlet.

termined by the quantity of surface of the vessel which can exchange mass; around the junction we have three surfaces that can exchange mass, and therefore higher values of c_t are found here.

In panel B, we change the boundary conditions on pressure, in order to change the advection field: $p_v|_{x_A} = 32$, $p_v|_{x_B} = 28.5$ and $p_v|_{x_C} = 23$. Under these conditions, the velocity field advects higher values of c_v in the lower branch; therefore we notice that higher values of c_t are found near Λ_2.

In Tab.(1.3) we report the diffusive and advective fluxes in the junction. The same considerations of the uncoupled case can be done.

1.6.4 Coupled 3D-1D problem on a complex network

As a final step, we test the code on a complex network. We consider the coupled domain (Ω, Λ) consisting of a non trivial one-dimensional manifold immersed in a three-dimensional unitary cube. The discretization of Ω is a regular mesh of tetrahedra with size $h = 0.1$ (11 points for each side of the cube Ω). The network is made of 47 branches of variable length; the total length of the network is 15.0. Each branch is discretized with 31 equidistant points; the radius is constant in the network, $R = 4 \cdot 10^{-6}$.

A

	BC on p_v	BC on c_v	Radius	Diffusive flux	Advective flux
Λ_0 (Inlet)	$p_v = 32$	$c_v = 1$	0.1	-2.422754e-02	3.565106e-01
Λ_1 (Outlet)	$p_v = 28.5$	$c_v = 0$	0.0793	-1.302717e-02	1.782553e-01
Λ_2 (Outlet)	$p_v = 28.5$	$c_v = 0$	0.0793	-1.302749e-02	1.782552e-01
$\sum_{\Lambda_i}$				-1.827132e-03	-9.167003e-08

B

	BC on p_v	BC on c_v	Radius	Diffusive flux	Advective flux
Λ_0 (Inlet)	$p_v = 32$	$c_v = 1$	0.1	-2.279719e-02	7.065469e-01
Λ_1 (Outlet)	$p_v = 28.5$	$c_v = 0$	0.0793	-2.285698e-02	7.489529e-02
Λ_2 (Outlet)	$p_v = 23$	$c_v = 0$	0.0793	-2.098504e-03	6.316516e-01
$\sum_{\Lambda_i}$				-2.158300e-03	-9.765010e-08

Table 1.3: Boundary conditions of the test cases on the coupled bifurcation, and mass balance at the junction. In each table, we have: the list of the branches (first column), the value of the Dirichlet conditions on the pressure (second column), the value of the Dirichlet conditions on the concentration (third column), the radius in the branch (fourth column), the diffusive flux $\pi R_i'^2 A_v \frac{\partial c_v}{\partial s}$ at the junction (fifth column) and the advective flux $\pi R_i'^2 u_v c_v$ at the junction (sixth column). The last row of each table give the mass balance in the junction due to diffusive and advective fluxes, respectively. Table A refers to the simulation with the same Dirichlet condition on pressure on the two outlets, and same radius in the outlet branches. Table B refers to the simulation where the Dirichlet condition on pressure is different on the two outlets.

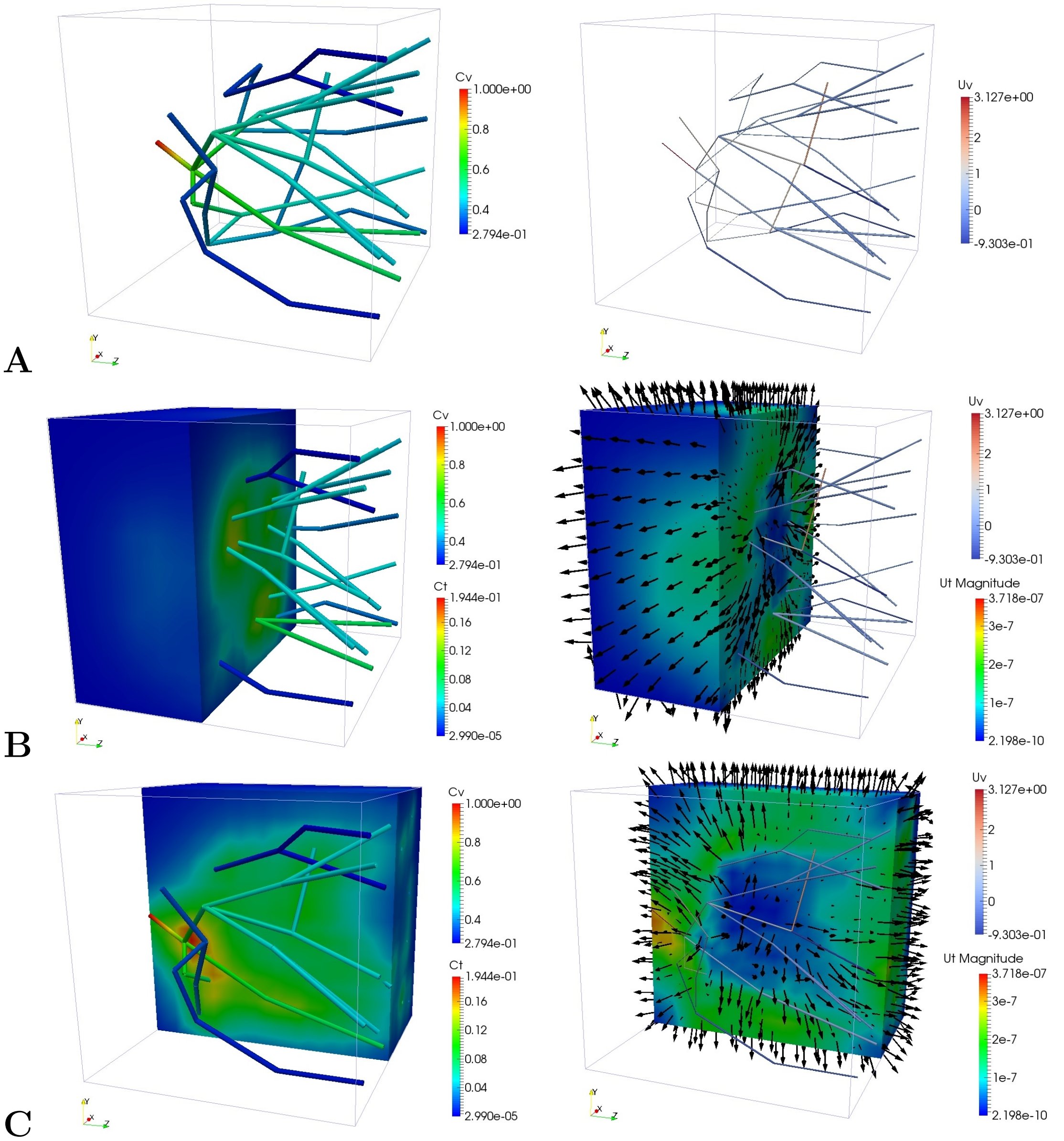

Figure 1.8: Complex network with physiological parameters from table 1.2. The figure shows different points of view of the same simulation on a network of 47 branches, each discretized with 31 points; each side ofΩ is subdivided with 11 points. The boundary conditions on the inlet points are $p_v = 32$ and $c_v = 1$; the boundary condition on the outlet points are $p_v = 28.5$ and $-A_v \frac{\partial c_v}{\partial s} = 0.1 c_v$. The boundary conditions on the faces of Ω are Robin-like for both pressure and concentration, namely $-\kappa_t \nabla p_t \cdot \boldsymbol{n} = 0.1 p_t$ and $-A_t \nabla c_t \cdot \boldsymbol{n} = 0.1 c_t$. The radius is constant in the network, and it is used the physiological value $R = 4 \times 10^{-6}$. On the left we have the concentrations c_t and c_v, while on the right we have the advection field $\boldsymbol{u}_t$ and $\boldsymbol{u}_v$, described by both the color plot and the vectors. Panel A shows only c_v and $\boldsymbol{u}_v$ in the whole network. Panel B shows also tissue values c_t and $\boldsymbol{u}_t$, with the domain Ω cut in half by an x-y plane. Panel C shows all the variables with the domain Ω cut in half by an y-z plane.

The boundary conditions on concentration are:

$$\begin{aligned} c_v &= 1 && \text{on } \partial\Lambda^{IN} \times (0,T)\,, \\ -A_v \frac{\partial c_v}{\partial s} &= \beta_v c_v && \text{on } \partial\Lambda^{OUT} \times (0,T)\,, \\ -A_t \nabla c_t \cdot \boldsymbol{n} &= \beta_t c_t && \text{on } \partial\Omega \times (0,T)\,. \end{aligned}$$

We choose the parameters from Tab. (1.2); under these assumption, we have a diffusion-dominated problem, where $Pe_v = 2.728e - 01$ and $Pe_t = 3.848e - 05$.

Since the validation on the simple geometries, and the absence of evident anomalies in Fig. (1.8), we can deduce the correctness of the solution. We can observe, as in the bifurcation, that the higher values of c_t are near groups of many branches. Nevertheless, one can observe also that the regions where the branches are more tangled contains less particles; in fact, the mass is advected more efficiently in sequence of vessels with few bifurcations. Although these complex regions with many bifurcation have large surface for exchanging mass, they have so low values of c_v that cannot relevantly affect the values of c_t. This is an important result, since it reproduces an experimental phenomenon of one of the many applications of this model: the cardiovascular system around tumoral cells is more tangled with respect to an healthy one; for this reason, these cells receive less oxygen but, on the other hand, it is harder to deliver them drugs such as chemotherapy [42, 23, 10, 49].

Chapter 2

Numerical approximation and a-priori error analysis

In the previous chapter, we presented a physiological model for transport of particles in a one-dimensional manifold embedded in a three-dimensional domain. As we already mentioned, the theoretical analysis of that model reduction has not been discussed thoroughly in literature. We now employ the approach from [33] in order to discuss the topological model reduction for elliptic problems.
In Section 2.1 we address the geometrical configuration and we derive the equations before and after the model reduction. In Section 2.2 we discuss the well-posedness of the reduced model. In Section 2.2.2 we provide the numerical approximation of the equations and discuss the convergence error.

2.1 Setting

This section describes the geometrical framework and the definition of the coupling terms between the 3D domain Ω and the 1D manifold Λ.

2.1.1 Geometry

The three-dimensional domain Ω contains a generalized cylinder Σ, which represent the vessel completely embedded in the tissue; the remaining domain is defined as $\Omega_{\oplus} := \Omega \setminus \overline{\Sigma}$. Let $\boldsymbol{\lambda}(s) = [\xi(s), \nu(s), \zeta(s)],\ s \in (0, S)$ be a $\mathcal{C}^2$-regular curve in the three-dimensional space, and $\Lambda(s) = \{\boldsymbol{\lambda}(s)\,,\ s \in (0, S)\}$ the centerline of the cylinder and Γ the boundary of the cylinder.

We define $\mathcal{D}(s) = [x\,(r, t; s)\,, y\,(r, t; s)] :\ (0, R) \times (0, T) \to \mathbb{R}^2$ the parametrization of the cross section of the cylinder Σ, and $\partial\mathcal{D}(s) = [\partial x\,(r, t; s)\,, \partial y\,(r, t; s)] : (0, R) \times (0, T) \to \mathbb{R}^2$ the parametrization of the boundary of the cross section;

let $\partial\mathcal{D}(s)$ be a piecewise $\mathcal{C}^2$-regular curve. Besides, let us suppose that the shape and the size of the cross section is constant along the centerline $\boldsymbol{\lambda}(s)$: therefore, $\mathcal{D}(s) = \mathcal{D}$, $\partial\mathcal{D}(s) = \partial\mathcal{D}$ and, in particular, $|\mathcal{D}(s)| = |\mathcal{D}|$, $|\partial\mathcal{D}(s)| = |\partial\mathcal{D}|$. Through the Frenet frame $\boldsymbol{T}$, $\boldsymbol{N}$, $\boldsymbol{B}$ related to $\lambda(s)$, we can parametrize the cylinder:

$$\Sigma = \left\{\boldsymbol{\lambda}\left(s\right) + x\left(r,t;\, s\right)\boldsymbol{N}\left(s\right) + y\left(r,t;\, s\right)\boldsymbol{B}\left(s\right),\, r \in \left(0,R\right),\, s \in \left(0,S\right),\, t \in \left(0,T\right)\right\},$$
$$\Gamma = \left\{\boldsymbol{\lambda}\left(s\right) + \partial x\left(r,t;\, s\right)\boldsymbol{N}\left(s\right) + \partial y\left(r,t;\, s\right)\boldsymbol{B}\left(s\right),\, r \in \left(0,R\right),\, s \in \left(0,S\right),\, t \in \left(0,T\right)\right\}.$$

Notice that Γ parametrize only the lateral boundary of Σ: we call the two bases of the cylinder $\Gamma_0 \coloneqq \lambda\left(0\right) + \mathcal{D}$ and $\Gamma_S \coloneqq \lambda\left(S\right) + \mathcal{D}$.

For a sufficiently regular function w, we define the surface average $\overline{\overline{w}}$ on a cross section and the line average $\overline{w}$ on his boundary:

$$\overline{\overline{w}}\left(s\right) = \left|\mathcal{D}\right|^{-1}\int_{\mathcal{D}} w d\sigma, \tag{2.1a}$$

$$\overline{w}\left(s\right) = \left|\partial\mathcal{D}\right|^{-1}\int_{\partial\mathcal{D}} w d\gamma. \tag{2.1b}$$

Therefore we can decompose integrals as follows:

$$\int_{\Sigma} w d\omega = \int_{\Lambda}\int_{\mathcal{D}(s)} w d\sigma ds = \int_{\Lambda} |\mathcal{D}|\overline{\overline{w}}(s) ds\,,$$
$$\int_{\partial\Sigma} w d\sigma = \int_{\Lambda}\int_{\partial\mathcal{D}(s)} w d\gamma ds = \int_{\Lambda} |\partial\mathcal{D}|\overline{w}(s) ds\,,$$

being $d\omega$, $d\sigma$, $d\gamma$ represent generic volume, surface and curvilinear Lebesgue measures. With little abuse of notation for a straight cylinder, we identify the function $\overline{\overline{w}}(s) : \Lambda \to \mathbb{R}$ with the function on Σ obtained by extending the mean value to each cross section $\mathcal{D}(s)$. The same extension can be also applied to Γ, namely $\overline{w}(s)$ can be either regarded as a function on Λ or on Γ, defined by uniform extension on every section boundary $\partial\mathcal{D}(s)$.

Finally, let us formulate a fundamental assumption on the proportions of Σ.

A0) We assume that *the transversal diameter of* Σ *is small compared to the diameter of* Ω. The small parameter (defined below) is denoted with the symbol ϵ.

We now want to rescale the domains Ω and Σ in order to highlight the small parameter. Let $D = \operatorname{diam}(\mathcal{D})$ be the diameter of the cross sections of Σ, that is the transversal diameter of Σ. The central assumption of this work is that $D \ll \operatorname{diam}(\Omega)$.Let $\chi_\Omega(\boldsymbol{x}) = \boldsymbol{x}/\operatorname{diam}(\Omega)$ be a scaling function and let be $\Omega_\chi = \chi_\Omega(\Omega)$, $\Sigma_\chi = \chi_\Omega(\Sigma)$ be the scaled domains. The previous assumption implies that for the scaled domains $\epsilon = D_\chi = /\operatorname{diam}(\Omega)$ is such that $0 < \epsilon \ll 1$. For simplicity of notation, and without loss of generality, from now on we will implicitly refer to the scaled domains dropping the subindex χ.

2.1.2 Reference problem

In this section, we present the reference elliptic problem. We use a different notation for our PDEs, with respect to Chapter 1: we want to take distance from the notation of biological quantities in (1.1), namely c_* for concentration, with subscripts $(\cdot)_t$ for tissue and $(\cdot)_v$ for vessels. In fact, the following elliptic equations can be addressed for many different physical problems; therefore, we now consider the general functions u_* with subscript $(\cdot)_\oplus$ for quantities in the three-dimensional domain $\Omega_\oplus$, and the subscript $(\cdot)_\ominus$ for quantities in the cylinder Σ. We provide the problem *Robin-Neumann* boundary conditions, so that our reference problem is:

$$
\begin{aligned}
-\Delta u_\oplus &= f && \text{in } \Omega_\oplus, && \text{(2.2a)}\\
-\Delta u_\ominus &= g && \text{in } \Sigma, && \text{(2.2b)}\\
-\nabla u_\oplus \cdot \boldsymbol{n}_\oplus &= \kappa\,(u_\oplus - u_\ominus) && \text{on } \Gamma, && \text{(2.2c)}\\
-\nabla u_\ominus \cdot \boldsymbol{n}_\ominus &= \kappa\,(u_\ominus - u_\oplus) && \text{on } \Gamma, && \text{(2.2d)}\\
-\nabla u_\oplus \cdot \boldsymbol{n}_\oplus &= 0 && \text{on } \Gamma_0 \cup \Gamma_S, && \text{(2.2e)}\\
-\nabla u_\ominus \cdot \boldsymbol{n}_\ominus &= 0 && \text{on } \Gamma_0 \cup \Gamma_S, && \text{(2.2f)}\\
u_\oplus &= 0 && \text{on } \partial\Omega\,. && \text{(2.2g)}
\end{aligned}
$$

The elliptic problems on $\Omega_\oplus$ and Σ are coupled by an exchange term: the wall Γ is assumed to be permeable, therefore it is crossed by a normal flux proportional to $\kappa\,(u_\oplus - u_\ominus)$. The coefficient κ plays the role of *permeability* or *transfer coefficient* and it assumes a uniform value on each cross section $\partial\mathcal{D}(s)$. As a result of that κ is only a (regular) function of the arc-length s. For the boundary conditions on the top and bottom faces of the cylinder, we make the assumption that $|\mathcal{D}(0)|$, $|\mathcal{D}(S)| > 0$. The numerical approximation of this PDEs may be expensive, especially in real applications: normally the domain Σ is extended to a collection $\Omega_\ominus$, made of many cylinders, representing channels carrying flow, fibers or inclusions. This results in a very complex shape to discretize, requiring the resolution of the full geometry of a large number of inclusions. In addition, the degrees of freedom of a uniform discretization of both the scales, arising from assumption A0, may be demanding. For this reason, we aim to apply topological model reduction techniques, based on averaging, in order to transform the problem on $\Omega_\ominus$ into a simpler one.

The objective of Sections 2.1.3 and 2.1.4 is to derived a simplified version of problem (2.2), where the domain Σ shrinks to its centerline Λ and the corresponding partial differential equation is averaged on the cylinder cross section, namely $\mathcal{D}$. This new problem setting will be also called the *reduced* problem. We will carefully describe this topological reduction: while the computational cost will decrease, from the mathematical standpoint the reduced formulation is more challenging than (2.2), because it involves the coupling of 3D-1D elliptic problems.

2.1.3 Topological model reduction of the problem on Σ

We apply the averaging technique to equation (2.2b). In particular, we consider an arbitrary portion $\mathcal{P}$ of the cylinder, bounded by two perpendicular sections to Λ, namely $\mathcal{D}(s_1)$, $\mathcal{D}(s_2)$ with $s_1 < s_2$. We have,

$$\int_{\mathcal{P}} \Delta u_\ominus d\Omega = \int_{\partial\mathcal{P}} \nabla u_\ominus \cdot \boldsymbol{n}_\ominus = -\int_{\mathcal{D}(s_1)} \partial_s u_\ominus d\sigma + \int_{\mathcal{D}(s_2)} \partial_s u_\ominus d\sigma + \int_\Gamma \nabla u_\ominus \cdot \boldsymbol{n}_\ominus d\sigma.$$

By the fundamental theorem of integral calculus we have,

$$-\int_{\mathcal{D}(s_1)} \partial_s u_\ominus d\sigma + \int_{\mathcal{D}(s_2)} \partial_s u_\ominus d\sigma = \int_{s_1}^{s_2} \int_{\mathcal{D}(s)} \partial^2_{ss} u_\ominus d\sigma = \int_{s_1}^{s_2} |\mathcal{D}| d^2_{ss} \overline{\overline{u}}_\ominus ds$$

By means of (2.2d) we obtain,

$$\begin{aligned}\int_\Gamma \nabla u_\ominus \cdot \boldsymbol{n}_\ominus d\sigma &= -\int_\Gamma \kappa(u_\ominus - u_\oplus) d\sigma \\ &= -\int_{s_1}^{s_2} \int_{\partial\mathcal{D}(s)} \kappa(u_\ominus - u_\oplus) R d\theta ds \\ &= -\int_{s_1}^{s_2} \kappa |\partial\mathcal{D}| (\overline{u}_\ominus - \overline{u}_\oplus) ds\,.\end{aligned}$$

From the combination of all the above terms with the right hand side, we obtain that the solution $u_\ominus$ of (2.2) satisfies,

$$\int_{s_1}^{s_2} \left[-|\mathcal{D}| d^2_{ss} \overline{\overline{u}}_\ominus + |\partial\mathcal{D}| \kappa(\overline{u}_\ominus - \overline{u}_\oplus)\right] ds = \int_{s_1}^{s_2} |\mathcal{D}| \overline{\overline{g}} ds\,.$$

Since the choice of the points s_1, s_2 is completely arbitrary, we conclude that the following equation holds true,

$$-|\mathcal{D}| d^2_{ss} \overline{\overline{u}}_\ominus + |\partial\mathcal{D}| \kappa(\overline{u}_\ominus - \overline{u}_\oplus) = |\mathcal{D}| \overline{\overline{g}} \quad \text{on } \Lambda\,. \tag{2.3}$$

Let us now formulate the modelling assumption that allows us to reduce equation (2.3) to a solvable one-dimensional (1D) model. More precisely, we assume that:

A1) the function $u_\ominus$ has a *uniform profile* on each cross section $\mathcal{D}(s)$, namely in cylindrical coordinates $u_\ominus(r, s, t) = U(s)$.

We call U the unknown of the one dimensional problem defined on Λ, that is the solution of the following problem,

$$-|\mathcal{D}|d_{ss}^2 U + |\partial\mathcal{D}|\kappa U = |\partial\mathcal{D}|\kappa\overline{u}_\oplus + |\mathcal{D}|\overline{\overline{g}} \qquad \text{on } \Lambda\,, \tag{2.4a}$$

$$|\mathcal{D}|d_s U = 0 \qquad \text{on } s = 0, L\,. \tag{2.4b}$$

For given functions $u_\oplus$ and g, regular enough, the weak form of the previous problem consists to find $U \in H^1(\Lambda)$ such that

$$(d_s U, d_s V)_{\Lambda,|\mathcal{D}|} + (\kappa U, V)_{\Lambda,|\partial\mathcal{D}|} = (\kappa\overline{u}_\oplus, V)_{\Lambda,|\partial\mathcal{D}|} + (\overline{\overline{g}}, V)_{\Lambda,|\mathcal{D}|} \quad \forall V \in H^1(\Lambda)\,. \tag{2.5}$$

where we have introduced the following weighted inner product notation,

$$(U,V)_{\Lambda,w} = \int_0^S w(s)U(s)V(s)ds\,.$$

2.1.4 Topological model reduction of the problem on $\Omega_\oplus$

We focus here on the subproblem of (2.2) related to $\Omega_\oplus$, that is

$$-\Delta u_\oplus = f \qquad \text{in } \Omega_\oplus, \tag{2.6a}$$

$$-\nabla u_\oplus \cdot \boldsymbol{n}_\oplus = \kappa\,(u_\oplus - u_\ominus) \qquad \text{on } \Gamma, \tag{2.6b}$$

$$u_\oplus = 0 \qquad \text{on } \partial\Omega\,. \tag{2.6c}$$

First, we multiply both sides of (2.6a) for a test function $v \in H_0^1(\Omega)$ and we enforce boundary and interface conditions,

$$-\int_{\Omega_\oplus} \Delta u_\oplus v\, d\Omega = \int_{\Omega_\oplus} fv\, d\Omega.$$

Integrating by parts and using boundary and interface conditions, we obtain:

$$\begin{aligned}\int_{\Omega_\oplus} fv\, d\Omega = -\int_{\Omega_\oplus} \Delta u_\oplus v\, d\Omega &= \int_{\Omega_\oplus} \nabla u_\oplus \cdot \nabla v\, d\Omega - \int_{\partial\Omega_\oplus} \nabla u_\oplus \cdot \boldsymbol{n}_\oplus v\, d\sigma \\ &= \int_{\Omega_\oplus} \nabla u_\oplus \cdot \nabla v\, d\Omega + \int_\Gamma \kappa(u_\oplus - u_\ominus)v\, d\sigma\,.\end{aligned}$$

Now, we apply a topological model reduction of the interface conditions, namely we go from a 3D-3D to a 3D-1D formulation. To this purpose, let us write the solution and the test functions on every cross section $\partial\mathcal{D}(s)$ as their average plus some fluctuation,

$$u_\oplus = \overline{u}_\oplus + \tilde{u}_\oplus, \qquad u_\ominus = \overline{u}_\ominus + \tilde{u}_\ominus, \qquad v = \overline{v} + \tilde{v}, \quad \text{on } \partial\mathcal{D}(s)\,,$$

where $\overline{\tilde{u}}_\oplus = \overline{\tilde{u}}_\ominus = \overline{\tilde{v}} = 0$. Therefore, using the coordinates system (r, s, t) on Γ, for $* = \oplus, \ominus$ we have,

$$\int_\Gamma \kappa u_* v\, d\sigma = \int_\Lambda \kappa \int_{\partial\mathcal{D}(s)} (\overline{u}_* + \tilde{u}_*)(\overline{v} + \tilde{v}) d\gamma ds = \int_\Lambda \kappa |\partial\mathcal{D}(s)| \overline{u}_* \overline{v}_*\, ds + \int_\Lambda \kappa \int_{\partial\mathcal{D}(s)} \tilde{u}_* \tilde{v} d\gamma ds\,.$$

Then, we make the following modelling assumptions:

A2) we identify the domain $\Omega_\oplus$ with the entire Ω, namely

$$\int_{\Omega_\oplus} d\omega \simeq \int_\Omega d\omega\,,$$

and we call u the unknown of the partial differential equation defined on Ω.

A3) we assume that the product of fluctuations is small, namely

$$\int_{\partial\mathcal{D}(s)} \tilde{u}_* \tilde{v} d\gamma \simeq 0\,.$$

By means of the previous deductions, reminding that for assumption A1 we have that $\overline{u}_\ominus = U$ and putting together the terms of the weak form of (2.6), we obtain that u solves the following problem,

$$(\nabla u, \nabla v)_\Omega + (\kappa \overline{u}, \overline{v})_{\Lambda, |\partial\mathcal{D}|} = (\kappa U, \overline{v})_{\Lambda, |\partial\mathcal{D}|} + (f, v)_\Omega\,, \quad \forall v \in H_0^1(\Omega)\,. \tag{2.7}$$

2.1.5 Extension of the 1D problem to a metric graph

The embedded domain Σ was defined starting from its centerline, namely the curve Λ. We now discuss the generalization to the case where Λ is a network. In our case, the edges of the network are curves $\boldsymbol{\lambda}_i(s_i) = [\xi_i(s_i), \nu_i(s_i), \zeta_i(s_i)]$, $s_i \in (0, S_i)$, $i = 1, \dots, N$ that are connected at a number M of vertices,

$$\boldsymbol{y}_j = \boldsymbol{\lambda}_i(0) = \boldsymbol{\lambda}_{\hat{\imath}}(S_{\hat{\imath}}), \quad i, \hat{\imath} \in \{1, \dots, N\},\, j = 1, \dots, M.$$

The set of vertices is denoted with $\boldsymbol{Y} = \{\boldsymbol{y}_j \in \boldsymbol{R}^d,\ j = 1, \dots, M\}$, while $\mathcal{K}_j$, represent all the indices i that are connected with the vertex j. Furthermore, $\mathcal{K}_j$ can be decomposed into $\mathcal{K}_j^- = \{i \in \{1, \dots, N\} :\ \boldsymbol{y}_j = \boldsymbol{\lambda}_i(0)\}$ that are the branches originating in the $j-$th vertex, according to their orientation. The complementary is $\mathcal{K}_j^+$ denoting the branches that end into the same vertex. We denote with $i \in \mathcal{B}$ the indices of segments with a dead-end, which can be similarly split into $\mathcal{B}^+$, $\mathcal{B}^-$. Obviously, each edge has an arc-coordinate s_i and a length S_i, under the assumption $\|\boldsymbol{\lambda}_i'\| = 1$. With these two properties, the network is also a *metric* *graph*. In this more general setting the embedded domain Σ is defined as the union of all the generalized cylinders generated by swiping suitable sections $\partial\mathcal{D}_i(s_i)$ along the centerlines $\Lambda_i = \{\boldsymbol{\lambda}_i(s_i),\ s_i \in (0, S_i)\}$, namely $\Sigma = \bigcup_{i=1}^N \Sigma_i$.

We observe that the topological model reduction approach can still be applied branch by branch individually, but it can not be adapted to the entire Σ at once, because in proximity of the junctions Σ is no longer a generalized cylinder. For this reason we define the reduced problem directly from the differential formulation of a single branch. Equation (2.4) applies to each edge Λ_i and it must be complemented with suitable matching conditions at the vertices. Such conditions are the Kirchhoff conditions that for the j-th vertex can be written as,

$$\begin{aligned}
&\sum_{i\in\mathcal{K}_j^+} |\mathcal{D}| d_{s_i} U_i(S_i) - \sum_{i\in\mathcal{K}_j^-} |\mathcal{D}| d_{s_i} U_i(0) = 0\,, && \forall j = 1,\dots,M\,,\\
&U_i(0) = U_{\hat{\imath}}(S_{\hat{\imath}}), \quad \forall i \in \mathcal{K}_j^-, \hat{\imath} \in \mathcal{K}_j^+ && \forall j = 1,\dots,M\,.
\end{aligned}$$

The first conditions corresponds to balance of current or fluxes, while the second states that the solution on each edge must be continuous at the vertices.

The reduced problem on the network consists to find a collection of functions $U_i,\ i = 1,\dots,N$ such that

$$\begin{aligned}
&-|\mathcal{D}| d_{ss}^2 U_i + |\partial\mathcal{D}|\kappa_i U_i = |\partial\mathcal{D}|\kappa_i \overline{u}_\oplus + |\mathcal{D}|\overline{\overline{g}} && \text{on } \Lambda_i,\ \forall i = 1,\dots,N\,, && \text{(2.8a)}\\
&\sum_{i\in\mathcal{K}_j^+} |\partial\mathcal{D}| d_{s_i} U_i(S_i) - \sum_{i\in\mathcal{K}_j^-} |\partial\mathcal{D}| d_{s_i} U_i(0) = 0\,, && \forall j = 1,\dots,M\,, && \text{(2.8b)}\\
&U_i(0) = U_{\hat{\imath}}(S_{\hat{\imath}}), && \forall i \in \mathcal{K}_j^-,\ \forall \hat{\imath} \in \mathcal{K}_j^+\ \forall j = 1,\dots,M\,, && \text{(2.8c)}\\
&|\mathcal{D}| d_s U_i(0) = 0, && \forall\ i \in \mathcal{B}^-\,, && \text{(2.8d)}\\
&|\mathcal{D}| d_s U_i(S_i) = 0, && \forall\ i \in \mathcal{B}^+\,. && \text{(2.8e)}
\end{aligned}$$

For the definition of the variational formulation of problem (2.8) we introduce Sobolev spaces defined on metric graphs, see for example [50] and references therein. In particular $H^1(\Lambda)$ is defined as the space of *continuous functions* V on Λ, such that their restriction to each edge $\Lambda_i,\ i = 1,\dots,N$ belongs to $H^1(\Lambda_i)$. The norm of $H^1(\Lambda)$ is naturally defined as, $\|V\|^2_{H^1(\Lambda)} = \sum_{i=1}^N \|V_i\|^2_{H^1(\Lambda_i)}$.

Let us now take $U, V \in H^1(\Lambda)$ and derive the variational formulation of (2.8). From (2.8a) we obtain,

$$\begin{aligned}
\sum_{i=1}^N \big[(d_s U_i, d_s V_i)_{\Lambda_i,|\mathcal{D}|} + (\kappa_i U_i, V_i)_{\Lambda_i,|\partial\mathcal{D}|} + |\mathcal{D}| d_{s_i} U_i(S_i) V_i(S_i) - |\mathcal{D}| d_{s_i} U_i(0) V_i(0)\big]&\\
= \sum_{i=1}^N (\kappa_i \overline{u}_\oplus, V)_{\Lambda,|\partial\mathcal{D}|} + (\overline{\overline{g}}, V)_{\Lambda,|\mathcal{D}|}\,.&
\end{aligned}$$

By reordering the terms at the endpoints of each edge we have,

$$\begin{aligned}\sum_{i=1}^{N}&\left[|\mathcal{D}|d_{s_i}U_i(S_i)V_i(S_i)-|\mathcal{D}|d_{s_i}U_i(0)V_i(0)\right]\\&=\sum_{j=1}^{M}\left[\sum_{i\in\mathcal{K}_j^+}|\mathcal{D}|d_{s_i}U_i(S_i)V_i(S_i)-\sum_{i\in\mathcal{K}_j^-}|\mathcal{D}|d_{s_i}U_i(0)V_i(0)\right]\\&\qquad+\sum_{i\in\mathcal{B}^+}|\mathcal{D}|d_{s_i}U_i(S_i)V_i(S_i)-\sum_{i\in\mathcal{B}^-}|\mathcal{D}|d_{s_i}U_i(0)V_i(0)\end{aligned}$$

Conditions (2.8b) can be weakly enforced in the variational formulation. The terms on $\mathcal{K}_j$ are not equivalent to (2.8d)-(2.8e), because each one is multiplied by a different the test function. However, since V are continuous on Λ, the test functions can be factorized and these terms disappear owing to (2.8b)-(2.8d)-(2.8e). Finally, conditions (2.8c) are stongly enforced through the definition of $H^1(\Lambda)$. As a result of that, the variational formulation of the reduced problem on the network consists of finding $U\in H^1(\Lambda)$ such that

$$a_\Lambda(U,V)+b_\Lambda^\epsilon(U,V)=b_\Lambda^\epsilon(\overline{u},V)+(\overline{\overline{g}},V)_{\Lambda,|\mathcal{D}|}\quad\forall V\in H^1(\Lambda)\,. \tag{2.9}$$

Endowed with problem (2.9) the metric graph Λ becomes a *quantum graph*, namely a metric graph equipped with a differential operator on the edges complemented with vertex conditions, see for example [4]. The differential operator is in our case $\mathcal{L}(U)=|\mathcal{D}|d_{ss}^2U+|\partial\mathcal{D}|\kappa U$ (also called as a Schrodinger-type or Hamiltonian operator) and the vertex conditions are the Kirchhoff equations reported above.

2.1.6 Coupled problems with hybrid dimensionality

Let us now introduce the following bilinear forms:

$$\begin{aligned}a_\Omega(w,v)&=(\nabla w,\nabla v)_\Omega,\\a_\Lambda(w,v)&=(d_sw,d_sv)_{\Lambda,|\mathcal{D}|},\\b_\Lambda^\epsilon(w,v)&=(\kappa w,v)_{\Lambda,|\partial\mathcal{D}|}.\end{aligned}$$

After averaging the equation on $\Omega_\ominus$ and the interface conditions, for any $f\in L^2(\Omega)$, $\overline{\overline{g}}\in L^2(\Lambda)$, the weak formulation of problem (2.2) consists to find $u\in H_0^1(\Omega)$, $U\in H^1(\Lambda)$ such that

$$a_\Omega(u,v)+b_\Lambda^\epsilon(\overline{u},\overline{v})=b_\Lambda^\epsilon(U,\overline{v})+(f,v)_\Omega\qquad\forall v\in H_0^1(\Omega)\,, \tag{2.10a}$$

$$a_\Lambda(U,V)+b_\Lambda^\epsilon(U,V)=b_\Lambda^\epsilon(\overline{u},V)+(\overline{\overline{g}},V)_{\Lambda,|\mathcal{D}|}\qquad\forall V\in H^1(\Lambda)\,. \tag{2.10b}$$

This problem is an extension to 3D of the one considered in [28] for two space dimensions.

For what follows, it is convenient to introduce a compact formulation for problem (2.10). In particular, we define $\mathcal{V} = [v, V]$ a generic function of the space $\mathbb{V} = H_0^1(\Omega) \times H^1(\Lambda)$ and we name $\mathcal{U} = [u, U]$ the couple of unknowns of problem (2.10). Any function $\mathcal{V} \in \mathbb{V}$ is endowed with the norm $|||\mathcal{V}|||^2 = \|v\|^2_{H^1(\Omega)} + \|V\|^2_{H^1(\Lambda),|\mathcal{D}|}$. Then, we introduce the following bilinear form in $\mathbb{V} \times \mathbb{V}$,

$$\mathcal{A}(\mathcal{U}, \mathcal{V}) = a_\Omega(u, v) + a_\Lambda(U, V) + b^\epsilon_\Lambda(\overline{u} - U, \overline{v} - V)\,,$$

and the linear functional in $\mathbb{V}$, $\mathcal{F}(\mathcal{V}) = (f, v)_\Omega + (\overline{\overline{g}}, V)_{\Lambda,|\mathcal{D}|}$. Then, the compact form of problem (2.10) consists of finding $\mathcal{U} \in \mathbb{V}$ such that

$$\mathcal{A}(\mathcal{U}, \mathcal{V}) = \mathcal{F}(\mathcal{V}), \quad \forall \mathcal{V} \in \mathbb{V}\,. \tag{2.11}$$

2.2 Well-posedness analysis

The solutions of problem (2.11) are studied below.

Theorem 2.2.1. *Problem* (2.11) *has a unique solution* $\mathcal{U} \in \mathbb{V}$ *satisfying the following stability estimate,*

$$|||\mathcal{U}||| \leq \frac{2\sqrt{1+\beta^2}}{\min\left(\frac{\beta}{1+C_P(\Omega)}, 2(1+\beta), C\kappa_{min}\right)} \left(\|f\|_{L^2(\Omega)} + \|\overline{\overline{g}}\|_{L^2(\Lambda),|D|}\right) \tag{2.12}$$

with $\beta = (1 + C_P(\Omega))\, C_T(\Gamma, \Omega_\oplus)\|\kappa\|_{L^\infty}$ *(where the meaning of constants will be clarified in what follows).*

Before addressing the central result, we present some auxiliary tools that will be useful in the analysis.

Lemma 1. *If* $v \in H^1(\Omega)$ *or alternatively* $v \in L^2(\Gamma)$*, then* $\overline{v} \in L^2(\Lambda)$ *and the following inequality holds*

$$\|\overline{v}\|^2_{L^2(\Lambda),|\partial\mathcal{D}|} \leq \|v\|^2_{L^2(\Gamma)} \leq C_T\,(\Gamma, \Omega_\oplus)\,\|v\|^2_{H^1(\Omega)}, \tag{2.13}$$

being $C_T\,(\Gamma, \Omega_\oplus)$ *the (positive) constant of the trace inequality from* $L^2(\Gamma)$ *to* $H^1(\Omega_\oplus)$*.*

Proof. If the inequality (2.13) holds, it follows immediately that $\overline{v} \in L^2(\Lambda)$, since $v \in H^1(\Omega)$, or alternatively $v \in L^2(\Gamma)$. Therefore, we consider

$$\|\overline{v}\|^2_{L^2(\Lambda),|\partial\mathcal{D}|} = \int_\Lambda |\partial\mathcal{D}(s)|\overline{v}^2\, ds = \int_\Lambda \frac{1}{|\partial\mathcal{D}|}\left(\int_{\partial\mathcal{D}(s)} v\, d\gamma\right)^2 ds. \tag{2.14}$$

Using Jensen's inequality, we obtain

$$\int_\Lambda \frac{1}{|\partial\mathcal{D}|}\left(\int_{\partial\mathcal{D}(s)} v\,d\gamma\right)^2 ds \leq \int_\Lambda \int_{\partial\mathcal{D}(s)} v^2\,d\gamma\,ds \tag{2.15}$$

and consequently

$$\|\overline{v}\|^2_{L^2(\Lambda),|\partial\mathcal{D}|} \leq \int_\Lambda \int_{\partial\mathcal{D}(s)} v^2\,d\gamma\,ds = \|v\|^2_{L^2(\Gamma)} \leq C_T\left(\Gamma,\Omega_\oplus\right)\|v\|^2_{H^1(\Omega)}. \tag{2.16}$$

□

Lemma 2 (Poincaré inequality)**.** *For any $v \in H^1_0(\Omega)$, there exists a positive constant, $C_P(\Omega)$, s.t.*

$$\|v\|^2_{L^2(\Omega)} \leq C_P(\Omega)\|\nabla v\|^2_{L^2(\Omega)}.$$

We now address the well-posedness of problem (2.11) on the basis of the theory for linear variational problems in Banach spaces. More precisely we use Theorem 2.6 of [16] (also named the Banach-Necas-Babuska Theorem), which for the sake of clarity is adapted here to the notation used for (2.11).

Theorem 2.2.2. *Let $\mathbb{V}$ be a reflexive Banach space and let $\mathcal{F} \in \mathbb{V}'$. Then, problem* (2.11) *is well-posed if and only if:*

$$\exists\alpha > 0 : \inf_{\mathcal{W}\in\mathbb{V}} \sup_{\mathcal{V}\in\mathbb{V}} \frac{\mathcal{A}(\mathcal{W},\mathcal{V})}{|||\mathcal{W}|||\,|||\mathcal{V}|||} \geq \alpha\,, \tag{BNB1}$$

$$\forall\mathcal{V} \in \mathbb{V} : \left(\mathcal{A}(\mathcal{W},\mathcal{V}) = 0\ \forall\mathcal{W} \in \mathbb{V}\right) \Rightarrow \mathcal{V} = 0\,. \tag{BNB2}$$

Lemma 3. *Under the assumption that $\kappa \in L^\infty(\Lambda)$ is strictly positive and lower bounded by κ_{min}, the operator $\mathcal{A}$ satisfies the conditions of Theorem 2.2.2.*

Proof. In order to prove that the bilinear form $\mathcal{A}$ satisfies (BNB1) it is sufficient to prove that there exists a positive constant α such that $\forall\mathcal{W} \in \mathbb{V}$ we can find $\mathcal{V} \in \mathbb{V}$ satisfying

$$\frac{\mathcal{A}(\mathcal{W},\mathcal{V})}{|||\mathcal{W}|||\,|||\mathcal{V}|||} \geq \alpha.$$

We subdivide the proof in the following steps. We prove that:

(i) $\exists m_1,\ m_2,\ m_3 > 0 :$

$$\mathcal{A}(\mathcal{V},\mathcal{V}) \geq m_1\|v\|^2_{H^1(\Omega)} + m_2|V|^2_{H^1(\Lambda),|\mathcal{D}|} + m_3\|\overline{v} - V\|^2_{L^2(\Lambda),|\partial\mathcal{D}|}\,, \quad \forall\mathcal{V} \in \mathbb{V}. \tag{2.17}$$

(ii) $\forall \mathcal{W} \in \mathbb{V}\ \exists \mathcal{V} \in \mathbb{V}$ and $\alpha_1 > 0$:

$$\mathcal{A}(\mathcal{W},\mathcal{V}) \geq \alpha_1 |||\mathcal{W}|||^2 \tag{2.18}$$

(iii) and $\exists \alpha_2 > 0$:

$$|||\mathcal{W}||| \geq \alpha_2 |||\mathcal{V}|||.$$

From the last two inequalities we obtain that (BNB1) holds for $\alpha = \alpha_1\alpha_2$. In details:

(i) By definition of $\mathcal{A}$,

$$\mathcal{A}(\mathcal{V},\mathcal{V}) = a_\Omega(v,v) + a_\Lambda(V,V) + b_\Lambda^\epsilon(\overline{v}-V,\overline{v}-V)$$

and for the first term we have

$$a_\Omega(v,v) = (\nabla v, \nabla v)_\Omega \geq (1+C_P(\Omega))^{-1}\|v\|^2_{H^1(\Omega)},$$

where $C_P(\Omega)$ is the Poincaré constant. For the second term, it follows immediately that

$$a_\Lambda(V,V) = (d_sV, d_sV)_{\Lambda,|\mathcal{D}|} = |V|^2_{H^1(\Lambda),|\mathcal{D}|},$$

whereas for the last one we have

$$b_\Lambda^\epsilon(\overline{v}-V,\overline{v}-V) = (\kappa(\overline{v}-V),\overline{v}-V)_{\Lambda,|\partial\mathcal{D}|} \geq \kappa_{min}\|\overline{v}-V\|^2_{L^2(\Lambda),\partial\mathcal{D}}.$$

Therefore (2.17) holds and $m_1 = (1+C_P(\Omega))^{-1}$, $m_2 = 1$, $m_3 = \kappa_{min}$.

(ii) For any $\mathcal{W} = [w, W]$, we choose $\mathcal{V} = \mathcal{W} + \delta[0, W]$ and from (i) we have

$$\begin{aligned}
\mathcal{A}(\mathcal{W},\mathcal{W}+\delta[0,W]) =& \mathcal{A}(\mathcal{W},\mathcal{W}) + \delta\mathcal{A}(\mathcal{W},[0,W]) \\
\geq& m_1\|w\|^2_{H^1(\Omega)} + m_2|W|^2_{H^1(\Lambda),|\mathcal{D}|} + m_3\|\overline{w}-W\|^2_{L^2(\Lambda),|\partial\mathcal{D}|} \\
&+ \delta\left(a_\Omega(w,0) + a_\Lambda(W,W) + b_\Lambda^\epsilon(\overline{w}-W,-W)\right) \\
\geq& m_1\|w\|^2_{H^1(\Omega)} + m_2|W|^2_{H^1(\Lambda),|\mathcal{D}|} \\
&+ \delta\left(|W|^2_{H^1(\Lambda),|\mathcal{D}|} + (\kappa(\overline{w}-W),-W)_{\Lambda,|\partial\mathcal{D}|}\right) \\
\geq& m_1\|w\|^2_{H^1(\Omega)} + (m_2+\delta)|W|^2_{H^1(\Lambda),|\mathcal{D}|} \\
&- \delta\left((\kappa\overline{w},W)_{\Lambda,|\partial\mathcal{D}|} - (\kappa W,W)_{\Lambda,|\partial\mathcal{D}|}\right).
\end{aligned} \tag{2.19}$$

We notice that using Young inequality and Lemma 1 we obtain

$$\begin{aligned}
(\kappa\overline{w},W)_{\Lambda,|\partial\mathcal{D}|} =& \int_\Lambda |\partial\mathcal{D}|\kappa\overline{w}W\,ds \leq \frac{1}{2}\left(\int_\Lambda |\partial\mathcal{D}|\kappa\overline{w}^2\,ds + \int_\Lambda |\partial\mathcal{D}|\kappa W^2\,ds\right) \\
\leq& \frac{1}{2}\left(\|\kappa\|_{L^\infty}\|\overline{w}\|^2_{L^2(\Lambda),|\partial\mathcal{D}|} + (\kappa W,W)_{\Lambda,|\partial\mathcal{D}|}\right) \\
\leq& \frac{1}{2}\left(C_T(\Gamma,\Omega_\oplus)\|\kappa\|_{L^\infty}\|w\|^2_{H^1(\Omega)} + (\kappa W,W)_{\Lambda,|\partial\mathcal{D}|}\right).
\end{aligned}$$

Substituting in (2.19) we have,

$$\begin{aligned}\mathcal{A}(\mathcal{W},\mathcal{W}+\delta[0,W]) \geq &\left(m_1-\frac{\delta}{2}C_T(\Gamma,\Omega_\oplus)\|\kappa\|_{L^\infty}\right)\|w\|^2_{H^1(\Omega)}\\ &+(m_2+\delta)|W|^2_{H^1(\Lambda),|\mathcal{D}|}+\frac{\delta}{2}(\kappa W,W)_{\Lambda,|\partial\mathcal{D}|}\end{aligned}$$

and we choose δ sufficiently small such that $m_1-\frac{\delta}{2}\|\kappa\|_{L^\infty}C_T(\Gamma,\Omega_\oplus)$ is positive. Moreover, we assume that there exist positive constants $C_\mathcal{D}$ and $C_{\partial\mathcal{D}}$ dependent on the shape of the cross section solely, such that

$$|\mathcal{D}(s)|=C_\mathcal{D}\,(\mathrm{diam}(\mathcal{D}(s)))^2,\qquad |\partial\mathcal{D}(s)|=C_{\partial\mathcal{D}}\,\mathrm{diam}(\mathcal{D}(s)),\tag{2.20}$$

thus

$$\frac{|\partial\mathcal{D}(s)|}{|\mathcal{D}(s)|}=\frac{C}{\mathrm{diam}(\mathcal{D}(s))}\qquad\forall s,\tag{2.21}$$

with $C=C_{\partial\mathcal{D}}/C_\mathcal{D}$. The assumption that $C_\mathcal{D}$ and $C_{\partial\mathcal{D}}$ are independent of s means that the section of the generalized cylinder Σ can not change its shape, but it can be subject to a homothetic map and rotations. Then, we have,

$$\begin{aligned}\frac{\delta}{2}(\kappa W,W)_{\Lambda,|\partial\mathcal{D}|}&\geq\frac{\delta}{2}\kappa_{min}\int_\Lambda|\partial\mathcal{D}(s)|W^2\,ds=\frac{\delta}{2}\kappa_{min}\int_\Lambda\frac{C}{\mathrm{diam}(\mathcal{D}(s))}|\mathcal{D}(s)|W^2\,ds\\ &\geq\frac{\delta}{2}C\kappa_{min}\|W\|^2_{L^2(\Lambda),|\mathcal{D}|}.\end{aligned}$$

Therefore

$$\begin{aligned}\mathcal{A}(\mathcal{W},\mathcal{W}+\delta[0,W])\geq&\left(m_1-\frac{\delta}{2}C_T(\Gamma,\Omega_\oplus)\|\kappa\|_{L^\infty}\right)\|w\|^2_{H^1(\Omega)}\\ &+(m_2+\delta)|W|^2_{H^1(\Lambda),|\mathcal{D}|}+\frac{\delta}{2}C\kappa_{min}\|W\|^2_{L^2(\Lambda),|\mathcal{D}|}\\ \geq&\left(m_1-\frac{\delta}{2}C_T(\Gamma,\Omega_\oplus)\|\kappa\|_{L^\infty}\right)\|w\|^2_{H^1(\Omega)}\\ &+\min\left(m_2+\delta,\,\frac{\delta}{2}C\kappa_{min}\right)\|W\|^2_{H^1(\Lambda),|\mathcal{D}|}\\ \geq&\alpha_1|||\mathcal{W}|||^2\end{aligned}$$

with $\alpha_1=\min\left(m_1-\frac{\delta}{2}C_T(\Gamma,\Omega_\oplus)\|\kappa\|_{L^\infty},\,m_2+\delta,\,\frac{\delta}{2}C\kappa_{min}\right).$

(iii) We show that there exists a constant α_2 such that

$$|||\mathcal{W}|||\geq\alpha_2|||\mathcal{W}+\delta[0,W]|||.\tag{2.22}$$

The inequality above can be proved as follows:

$$|||\mathcal{W}+\delta[0,W]|||^2 \leq |||\mathcal{W}|||^2+|||\delta[0,W]|||^2 = \|w\|^2_{H^1(\Omega)}+(1+\delta^2)\|W\|^2_{H^1(\Lambda),|\mathcal{D}|} \leq (1+\delta^2)|||\mathcal{W}|||^2.$$

Therefore (2.22) holds with $\alpha_2 = (\sqrt{1+\delta^2})^{-1}$. For the proof of (BNB2) we choose $\mathcal{W}=\mathcal{V}$ and being $\mathcal{A}(\mathcal{V},\mathcal{V})=0$, from (i) we have

$$m_1\|v\|^2_{H^1(\Omega)} + m_2|V|^2_{H^1(\Lambda),|\mathcal{D}|} + m_3\|\overline{v}-V\|^2_{L^2(\Lambda),|\partial\mathcal{D}|} = 0,$$

and consequently

$$\|v\|_{H^1(\Omega)} = 0,\ |V|_{H^1(\Lambda),|\mathcal{D}|} = 0,\ \|\overline{v}-V\|_{L^2(\Lambda),|\partial\mathcal{D}|} = 0. \tag{2.23}$$

Then, $v=0$ and $|V|_{H^1(\Lambda),|\mathcal{D}|}=0$ with $\|V\|^2_{L^2(\Lambda),|\partial\mathcal{D}|}=0$ imply $V=0$. □

Combining Lemma 3 and Theorem 2.2.2, we obtain the well-posedness of (2.11). In order complete the proof Theorem 2.2.1, it remains to show that the stability estimate (2.12) holds. Hence,

$$|||\mathcal{U}||| \leq \frac{1}{\alpha}\sup_{\mathcal{V}\in\mathbb{V}}\frac{\mathcal{A}(\mathcal{U},\mathcal{V})}{|||\mathcal{V}|||} = \frac{1}{\alpha}\sup_{\mathcal{V}\in\mathbb{V}}\frac{\mathcal{F}(\mathcal{V})}{|||\mathcal{V}|||} \leq \frac{1}{\alpha}\left(\|f\|_{L^2(\Omega)}+\|\overline{\overline{g}}\|_{L^2(\Lambda),|D|}\right)$$

where the last inequality follows from

$$\begin{aligned}\mathcal{F}(\mathcal{V}) = (f,v)_\Omega + (\overline{\overline{g}},V)_{\Lambda,|\mathcal{D}|} &\leq \|f\|_{L^2(\Omega)}\|v\|_{L^2(\Omega)} + \|\overline{\overline{g}}\|_{L^2(\Lambda),|\mathcal{D}|}\|V\|_{L^2(\Lambda),|\mathcal{D}|}\\ &\leq \left(\|f\|_{L^2(\Omega)}+\|\overline{\overline{g}}\|_{L^2(\Lambda),|\mathcal{D}|}\right)|||\mathcal{V}|||.\end{aligned}$$

For the particular choice

$$\delta = \frac{m_1}{C_T(\Gamma,\Omega_\oplus)\|\kappa\|_{L^\infty}}$$

we obtain (2.12).

2.2.1 Additional regularity of the solution of the problem in Ω

We observe that the weak formulation (2.10a) could have been formally written in strong form as

$$-\Delta u = f - \kappa\mathcal{E}_\Gamma\left(\overline{u}-U\right)\delta_\Gamma \text{ in } \Omega, \quad u=0 \text{ on } \partial\Omega, \tag{2.24}$$

where $\mathcal{E}_\Gamma$ denotes an extension operator from Λ to Γ. More precisely, given a continuous function $\zeta\in C^0(\Lambda)$, for any $s\in(0,S)$ the extension operator is such that

$$\mathcal{E}_\Gamma\zeta(r,t;s) = \zeta(s) \qquad \forall r\in(0,R), t\in(0,T),$$

namely, the extension operator spans the point-wise value $\zeta(s)$ on $\{\boldsymbol{\lambda}(s)+\partial\mathcal{D}(s)\}$, preserving the regularity of the function. It is straightforward to show that $\left(\kappa\mathcal{E}_\Gamma\left(\overline{u}-U\right)\delta_\Gamma, v\right)_\Omega$ becomes $b_\Lambda^\epsilon(\overline{u}-U,\overline{v})$ in the variational formulation, as follows

$$\begin{aligned}\int_\Omega \kappa\mathcal{E}_\Gamma\left(\overline{u}-U\right)v\delta_\Gamma\,d\Omega &= \int_\Gamma \kappa\mathcal{E}_\Gamma(\overline{u}-U)v\,d\sigma\\ &= \int_\Lambda \kappa(\overline{u}-U)\int_{\partial\mathcal{D}(s)} v\,d\gamma\,ds\\ &= \int_\Lambda |\partial\mathcal{D}|\kappa(\overline{u}-U)\overline{v}\,ds.\end{aligned}$$

Due to the presence of the Dirac source δ_Γ, global H^2-regularity can not be recovered and the issue arises to which interspace X with $H^2(\Omega)\subset X\subset H_0^1(\Omega)$ the solution u belongs to.

Theorem 2.2.3. *The sub-problem on* Ω *enjoys additional regularity* $u\in H^{\frac{3}{2}-\eta}(\Omega)$ *for any* $\eta>0$.

The proof of Theorem 2.2.3 is based on the following result.

Lemma 4. *Let* Ω *be a bounded, convex, polygonal or polyhedral domain in* $\mathbb{R}^3$ *with its boundary* $\partial\Omega$. *Let* $\gamma\subset\Omega$ *be a* C^2-*surface s.t. the distance between* γ *and* $\partial\Omega$ *is positive and* $\gamma\subset\partial D$ *for some three-dimensional* C^2-*domain* $D\subset\subset\Omega$. *Consider the following problem*

$$\begin{cases}-\Delta y = z\delta_\gamma & \text{in } \Omega\\ y=0 & \text{on } \partial\Omega,\end{cases}\tag{2.25}$$

with δ_γ *being the Dirac measure of* γ *and* $z(x)\in L^2(\gamma)$. *Problem* (2.25) *has a unique solution* y *and* $y\in H^{\frac{3}{2}-\eta}(\Omega)\cap H_0^1(\Omega)$ *for each* $\eta>0$.

Proof. For the proof see [24, Theorem 2.1, case (iii)]. ☐

Since $y\in H^{\frac{3}{2}-\eta}(\Omega)$, Δy and the right hand side of (2.25) belong to $H^{-\frac{1}{2}-\eta}(\Omega)$. Then, the theory of pseudo-differential operators and in particular the generalization of Garding inequality to fractional Sobolev spaces (see [2] for details), guarantees that there exists a constant C_R such that

$$\|y\|_{H^{\frac{3}{2}-\eta}(\Omega)}\le C_R\|z\delta_\gamma\|_{H^{-\frac{1}{2}-\eta}(\Omega)}.\tag{2.26}$$

We notice that we cannot apply directly Lemma 4 to problem (2.24) because of the term $\kappa\mathcal{E}_\Gamma\left(\overline{u}-U\right)$ on the right hand side. We can get around this issue by introducing a suitable sequence that converges to the solution u, as shown in the following.

Lemma 5. *The constant* $C_T(\Gamma, \Omega_\oplus)$ *in the Sobolev trace inequality from* $L^2(\Gamma)$ *to* $H^1(\Omega_\oplus)$*, namely*

$$\|v\|_{L^2(\Gamma)} \leq C_T(\Gamma, \Omega_\oplus)\|v\|_{H^1(\Omega_\oplus)} \quad \forall v \in H^1(\Omega_\oplus), \tag{2.27}$$

tends to 0 for $\epsilon \to 0$.

Proof. Let $v \in H^1_0(\Omega_\oplus)$, the trace of v on Γ is in $H^{\frac{1}{2}}(\Gamma)$ and by Sobolev embedding theorem we have that $H^{\frac{1}{2}}(\Gamma) \subset L^4(\Gamma)$. Using Hölder inequality,

$$\|v\|_{L^2(\Gamma)} \leq \left(\int_\Gamma 1\, d\sigma\right)^{\frac{1}{4}} \left(\int_\Gamma v^4\right)^{\frac{1}{4}} \leq |\Gamma|^{\frac{1}{4}}\|v\|_{L^4(\Gamma)} \leq |\Gamma|^{\frac{1}{4}} C_T(\partial\Omega_\oplus, \Omega_\oplus)\|v\|_{H^1(\Omega_\oplus)}$$

and $C_T(\partial\Omega_\oplus, \Omega_\oplus)$ is bounded as $\epsilon \to 0$. Indeed, the problem of studying the asymptotic behaviour of the constant in the trace inequality from $L^4(\partial\Omega_\oplus)$ to $H^1(\Omega_\oplus)$ as $\epsilon \to 0$ can be reformulated as the problem of studying the behaviour of the trace constant from $L^4(\partial\Omega_\oplus)$ to $H^1(\Omega_\oplus)$ as the external boundary $\partial\Omega$ expands (we recall that $\partial\Omega = \partial\Omega_\oplus \setminus \Gamma$) and from [17, Theorem 1.3] we have that $C_T(\partial\Omega_\oplus, \Omega_\oplus)$ is bounded. Therefore $C_T(\Gamma, \Omega_\oplus) = |\Gamma|^{\frac{1}{4}} C_T(\partial\Omega_\oplus, \Omega_\oplus) \to 0$ when $\epsilon \to 0$.

□

Theorem 2.2.4. *For* ϵ *small enough, there exists a sequence* $\{u_n\}_{n\geq 0}$ *such that* $u_n \in H^{\frac{3}{2}-\eta}(\Omega)$ *for any* $\eta > 0$*, which converges to the solution* u *of* (2.24) *in the* $H^{\frac{3}{2}-\eta}$*-norm.*

Proof. Let us consider the sequence $\{u_n\}_{n\geq 0}$, where u_{n+1} is the solution of

$$-\Delta u_{n+1} = f - \kappa\mathcal{E}_\Gamma\left(\overline{u}_n - U\right)\delta_\Gamma \text{ in } \Omega, \quad u_{n+1} = 0 \text{ on } \partial\Omega, \tag{2.28}$$

for $n \geq 0$ and u_0 is arbitrarily chosen in $H^1_0(\Omega)$.

Using induction on n we show that for any $n > 0$, $u_n \in H^{\frac{3}{2}-\eta}(\Omega) \cap H^1_0(\Omega)$ for each $\eta > 0$. For $n = 0$, the term $\kappa\mathcal{E}_\Gamma(\overline{u}_0 - U)$ on the right side belongs to $L^2(\Gamma)$ because, for Lemma 2.13, $\overline{u}_0 \in L^2(\Lambda)$ and the extension operator $\mathcal{E}_\Gamma$ does not change the regularity of the functions. Thus, setting $\gamma = \Gamma$, we can use Lemma 4 and we obtain that $u_1 \in H^{\frac{3}{2}-\eta}(\Omega) \cap H^1_0(\Omega)$ for each $\eta > 0$. Supposing that the property is valid for u_n, the same considerations apply to $\kappa\mathcal{E}_\Gamma(\overline{u}_n - U)$ and consequently the property is satisfied also by u_{n+1}.

We prove now that the sequence $\{u_n\}_{n\geq 0}$ converges to the solution u of (2.24) in $H^{\frac{3}{2}-\eta}(\Omega)$. Let us set $e_n = u - u_n$, hence e_{n+1} is solution of the problem

$$-\Delta e_{n+1} = -\kappa\mathcal{E}_\Gamma\overline{e}_n\delta_\Gamma \text{ in } \Omega, \quad e_{n+1} = 0 \text{ on } \partial\Omega$$

and it can be shown, using Lemma 4, that e_{n+1} still belongs to $H^{\frac{3}{2}-\eta}(\Omega)$. From (2.26) we have

$$\|e_{n+1}\|_{H^{\frac{3}{2}-\eta}(\Omega)} \leq C_R \|\kappa \mathcal{E}_\Gamma \overline{e}_n \delta_\Gamma\|_{H^{-\frac{1}{2}-\eta}(\Omega)} \tag{2.29}$$

where,

$$\|\kappa \mathcal{E}_\Gamma \overline{e}_n \delta_\Gamma\|_{H^{-\frac{1}{2}-\eta}(\Omega)} = \sup_{\substack{w \in H^{\frac{1}{2}+\eta}(\Omega) \\ w \neq 0}} \frac{(\kappa \mathcal{E}_\Gamma \overline{e}_n \delta_\Gamma, w)_\Omega}{\|w\|_{H^{\frac{1}{2}+\eta}(\Omega)}}.$$

Then we have,

$$\begin{aligned}(\kappa \mathcal{E}_\Gamma \overline{e}_n \delta_\Gamma, w)_\Omega = (\kappa \mathcal{E}_\Gamma \overline{e}_n, w)_\Gamma &\leq \|\kappa\|_{L^\infty} \|\mathcal{E}_\Gamma \overline{e}_n\|_{L^2(\Gamma)} \|w\|_{L^2(\Gamma)} \\ &\leq \sqrt{C_T'(\Gamma, \Omega_\oplus)} \|\kappa\|_{L^\infty} \|\mathcal{E}_\Gamma \overline{e}_n\|_{L^2(\Gamma)} \|w\|_{H^{\frac{1}{2}+\eta}(\Omega)},\end{aligned}$$

where $C_T'(\Gamma, \Omega_\oplus)$ is the constant in the trace inequality from $L^2(\Gamma)$ to $H^{\frac{1}{2}+\eta}(\Omega_\oplus)$. Substituting the previous inequality in the definition of $\|\kappa \mathcal{E}_\Gamma \overline{e}_n \delta_\Gamma\|_{H^{-\frac{1}{2}-\eta}(\Omega)}$ we obtain

$$\|\kappa \mathcal{E}_\Gamma \overline{e}_n \delta_\Gamma\|_{H^{-\frac{1}{2}-\eta}(\Omega)} \leq \sqrt{C_T'(\Gamma, \Omega_\oplus)} \|\kappa\|_{L^\infty} \|\mathcal{E}_\Gamma \overline{e}_n\|_{L^2(\Gamma)}.$$

and from (2.29) we infer that

$$\|e_{n+1}\|_{H^{\frac{3}{2}-\eta}} \leq C_R \sqrt{C_T'(\Gamma, \Omega_\oplus)} \|\kappa\|_{L^\infty} \|\mathcal{E}_\Gamma \overline{e}_n\|_{L^2(\Gamma)}. \tag{2.30}$$

Using Lemma 1, we can write $\|\mathcal{E}_\Gamma \overline{e}_n\|^2_{L^2(\Gamma)}$ as follows

$$\begin{aligned}\|\mathcal{E}_\Gamma \overline{e}_n\|^2_{L^2(\Gamma)} = \int_\Gamma (\mathcal{E}_\Gamma \overline{e}_n)^2 \, d\sigma = \int_\Lambda |\partial \mathcal{D}(s)| \overline{e}_n^2 \, ds &\leq C_T(\Gamma, \Omega_\oplus) \|e_n\|^2_{H^1(\Omega)} \\ &\leq C_T(\Gamma, \Omega_\oplus) \|e_n\|^2_{H^{\frac{3}{2}-\eta}(\Omega)}\end{aligned}$$

Therefore,

$$\begin{aligned}\|e_{n+1}\|_{H^{\frac{3}{2}-\eta}(\Omega)} &\leq C_R \sqrt{C_T'(\Gamma, \Omega_\oplus)} \sqrt{C_T(\Gamma, \Omega_\oplus)} \|\kappa\|_{L^\infty} \|e_n\|_{H^{\frac{3}{2}-\eta}(\Omega)} \\ &\leq (C_R \sqrt{C_T'(\Gamma, \Omega_\oplus)} \sqrt{C_T(\Gamma, \Omega_\oplus)} \|\kappa\|_{L^\infty})^2 \|e_{n-1}\|_{H^{\frac{3}{2}-\eta}(\Omega)} \leq \dots \\ &\leq (C_R \sqrt{C_T'(\Gamma, \Omega_\oplus)} \sqrt{C_T(\Gamma, \Omega_\oplus)} \|\kappa\|_{L^\infty})^n \|e_0\|_{H^1(\Omega)},\end{aligned} \tag{2.31}$$

and we conclude that for $(C_R \sqrt{C_T'(\Gamma, \Omega_\oplus)} \sqrt{C_T(\Gamma, \Omega_\oplus)} \|\kappa\|_{L^\infty}) < 1$ the iteration error e_n converges to 0 and equivalently u_n converges to u in $H^{\frac{3}{2}-\eta}(\Omega)$. The condition on the iteration constant that is guaranteed by ϵ sufficiently small owing to Lemma 5.

□

2.2.2 Finite element approximation

Let us consider a quasi-uniform partition $\mathcal{T}_\Omega^h$ of Ω and an admissible partition $\mathcal{T}_\Lambda^h$ of Λ with comparable characteristic size, denoted by h, and let $\mathbb{V}_h = V_h^\Omega \times V_h^\Lambda \subset \mathbb{V}$ be continuous k_1, k_2-order Lagrangian finite element spaces defined on $\mathcal{T}_\Omega^h$, $\mathcal{T}_\Lambda^h$ respectively. The numerical approximation of the variational formulation (2.11) consists of finding $\mathcal{U}_h \in \mathbb{V}_h$ solution of

$$\mathcal{A}(\mathcal{U}_h, \mathcal{V}_h) = \mathcal{F}(\mathcal{V}_h) \qquad \forall \mathcal{V}_h \in \mathbb{V}_h. \tag{2.32}$$

We notice that in problem (2.32) it is implicitly assumed that numerical integration is performed exactly. In practice, the average operator $\overline{(\cdot)}$ is approximated by means of numerical quadrature. The effect of the latter approximation shall be analyzed in a future development of this work.

We exploit the conformity of the finite element space combined with (BNB1) and Lemma 3, in order to prove that $\mathcal{U}_h$ satisfies a Ceá-type inequality ([16] [Lemma 2.28]),

$$|||\mathcal{U} - \mathcal{U}_h||| \leq \left(1 + \frac{|||\mathcal{A}|||}{\alpha}\right) \inf_{v_h \in V_h^\Omega, V_h \in V_h^\Lambda} \left(\|u - v_h\|_{H^1(\Omega)} + \|U - V_h\|_{H^1(\Lambda), |\mathcal{D}|}\right). \tag{2.33}$$

The convergence of the finite element method follows from (2.33) combined with approximation properties of the finite element spaces. For the latter property, we exploit the additional regularity of the solution in Ω proved in Theorem 2.2.4 and the fact that the solution U on Λ is in $H^2(\Lambda)$. The regularity of U descends from the standard theory of elliptic operators in convex domains, [22, Theorem 8.12], being in (2.10b) $\overline{\overline{g}}$ and $\overline{u}$ both in $L^2(\Lambda)$. From now on, let $a \lesssim b$ be equivalent to the inequality $a \leq Cb$ where C is a generic constant, possibly dependent on Ω, Λ but independent of the parameters of the problem. Concerning the solution u in Ω, let π^h be the Scott-Zhang interpolation operator from $W^{l,q}(\Omega) \cap H_0^1(\Omega)$ to V_h^Ω with $1 \leq q \leq \infty$ and $0 \leq l \leq k_1 + 1$, with the additional constraint $l \geq 1/q$ when $q > 1$. Then, the following interpolation estimate holds true in the norm of $W^{t,q}(\Omega)$ with $t \leq l$ (see for example [16, Lemma 1.130])

$$\|v - \pi^h v\|_{W^{t,q}(\Omega)} \lesssim h^{l-t} |v|_{W^{l,q}(\Omega)}.$$

The estimate above applies to the problem at hand, knowing that $u \in H^{\frac{3}{2}-\eta}(\Omega) \cap H_0^1(\Omega)$, with $t = 1$, $l = \frac{3}{2} - \epsilon$, $q = 2$, $k_1 = 1$, obtaining

$$\inf_{v_h \in V_h^\Omega} \|u - v_h\|_{H^1(\Omega)} \lesssim h^{\frac{1}{2}-\eta} \|u\|_{H^{\frac{3}{2}-\eta}(\Omega)}.$$

For the solution U on Λ and $k_2 = 1$, the standard finite element approximation estimate ensures that

$$\inf_{V_h \in V_h^\Lambda} \|U - V_h\|_{H^1(\Lambda)} \lesssim h \|U\|_{H^2(\Lambda)}.$$

Therefore, combining (2.33) and the previous inequalities for piecewise affine approximation, we obtain

$$|||\mathcal{U} - \mathcal{U}_h||| \lesssim h^{\frac{1}{2}-\eta} \|u\|_{H^{\frac{3}{2}-\eta}(\Omega)} + h\|U\|_{H^2(\Lambda)}.$$

Moreover, on the basis of the previous estimate, it can be proved by means of an Aubin-Nitsche argument (see [16, Lemma 2.31]), that the following error estimate holds

$$\|u - u_h\|_{L^2(\Omega)} + \|U - U_h\|_{L^2(\Lambda),|\mathcal{D}|} \lesssim h^{\frac{3}{2}-\eta} \|u\|_{H^{\frac{3}{2}-\eta}(\Omega)} + h^2\|U\|_{H^2(\Lambda)}. \qquad (2.34)$$

We have tested the previous convergence results by means of numerical experiments based on a problem for which the analytical solution is known. Precisely, we consider $\Omega = (-1, 1)^3 \subset \mathbb{R}^3$ and Σ is the cylinder with constant circular cross section of radius $R = 0.25$ and centerline $\Lambda = \{(x, 0, 0), x \in (-1, 1)\}$. We assume $U = 1$, therefore the problem reduces to find only the solution u in Ω. Concerning the other parameters, we choose $f = 0$ and $\kappa = 0.1$. With appropriate boundary conditions, the exact solution u_e of the problem can be obtained by uniform extension along the x-coordinate the 2D solution given in [28], which is

$$u_e^{2D}(y, z) = \begin{cases} U \frac{\kappa}{1+\kappa} \left(1 - R \ln \frac{r}{R}(y, z),\right) & r(y, z) > R, \\ U \frac{\kappa}{1+\kappa}, & r(y, z) \leq R, \end{cases}$$

where $r(y, z)$ is the Euclidean distance from the origin. In particular in our case $u_e(x, y, z) = u_e^{2D}(y, z)$. For the triangulation of Ω we consider a quasi-uniform mesh(see Figure 2.1) and we report in Table 2.1 the discretization error $e_h = u_e - u_h$ and the rates of convergence computed with respect to the L^2- and H^1- norms for different numbers of subdivisions along the y and z axes. The numerical results confirm the theoretical estimates.

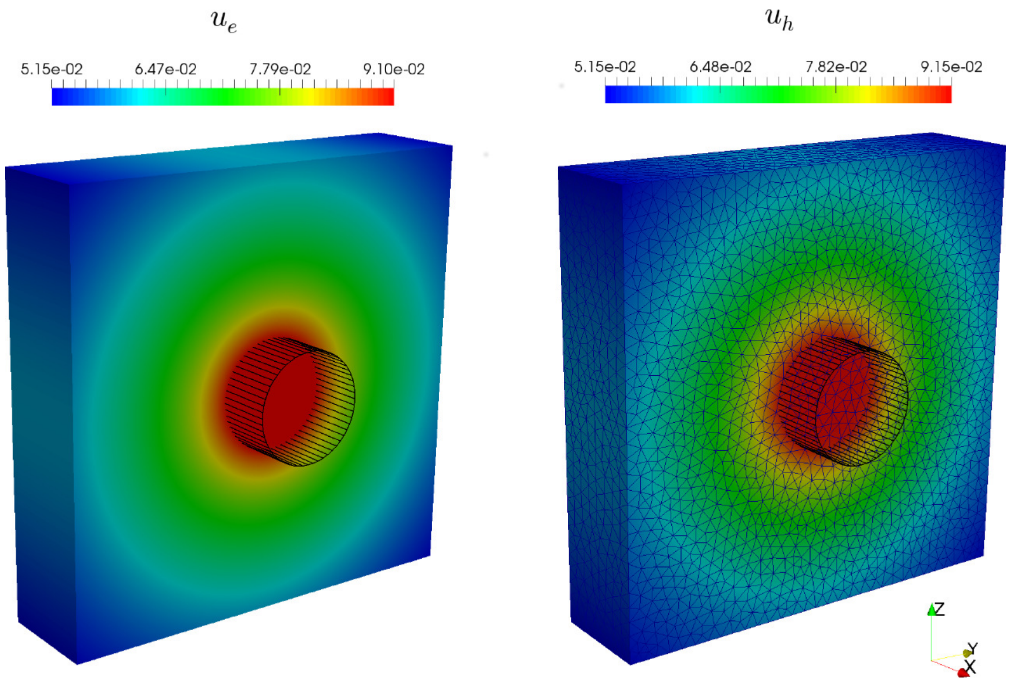

Figure 2.1: Visualization of the quasi-uniform mesh used for the convergence test, the exact solution u_e and the numerical solution u_h.

y,z sub.	$\|e_h\|_{L^2(\Omega)}$	Rate	$\|e_h\|_{H^1(\Omega)}$	Rate
8	$1.37341e-03$	0.67705	$1.77839e-02$	0.02115
16	$4.24798e-04$	1.69291	$1.21790e-02$	0.54618
32	$1.74336e-04$	1.28491	$8.63759e-03$	0.49569
64	$6.42597e-05$	1.43988	$6.10750e-03$	0.50005
	expected:	**1.50**	expected:	**0.50**

Table 2.1: The discretization error e_h and the rate of convergence computed with respect to the L^2- and H^1- norms for different numbers of subdivision of the y and z axes.

Chapter 3

Model error analysis

In Chapter 2 we discussed the formulation of a topological model reduction for equation (2.2). The analysis of Sections 2.2 and 2.2.2 guarantees the well-posedness of the reduced equation (2.10). We now want to study the error introduced by replacing the equation (2.2) with (2.10). In particular, the idea of the topological reduction was justified by the assumption A0 in Section 2.1: our goal is to characterize the dependence of the modeling error with respect to the small parameter of the model, which is the radius of the inclusion, namely ϵ.

The *a posteriori* analysis of modeling error developed in [7] is the starting point of our analysis: therefore, in Section 3.1 we recall the main steps for general abstract problems. Then, in Section 3.2 we apply the general theory to the particular case of topological model reductions for small cylindrical inclusions. In particular, we will discuss separately the contributes of the modeling error arising from the assumptions described in 2.1.3,2.1.4 namely A1, A2, A3.

3.1 Theory of dual-based estimator of modeling error

The following section describes the abstract theory of dual-based estimators for modeling error, as discussed in [7].

Let us introduce our reference problem: this is the weak formulation of the partial differential equations describing the complete model,

$$\text{find } u_{ref} \in X : \quad a_{ref}\left(u_{ref}, v\right) = \mathcal{F}_{ref}\left(v\right), \qquad \forall v \in X, \tag{3.1}$$

where $a_{ref}(\cdot,\cdot)$ and $\mathcal{F}_{ref}$ are, respectively, a bilinear and a linear form on the Hilbert space X.

Let us suppose that equation (3.1), representing the accurate model for our problem, can be decomposed in an expensive part of the model, which we don't want to compute, and a simple part of the model, which is our reduced model. In practice, we introduce the bilinear form $d(\cdot,\cdot)$ and the linear form $l(\cdot)$, representing the part of the model we want to neglect, such that:

$$a_{ref}\left(u,v\right) = a\left(u,v\right) + d\left(u,v\right), \forall u,v \in X, \tag{3.2}$$

$$\mathcal{F}_{ref}\left(v\right) = \mathcal{F}\left(v\right) + l\left(v\right), \forall v \in X. \tag{3.3}$$

Therefore, the reduced model is

$$\text{find } u \in X : \quad a\left(u,v\right) = \mathcal{F}\left(v\right), \qquad \forall v \in X. \tag{3.4}$$

Remark 3.1.1. We define the model error $e = u_{ref} - u$; by subtracting (3.1) to (3.4), we obtain the following *perturbated Galerkin orthogonality*:

$$a\left(e,v\right) = l\left(v\right) - d\left(u_{ref},v\right), \forall v \in X. \tag{3.5}$$

In order to estimate the model error e, we introduce the linear functional $j\left(\cdot\right) : X \to \mathbb{R}$; this functional will be the source term for the dual reference problem

$$\text{find } z_{ref} \in X : \quad a_{ref}\left(v,z_{ref}\right) = j\left(v\right), \qquad \forall v \in X, \tag{3.6}$$

and for his corresponding reduced problem

$$\text{find } z \in X : \quad a\left(v,z\right) = j\left(v\right), \qquad \forall v \in X. \tag{3.7}$$

Considering $v = e$ in the dual problems (3.6) and (3.7), and applying the (3.5), we can write the following *representation formula for the modeling error*:

$$j\left(e\right) = l\left(z_{ref}\right) - d\left(u,z_{ref}\right) \tag{3.8}$$

$$= l\left(z\right) - d\left(u_{ref},z\right). \tag{3.9}$$

This *formula* tells us that, thanks to the dual solution, it is possible to represent the modeling error by means of the terms $d(\cdot,\cdot)$ and $l(\cdot)$, that is the complex part of the model.

Remark 3.1.2. Notice that we are employing the model reduction in order to not build the expensive or complicated terms $d(\cdot,\cdot)$ and $l(\cdot)$; therefore, computing the error through these operators may look a not so good strategy.
For this reason, we assume that the overhead for solving the full variational problem (3.1) rather than the reduced one (3.4) is much higher than a single evaluation of $d(\cdot,\cdot)$ and $l(\cdot)$. This assumption is reasonable if we are using iterative methods, where we would compute those operators multiple times for every residual evaluation.

Unfortunately, (3.8) tells us also that the error depends on the solution of a reference problem (the dual or the primal one, depending on the version used): this is not feasible, therefore we must find an approximated version of the *representation formula*. In the following section we derive a *representation formula for the modeling error* depending only on reduced solutions.

3.1.1 Approximate error representation formula

Let us suppose that $l(\cdot) \equiv 0$; the following considerations will apply similarly to both the operators.
Our goal is to separate the contribution of the *representation formula* (3.8) depending on the reduced solutions u and z by the contribution depending on the reference solutions u_{ref} and z_{ref}. The functional $j(\cdot)$ applied to the error e can be written as:

$$j(e) = -d(u, z_{ref}) = -d(u, z) - d(u, z_{ref} - z). \tag{3.10}$$

Let us suppose that $d(\cdot,\cdot)$ is continuous; therefore, with $\|\cdot\|$ denoting the usual norms on X and $X \times X$, it holds

$$|d(u, z)| \leq \|d\| \|u\| \, \|z\|. \tag{3.11}$$

If the mapping $A : X \to X'$, $A(u) = a(u, \cdot)$ is bijective, the adjoint A^* is bijective too. Using the open mapping theorem, there exist a constant $\alpha > 0$ such that:

$$\|z\| \leq \alpha \sup_{v \in X} \frac{a(v, z)}{\|v\|}. \tag{3.12}$$

The last result we need is the *dual perturbed Galerkin orthogonality*: proceeding as in (3.5), we obtain

$$a(v, z_{ref} - z) = -d(v, z_{ref}), \quad \forall v \in X. \tag{3.13}$$

Combining the (3.12) with (3.13), we deduce the *a priori* estimate:

$$\|z_{ref} - z\| \leq \alpha \sup_{v \in X} \frac{a(v, z_{ref} - z)}{\|v\|} \leq \alpha \sup_{v \in X} \frac{d(v, z_{ref})}{\|v\|} \leq \alpha \|d\| \|z_{ref}\|. \tag{3.14}$$

Finally, employing the continuity of $d(\cdot,\cdot)$, we find:

$$|d(u, z_{ref} - z)| \leq \|d\| \|u\| \|z_{ref} - z\| \leq \alpha \|d\|^2 \|u\| \|z_{ref}\|. \tag{3.15}$$

In conclusion, the representation (3.10) can be bounded estimated as:

$$|j(e)| \leq \|d\| \|u\| \|z\| + \alpha \|d\|^2 \|u\| \|z_{ref}\|. \tag{3.16}$$

We achieved our goal to separate the contributions derived by the reduced and the reference solutions. Furthermore, if $\|d\| \to 0$, the contribution of the reference solutions vanishes at the first order.
Repeating the same estimate for $l(\cdot)$, at first order in $\|d\|$ and $\|l\|$, the error can be approximated as:

$$j(e) \approx l(z) - d(u, z). \tag{3.17}$$

The use of the *approximated representation formula for the modeling error* is justified if $\|d\| \to 0$ and $\|l\| \to 0$. From assumption A0, one can look for a dependency between the norms $\|d\|$, $\|l\|$, and the small parameter ϵ.
The aim of the next section is to verify if the norms of the operators $d(\cdot,\cdot)$ and $l(\cdot)$ arising from each step, namely A1, A2, and A3, vanish as $\epsilon \to 0$.

Remark 3.1.3. The well-posedness analysis of sections 2.2 and 3.2 is based on the linearity of the functional $j(\cdot)$. This request limits the choice of the functional; as we will discuss further in Chapter 4, standard choices are, for example, the mean value in a region of the domain or the mean gradient on a boundary. One may be interested in using this method to compute L^2 norm of the error; this can be done from a theoretical point of view, defining $j(v) := (e, v)$, but obviously not in practice, where this is possible only defining the non-linear operator $j(v) := \|v\|_{L^2}$. Although the non-linear theory is not available for our specific problem, the dual-based analysis of the modeling error in a generic problem is extended to the non-linear case.
We briefly present here the main results for the non-linear case; we refer the interested reader to [7].
We define the forms $a(u)(\cdot)$ and $d(u)(\cdot)$ to be linear in the second argument; though, they may be not linear in u. We assume the operator $l(\cdot)$ to be zero. The reference and reduced primal problems are:

$$\begin{aligned} \text{find } u_{ref} \in X: &\quad a\left(u_{ref}\right)(v) + d\left(u_{ref}\right)(v) = (f, v) &\qquad \forall v \in X, \qquad (3.18)\\ \text{find } u \in X: &\quad a(u)(v) = (f, v) &\qquad \forall v \in X. \qquad (3.19)\end{aligned}$$

Let us define the first derivative of $a(u)(\cdot)$ and $d(u)(\cdot)$, denoted as $a'(u)(\cdot,\cdot)$ and $d'(u)(\cdot,\cdot)$, with:

$$a'(u)(w, v) = \lim_{\epsilon \to 0} \left\{ a(u + \epsilon w)(v) - a(u)(v) \right\}. \tag{3.20}$$

The first derivative of the nonlinear output functional $j(u)$ is

$$j'(v)(w) = \lim_{\epsilon \to 0} \left\{ j(v + \epsilon w) - j(v) \right\}. \tag{3.21}$$

The reference and reduced dual problems are:

$$\begin{aligned} \text{find } z_{ref} \in X: &\quad a'\left(u_{ref}\right)(v, z) + d'\left(u_{ref}\right)(v, z) = j'\left(u_{ref}\right)(v), &\quad \forall v \in X, \quad (3.22)\\ \text{find } z \in X: &\quad a'(u)(v, z) = j'(u)(v), &\quad \forall v \in X. \quad (3.23)\end{aligned}$$

The *representation formula for modeling error* corresponding to problems (3.18) and (3.22) is given by the following result:

Theorem 3.1.1. *If $a(u)(\cdot)$, $d(u)(\cdot)$ and the functional $j(u)$ are sufficiently differentiable with respect to u, then it holds that:*

$$j(u_{ref}) - j(u) = -\,d(u)(z) \tag{3.24}$$

$$-\frac{1}{2}\left\{d(u)(z_{ref} - z) + d'(u)(u_{ref} - u, z) - R\right\}, \tag{3.25}$$

where R is cubic in the error $e_{u,z} := \{u_{ref} - u, z_{ref} - z\}$.

By neglecting the higher order terms, we deduce the *approximated non-linear representation formula*:

$$j(u_{ref}) - j(u) \approx -d(u)(z). \tag{3.26}$$

In conclusion, notice that:

- if $a(u)(v) = a(u, v)$ is bilinear, then $a'(u)(w, v) = a(w, v)$;
- if $j(v)$ is linear, then $j'(v)(w) = j(w)$.

This confirms that (3.1.1) gives (3.8) in the linear case.

3.2 Modeling error analysis

In Section 3.1 we described the general theory for deriving the modeling error. In particular we showed the *reprensentation formula for modeling error* (3.8) depending on the forms $d(\cdot,\cdot)$ and $l(\cdot)$.
In this Section we aim to derive those operators for our specific problem. In particular, in Sections 2.1.3, 2.1.4 we described the three assumptions A1, A2 and A3 at the basis of our model reduction: we now want to characterize the complex parts of the equations we neglected after each assumption, namely $d^{(1)}(\cdot,\cdot)$, $d^{(2)}(\cdot,\cdot)$, $d^{(3)}(\cdot,\cdot)$, and $l^{(1)}(\cdot)$, $l^{(2)}(\cdot)$, $l^{(3)}(\cdot)$.
Furthermore, we will analyze the following properties for each case; in the following, $\|\cdot\|_\star$ and $\|\cdot\|_\circ$ are suitable norms defined on case by case.

Property 3.2.1. *There exist constants $\|d\|_{\star\circ}$, $\|l\|_\circ$ such that*

$$d(u, z_{\mathrm{ref}}) \le \|d\|_{\star\circ}\|u\|_\star\,\|z_{\mathrm{ref}}\|_\circ, \quad l(z_{\mathrm{ref}}) \le \|l\|_\circ\|z_{\mathrm{ref}}\|_\circ\,. \tag{3.27}$$

Furthermore, the constants $\|d\|_{\star\circ}$ and $\|l\|_\circ$ asymptotically vanish with $\epsilon \to 0$.

Property 3.2.2. *There exist constants $\|a\|_\star$ and $\|a_{\mathrm{ref}}\|_\circ$, uniformly bounded with ϵ, such that*

$$\|u\|_\star \le \|a\|_\star\|\mathcal{F}\|_{X'}\,, \quad \|z_{\mathrm{ref}}\|_\circ \le \|a_{\mathrm{ref}}\|_\circ\|j\|_{X'}\,. \tag{3.28}$$

Property 3.2.1 generalizes the continuity of the operators $d(\cdot,\cdot)$ and $l(\cdot)$, requiring their boundedness under suitable norms, which may vary on case by case. Besides, it requests that the norms $\|d\|_{\star\circ}$, $\|l\|_{\circ}$ asymptotically vanish as the diameter of Σ decrease to zero; as explained in Section 3.1 this is a fundamental property in order to use the *approximated representation formula* (3.17) instead of the complete but non computable one (3.8).
Property 3.2.2 provides stability estimates for the solutions of the reduced primal and reference dual problems. This property let us derive an *a priori* estimate for the L^2 norm of the modeling error: in the case of $j(v) = (e, v)_{L^2}$, combining Properties 3.2.1 and 3.2.2, we find:

$$\begin{aligned}\|e\|^2_{L^2} = j(e) = l(z_{\text{ref}}) - d(u, z_{\text{ref}}) &\le \|l\|_{\circ}\|z_{\text{ref}}\|_{\circ} + \|d\|_{\star\circ}\|u\|_{\star}\|z_{\text{ref}}\|_{\circ} \\ &\le \left(\|l\|_{\circ} + \|d\|_{\star\circ}\|a\|_{\star}\|\mathcal{F}\|_{X'}\right)\|a_{\text{ref}}\|_{\circ}\|e\|_{L^2}\,.\end{aligned}$$

3.2.1 Useful results

Before proceeding, we introduce some results that will be useful in what follows.

Lemma 6 (Stekloff inequality [32])**.** *Let $\partial\mathcal{D}$ be an ellipse or a rhombus. For any function $v \in H^1(\mathcal{D})$ such that*

$$\int_{\partial\mathcal{D}} v\,d\gamma = 0\,,$$

there exists a constant C such that

$$\int_{\partial\mathcal{D}} v^2 d\gamma \le C\int_{\mathcal{D}} (\nabla v)^2 d\sigma\,. \tag{3.29}$$

More precisely if $\partial\mathcal{D}$ is an ellipse $(x_1/a_1)^2 + (x_2/a_2)^2 = 1$ then $C \le \max[a_1, a_2]$. If $\partial\mathcal{D}$ is a rhombus $|x_1/a_1| + |x_2/a_2| = 1$, then $C \le (a_1^2 + a_2^2)^{\frac{1}{2}}/\min[a_1/a_2, a_2/a_1]$.

From the previous lemma combined with assumption A0, we conclude that there exists C_S, independent of ϵ and with $C \le C_S\epsilon$, such that (3.29) holds true with constant C_S.

Lemma 7 (Poincaré-Wirtinger inequality [41])**.** *Let $\mathcal{D} \in \mathbb{R}^2$ be a convex domain of diameter $\mathrm{D}(\mathcal{D})$. For any function $v \in H^1(\mathcal{D})$ such that*

$$\int_{\mathcal{D}} v\,d\sigma = 0\,,$$

we have,

$$\int_{\mathcal{D}} v^2 d\sigma \le \frac{\mathrm{D}^2}{\pi^2}\int_{\mathcal{D}} (\nabla v)^2 d\sigma\,. \tag{3.30}$$

Lemma 8 (Extension theorem for domains having small geometric details [48])**.** *There exists an extension operator $\mathcal{E}_\Sigma$ from $H^1(\Omega_\oplus)$ to $H^1(\Sigma)$ such that*

$$\|\mathcal{E}_\Sigma u\|_{H^1(\Sigma)} \leq C_E \|u\|_{H^1(\Omega_\oplus)} \qquad \forall u \in H^1(\Omega_\oplus)$$

where the constant C_E is independent of $\Sigma = \Omega \setminus \overline{\Omega}_\oplus$.

Lemma 9 (Poincaré-Friedrichs inequality [8, 41])**.** *Let $\mathcal{D} \subset \mathbb{R}^2$ be a bounded domain of diameter $\mathrm{D}(\mathcal{D})$. For any $v \in H^1(\mathcal{D})$, there exists a positive constant, $C_{PF}(\mathcal{D})$, s.t.*

$$\|v\|^2_{L^2(\mathcal{D})} \leq C_{PF}(\mathcal{D}) \left(\|\nabla v\|^2_{L^2(\mathcal{D})} + \|v\|^2_{L^2(\partial\mathcal{D})} \right)$$

and $C_{PF}(\mathcal{D})$ tends to 0 for $\mathrm{D} \to 0$.

Proof. Integrating by parts we have:

$$\|v\|^2_{L^2(\mathcal{D})} = \int_{\mathcal{D}} v^2 \, d\sigma = \frac{1}{2} \sum_{i=1}^{2} \int_{\mathcal{D}} v^2 \cdot 1 = -\frac{1}{2} \sum_{i=1}^{2} \int_{\mathcal{D}} 2v \frac{\partial v}{\partial x_i} x_i \, d\sigma + \frac{1}{2} \sum_{i=1}^{2} \int_{\partial\mathcal{D}} v^2 x_i \nu_i \, d\gamma,$$

where ν_i is the $i-$th component of the outward unit surface normal to $\mathcal{D}$. Then, using Schwarz and Young inequalities we obtain

$$\begin{aligned}
\|v\|^2_{L^2(\mathcal{D})} &\leq \frac{1}{2} \sum_{i=1}^{2} 2\mathrm{D} \|v\|_{L^2(\mathcal{D})} \left\| \frac{\partial v}{\partial x_i} \right\|_{L^2(\mathcal{D})} + \frac{1}{2} \sum_{i=1}^{2} \mathrm{D} \|v\|^2_{L^2(\partial\mathcal{D})} \\
&\leq \frac{1}{2} \|v\|^2_{L^2(\mathcal{D})} + \frac{1}{2} \sum_{i=1}^{2} 2\mathrm{D}^2 \left\| \frac{\partial v}{\partial x_i} \right\|^2_{L^2(\mathcal{D})} + \mathrm{D} \|v\|^2_{L^2(\partial\mathcal{D})} \\
&\leq \frac{1}{2} \|v\|^2_{L^2(\mathcal{D})} + \mathrm{D}^2 \|\nabla v\|^2_{L^2(\mathcal{D})} + \mathrm{D} \|v\|^2_{L^2(\partial\mathcal{D})}
\end{aligned}$$

from which it follows that

$$\|v\|^2_{L^2(\mathcal{D})} \leq \max\left(2\mathrm{D}^2, 2\mathrm{D}\right) \left(\|\nabla v\|^2_{L^2(\mathcal{D})} + \|v\|^2_{L^2(\partial\mathcal{D})} \right).$$

Thus, $C_{PF}(\mathcal{D}) = \max(4\mathrm{D}^2, 2\mathrm{D})$ and it tends to 0 when D tends to 0. □

Lemma 10. *From Lemma 9, it follows that for any $v \in H^1(\Sigma)$, there exists a positive constant, $C_{PF}(\Sigma)$, s.t.*

$$\|v\|^2_{L^2(\Sigma)} \leq C_{PF}(\Sigma) \left(\|\nabla v\|^2_{L^2(\Sigma)} + \|v\|^2_{L^2(\Gamma)} \right) \tag{3.31}$$

and $C_{PF}(\Sigma)$ tends to 0 for $\epsilon \to 0$.

3.2.2 Analysis of modeling error of the one dimensional problem (Assumption A1)

We want to characterize the modeling error of replacing the equation (2.2b) with (2.4). Let $u_\oplus \in H^1_{\partial\Omega}(\Omega_\oplus)$ and $g \in H^1(\Sigma)$ be suitable functions. We consider the reference problem on the cylinder Σ and the reduced problem on his centerline Λ, namely:

$$\begin{aligned}
&\text{find } u_\ominus \in H^1(\Sigma) : \\
&(\nabla u_\ominus, \nabla v)_\Sigma + (\kappa u_\ominus, v)_\Gamma = (\kappa u_\oplus, v)_\Gamma + (g, v)_\Sigma,\ \forall v \in H^1(\Sigma), \qquad (3.32a)\\
&\text{find } U \in H^1(\Lambda) : \\
&(d_s U, d_s V)_{\Lambda,\mathcal{D}} + (\kappa U, V)_{\Lambda,\partial\mathcal{D}} = (\kappa \overline{u}_\oplus, V)_{\Lambda,\partial\mathcal{D}} + (\overline{\overline{g}}, V)_{\Lambda,\mathcal{D}},\ \forall v \in H^1(\Lambda)\,. \qquad (3.32b)
\end{aligned}$$

We define the modeling error $e^{(1)}$ as the difference between $u_\ominus$ and U.
To this purpose, we exploit the cylindrical configuration of the domain Σ and its local coordinate system. In particular, we uniformly extend $U(s)$ on every cross section $\mathcal{D}(s)$ of the cylinder and with abuse of notation we still denote the extended function with U. Thanks to the regularity of U on Λ, we have that the extension on Σ belongs to $H^1(\Sigma)$. Referring to the general notation introduced in the previous section we have that the solutions of the reference and reduced models are $u^{(1)}_{\text{ref}} = u_\ominus$ and $u^{(1)} = U$ both in the space $X = H^1(\Sigma)$, since we identify U on Λ and its uniform extension on Σ. As a result, the modeling error is $e^{(1)} = u^{(1)}_{\text{ref}} - u^{(1)} = u_\ominus - U \in H^1(\Sigma)$. Let us derive the operators $d^{(1)}(u, v) = a^{(1)}_{\text{ref}}(u, v) - a^{(1)}(u, v)$ and $l^{(1)}(v) = \mathcal{F}^{(1)}_{\text{ref}}(v) - \mathcal{F}^{(1)}(v)$. The bilinear forms of the reference and reduced problems are

$$\begin{aligned}
a^{(1)}_{\text{ref}}(u, v) &= (\nabla u, \nabla v)_\Sigma + (\kappa u, v)_\Gamma\,,\\
a^{(1)}(u, v) &= (d_s\overline{\overline{u}}, d_s\overline{\overline{v}})_{\Lambda,\mathcal{D}} + (\kappa\overline{u}, \overline{v})_{\Lambda,\partial\mathcal{D}}\,,
\end{aligned}$$

while the linear forms of the reference and reduced problems are

$$\begin{aligned}
\mathcal{F}^{(1)}_{\text{ref}}(v) &= (\kappa u_\oplus, v)_\Gamma + (g, v)_\Sigma\,,\\
\mathcal{F}^{(1)}(v) &= (\kappa\overline{u}_\oplus, v)_{\Lambda,\partial\mathcal{D}} + (\overline{\overline{g}}, v)_{\Lambda,\mathcal{D}}\,.
\end{aligned}$$

In order to quantify their difference, we recall the expression of the gradient in cylindrical coordinates for a generic function of $H^1(\Sigma)$: $\nabla(\cdot) = [d_s(\cdot), \partial_r(\cdot), r^{-1}\partial_\theta(\cdot)]'$. Using these expression:

$$\begin{aligned}
d^{(1)}(u, v) =& ((\mathcal{I} - \overline{\overline{(\cdot)}})d_s u, d_s v)_\Sigma + (\kappa(\mathcal{I} - \overline{(\cdot)})u, v)_\Gamma \\
&+ (\partial_r u, \partial_r v)_\Sigma + (r^{-1}\partial_\theta u, r^{-1}\partial_\theta v)_\Sigma\,, \qquad (3.33a)\\
l^{(1)}(v) =& ((\mathcal{I} - \overline{\overline{(\cdot)}})g, v)_\Sigma + (\kappa(\mathcal{I} - \overline{(\cdot)})u_\oplus, v)_\Gamma\,. \qquad (3.33b)
\end{aligned}$$

We now aim to prove properties 3.2.1 and 3.2.2 for the operators d, l and a, a_{ref} respectively.

Lemma 11 (Property 3.2.1 for $d^{(1)}$)**.** *The operator $d^{(1)}(\cdot,\cdot)$ satisfies Property 3.2.1 with $d^{(1)}(U,v)=0$ for any $v\in H^1(\Sigma)$.*

Proof. Let $U\in H^1(\Sigma)$ be the extension to Σ of the reduced problem on Λ. We observe that $d(U,v)=0$ for any $v\in H^1(\Sigma)$, because $\partial_r U=\partial_\theta u=0$ and $(\mathcal{I}-\overline{\overline{(\cdot)}})d_s U=0$. ☐

Lemma 12 (Property 3.2.1 for $l^{(1)}$)**.** *The operator $l^{(1)}(\cdot)$ satisfies Property 3.2.1 with the norm $\|\cdot\|_\circ^2=\|\cdot\|^2_{L^2(\Sigma)}+\|\cdot\|^2_{L^2(\Gamma)}$ and with the constant*

$$\|l^{(1)}\|_\circ=\frac{\epsilon}{\pi}\|g\|_{H^1(\Sigma)}+\|\kappa\|_{L^\infty}C_E\sqrt{C_S\epsilon}\|u_\oplus\|_{H^1(\Omega_\oplus)}\,.$$

Proof. For the upper bound of the right hand side, without loss of generality we assume that $g\in H^1(\Sigma),\ u_\oplus\in H^1(\Omega_\oplus)$. Then, $(\mathcal{I}-\overline{\overline{(\cdot)}})g$ satisfies the assumptions of the Poincaré-Wirtinger inequality, which allows us to conclude that

$$\begin{aligned}((\mathcal{I}-\overline{\overline{(\cdot)}})g,v)_\Sigma &\le \Big(\int_\Sigma((\mathcal{I}-\overline{\overline{(\cdot)}})g)^2\Big)^{\frac12}\Big(\int_\Sigma v^2\Big)^{\frac12}=\Big(\int_\Lambda\int_{\mathcal{D}(s)}((\mathcal{I}-\overline{\overline{(\cdot)}})g)^2d\sigma ds\Big)^{\frac12}\|v\|_{L^2(\Sigma)}\\ &\le\Big(\int_\Lambda\frac{D^2}{\pi^2}\int_{\mathcal{D}(s)}(\nabla_{\mathcal{D}}g)^2d\sigma ds\Big)^{\frac12}\|v\|_{L^2(\Sigma)}\le\frac{\epsilon}{\pi}\|g\|_{H^1(\Sigma)}\|v\|_\circ\,,\end{aligned}$$

where, from now on $\nabla_{\mathcal{D}}(\cdot)=[\partial_r(\cdot),r^{-1}\partial_\theta(\cdot)]'$ denotes the gradient in the local coordinate system of the disc $\mathcal{D}$. For the second term of l we use the Stekloff inequality,

$$\begin{aligned}(\kappa(\mathcal{I}-\overline{(\cdot)})u_\oplus,v)_\Gamma&\le\|\kappa\|_{L^\infty}\Big(\int_\Gamma(\mathcal{I}-\overline{(\cdot)})u_\oplus)^2\Big)^{\frac12}\Big(\int_\Gamma v^2\Big)^{\frac12}\\ &\le\|\kappa\|_{L^\infty}\sqrt{C_S\epsilon}\Big(\int_\Lambda\int_{\mathcal{D}(s)}(\nabla_{\mathcal{D}}\mathcal{E}_\Sigma u_\oplus)^2d\sigma ds\Big)^{\frac12}\|v\|_{L^2(\Gamma)}\\ &\le\|\kappa\|_{L^\infty}\sqrt{C_S\epsilon}\|\mathcal{E}_\Sigma u_\oplus\|_{H^1(\Sigma)}\|v\|_{L^2(\Gamma)}\le\|\kappa\|_{L^\infty}C_E\sqrt{C_S\epsilon}\|u_\oplus\|_{H^1(\Omega_\oplus)}\|v\|_\circ\,,\end{aligned}$$

where $\mathcal{E}_\Sigma$ denotes the extension operator of Lemma 8. The previous inequalities show that (3.27) is verified for this component of the modeling error with the constant,

$$l^{(1)}(v)\le\Big(\frac{\epsilon}{\pi}\|g\|_{H^1(\Sigma)}+\|\kappa\|_{L^\infty}C_E\sqrt{C_S\epsilon}\|u_\oplus\|_{H^1(\Omega_\oplus)}\Big)\|v\|_\circ,\ \forall v\in H^1(\Sigma)\,.$$

☐

The verification of (3.28) in this case consists of showing that problems (3.32a) and (3.32b) are stable in the norm $\|\cdot\|_\circ$ with constants uniformly bounded with respect to ϵ. More precisely, since $d(U, z_{\text{ref}}) = 0$, only the second of (3.28), namely the stability of the reference dual problem, is meaningful in this case.
For this reason, we define the reference dual problem

$$\text{find } z^{(1)}_{\text{ref}} \in H^1(\Sigma) : (\nabla v, \nabla z^{(1)}_{\text{ref}})_\Sigma + (\kappa v, z^{(1)}_{\text{ref}})_\Gamma = j^{(1)}(v),\ \forall v \in H^1(\Sigma)\,. \tag{3.34}$$

There are different choices for the functional $j^{(1)}(\cdot) : H^1(\Sigma) \to \mathbb{R}$. For example,

$$\begin{aligned}
&j^{(1)}(v) = j^{(1)}_\Sigma(v) = \int_\Sigma v\, d\Sigma,\\
&\text{or}\\
&j^{(1)}(v) = j^{(3)}_\Gamma(v) = \int_\Gamma \nabla v \cdot \boldsymbol{n}\, d\gamma,\\
&\text{or}\\
&j^{(1)}(v) = j^{(1)}_e(v) = (e^{(1)}, v)_\Sigma.
\end{aligned} \tag{3.35}$$

We now proceed to prove the stability of the dual solution in the particular case of $j^{(1)}(v) = j^{(1)}_e(v)$.

Lemma 13 (Property 3.2.2 for $z^{(1)}_{\text{ref}}$)**.** *The reference dual problem* (3.34) *with* $j^{(1)}(v) = j^{(1)}_e(v)$ *satisfies the following stability estimate with the norm* $\|\cdot\|_\circ = \|\cdot\|_{L^2(\Sigma)} + \|\cdot\|_{L^2(\Gamma)}$

$$\|z^{(1)}_{\text{ref}}\|_\circ \le \frac{2}{\min\left(2\, C^{-1}_{PF}(\Sigma),\ C^{-1}_{PF}(\Sigma)\, \kappa_{min},\ \kappa_{min}\right)} \|e^{(1)}\|_{L^2(\Sigma)}\,.$$

As a result, Property 3.2.2 is satisfied with the following constant,

$$\|a^{(1)}_{\text{ref}}\|_\circ = \frac{2}{\min\left(2\, C^{-1}_{PF}(\Sigma),\ C^{-1}_{PF}(\Sigma)\, \kappa_{min},\ \kappa_{min}\right)}\,.$$

Proof. Owing to Poincaré -Friedrichs inequality (3.31) we have,

$$\begin{aligned}
a_{\text{ref}}(v,v) = (\nabla v, \nabla v)_\Sigma + (\kappa v, v)_\Gamma &\ge \min\left(1, \frac{1}{2}\kappa_{min}\right) C^{-1}_{PF}(\Sigma)\|v\|^2_{L^2(\Sigma)} + \frac{1}{2}\kappa_{min}\|v\|^2_{L^2(\Gamma)},\\
&\ge \frac{1}{2}\min\left(2\, C^{-1}_{PF},\ C^{-1}_{PF}(\Sigma)\, \kappa_{min},\ \kappa_{min}\right)\|v\|^2_\circ,\ \forall v \in H^1(\Sigma)\,.
\end{aligned}$$

As a result of that the second of (3.28) is proved. Indeed:

$$\begin{aligned}
\frac{1}{2}\min\left(2\, C^{-1}_{PF},\ C^{-1}_{PF}(\Sigma)\, \kappa_{min},\ \kappa_{min}\right)\|z^{(1)}_{\text{ref}}\|^2_\circ &\le a_{\text{ref}}(z^{(1)}_{\text{ref}}, z^{(1)}_{\text{ref}}) = (e^{(1)}, z^{(1)}_{\text{ref}})_\Sigma\\
&\le \|e^{(1)}\|_{L^2(\Sigma)}\|z^{(1)}_{\text{ref}}\|_{L^2(\Sigma)} \le \|e^{(1)}\|_{L^2(\Sigma)}\|z^{(1)}_{\text{ref}}\|_\circ\,.
\end{aligned}$$

from which it follows that

$$\|a^{(1)}_{\text{ref}}\|_\circ = \frac{2}{\min\left(2\,C^{-1}_{PF}(\Sigma),\, C^{-1}_{PF}(\Sigma)\,\kappa_{min},\, \kappa_{min}\right)}$$

and for Lemma 10 $\|a^{(1)}_{\text{ref}}\|_\circ$ is bounded for $\epsilon \to 0$. □

3.2.3 Analysis of modeling error relative to the domain (Assumption A2)

We want to characterize the modeling error of identifying the domain $\Omega_\oplus$ with the entire domain Ω. Let $U \in H^1(\Sigma)$ and $f \in H^1(\Omega_\oplus)$ be suitable functions; let us denote by $\mathcal{E}_\Sigma)f$ the extension of f to $f \in H^1(\Sigma)$. We consider the reference problem on the domain $\Omega_\oplus$ and the reduced problem on the entire domain Ω, namely:

$$\begin{aligned}
&\text{find } u_\oplus \in H^1_{\partial\Omega}(\Omega_\oplus) : \\
&(\nabla u_\oplus, \nabla v)_{\Omega_\oplus} + (\kappa u_\oplus, v)_\Gamma = (f, v)_{\Omega_\oplus} + (\kappa U, v)_\Gamma,\ \forall v \in H^1_{\partial\Omega}(\Omega_\oplus), && \text{(3.36a)}\\
&\text{find } u^{(2)} \in H^1_0(\Omega) : \\
&(\nabla u^{(2)}, \nabla v)_\Omega + (\kappa u^{(2)}, v)_\Gamma = ((\mathcal{I}_{\Omega_\oplus} + \mathcal{E}_\Sigma)f, v)_\Omega + (\kappa U, v)_\Gamma,\ \forall v \in H^1_0(\Omega)\,, && \text{(3.36b)}
\end{aligned}$$

where $H^1_{\partial\Omega}(\Omega_\oplus)$ denotes the space of functions of $H^1(\Omega_\oplus)$ with null trace on $\partial\Omega$. More precisely, we extend the solution of (3.36a) from $\Omega_\oplus$ to Ω, with the extension operator $\mathcal{E}_\Sigma$ which takes the function $u_\oplus$ on $\Omega_\oplus$ and extends it to the interior of the domain. Then, the reference solution relative to assumption A2 is $u^{(2)}_{\text{ref}} = (\mathcal{I}_{\Omega_\oplus} + \mathcal{E}_\Sigma)u_\oplus$, belonging to the space $X^{(2)} = H^1_0(\Omega)$. The solution of the reduced problem is instead $u^{(2)} \in H^1_0(\Omega)$. The functional space where we set the modeling error is $H^1_0(\Omega)$ and error is $e^{(2)} = u^{(2)}_{\text{ref}} - u^{(2)} = (\mathcal{I}_{\Omega_\oplus} + \mathcal{E}_\Sigma)u_\oplus - u^{(2)} \in H^1_0(\Omega)$. Let us derive the operators $d^{(2)}(u, v) = a^{(2)}_{\text{ref}}(u, v) - a^{(2)}(u, v)$ and $l^{(2)}(v) = \mathcal{F}^{(2)}_{\text{ref}}(v) - \mathcal{F}^{(2)}(v)$. The bilinear forms of the reference and reduced problems are

$$\begin{aligned}
a^{(2)}_{\text{ref}}(u, v) &= (\nabla u, \nabla v)_{\Omega_\oplus} + (\kappa u, v)_\Gamma\,,\\
a^{(2)}(u, v) &= (\nabla u, \nabla v)_\Omega + (\kappa u, v)_\Gamma\,,
\end{aligned}$$

while the linear forms of the reference and reduced problems are

$$\begin{aligned}
\mathcal{F}^{(2)}_{\text{ref}}(v) &= (f, v)_{\Omega_\oplus} + (\kappa U, v)_\Gamma\,,\\
\mathcal{F}^{(2)}(v) &= ((\mathcal{I}_{\Omega_\oplus} + \mathcal{E}_\Sigma)f, v)_\Omega + (\kappa U, v)_\Gamma\,.
\end{aligned}$$

Then, subtracting (3.36b) from (3.36a), it is straightforward to determine the expression of the difference operators $d^{(2)}(u,v)$ and $l^{(2)}(v)$,

$$d^{(2)}(u,v) = -(\nabla u, \nabla v)_\Sigma \,, \tag{3.37a}$$

$$l^{(2)}(v) = -(\mathcal{E}_\Sigma f, v)_\Sigma \,. \tag{3.37b}$$

We now aim to prove properties 3.2.1 and 3.2.2 for the operators d, l and a, a_{ref} respectively.

Lemma 14 (Property 3.2.1 for $d^{(2)}$ $l^{(2)}$)**.** *The operators* $d^{(2)}(\cdot,\cdot)$ *and* $l^{(2)}(\cdot)$ *satisfy Property 3.2.1 with the norms* $\|\cdot\|_\star = \|\cdot\|_{H^{\frac{3}{2}-\eta}(\Omega)}$*, fora any* $\eta > 0$*, and* $\|\cdot\|_\circ = \|\cdot\|_{H^1(\Omega_\oplus)}$ *and inequality* (3.27) *is satisfied with constants*

$$\begin{aligned}
\|d^{(2)}\|_{\star\circ} =& C_E(SC_{\mathcal{D}})^{\frac{1-2\eta}{6}}\epsilon^{\frac{1-2\eta}{3}}C(1/2-\eta, 3/(1+\eta), \Omega)\,,\\
\|l^{(2)}\|_\circ =& (1+C_E)C_E(SC_{\mathcal{D}})^{\frac{1}{2}}\epsilon\|f\|_{H^1(\Omega_\oplus)}\,.
\end{aligned}$$

Proof. Let us start with the upper bound for $d^{(2)}(u,v)$. We observe that $d^{(2)}(u,v) \leq \|\nabla u\|_{L^2(\Sigma)}\|\nabla v\|_{L^2(\Sigma)}$. Let us assume that $u \in H^k(\Omega)$ with $1 < k \leq 2$, then $\nabla u \in H^{k-1}(\Omega)$ and for Sobolev embedding theorem we have $\nabla u \in L^{p^*}(\Omega)$ with $p^* = 6/(5-2k)$. Then we apply Hölder inequality and (2.20) as follows,

$$\begin{aligned}
\|\nabla u\|_{L^2(\Sigma)} &= \Big(\int_\Sigma 1(\nabla u)^2 d\Omega\Big)^{\frac{1}{2}} \leq \|1\|^{\frac{1}{2}}_{L^q(\Sigma)}\|(\nabla u)^2\|^{\frac{1}{2}}_{L^r(\Sigma)}\\
&\leq \Big(\int_\Sigma 1\Big)^{\frac{1}{2q}}\Big(\int_\Sigma (\nabla u)^{2r}\Big)^{\frac{1}{2r}} \leq |\Sigma|^{\frac{1}{2q}}\|\nabla u\|_{L^{2r}(\Sigma)} \leq (SC_{\mathcal{D}})^{\frac{1}{2q}}\epsilon^{\frac{1}{q}}\|\nabla u\|_{L^{2r}(\Sigma)}
\end{aligned}$$

where q, r must satisfy $1/q + 1/r = 1$. The maximum exponent for which the previous inequality holds true is $p^* = 2r = 6/(5-2k)$. Then, $r = 3/(5-2k)$ and $1/q = 2(k-1)/3$. Denoting with $C(k-1, p^*, \Omega)$ the Sobolev constant of the embedding of $H^{k-1}(\Omega)$ in $L^{p^*}(\Omega)$, we have

$$\begin{aligned}
\|\nabla u\|_{L^2(\Sigma)} &\leq (SC_{\mathcal{D}})^{\frac{1}{2q}}\epsilon^{\frac{1}{q}}\|\nabla u\|_{L^{p^*}(\Sigma)} \leq (SC_{\mathcal{D}})^{\frac{1}{2q}}\epsilon^{\frac{1}{q}}\|\nabla u\|_{L^{p^*}(\Omega)}\\
&\leq (SC_{\mathcal{D}})^{\frac{1}{2q}}\epsilon^{\frac{1}{q}}C(k-1, p^*, \Omega)\|\nabla u\|_{H^{k-1}(\Omega)}\\
&\leq (SC_{\mathcal{D}})^{\frac{1}{2q}}\epsilon^{\frac{1}{q}}C(k-1, p^*, \Omega)\|u\|_{H^k(\Omega)}.
\end{aligned}$$

Being $u^{(2)} \in H^{\frac{3}{2}-\eta}(\Omega)$ and $z^{(2)}_{\mathrm{ref}} \in H^1_{\partial\Omega}(\Omega_\oplus)$, we obtain,

$$\begin{aligned}
d(u^{(2)},&(\mathcal{I}_{\Omega_\oplus} + \mathcal{E}_\Sigma)z_{\mathrm{ref}})\\
&\leq C_E(SC_{\mathcal{D}})^{\frac{1-2\eta}{6}}\epsilon^{\frac{1-2\eta}{3}}C\left(1/2-\eta, 3/(1+\eta), \Omega\right)\|u^{(2)}\|_{H^{\frac{3}{2}-\eta}(\Omega)}\|z_{\mathrm{ref}}\|_{H^1(\Omega_\oplus)}\,.
\end{aligned}$$

Proceeding similarly, using the minimal regularity requirement $\mathcal{E}_\Sigma f \in H^1(\Sigma)$ combined with Hölder inequality and Sobolev embeddings, namely $H^1(\Sigma) \subset L^6(\Sigma)$, we have

$$\begin{aligned} &l((\mathcal{I}_{\Omega_\oplus} + \mathcal{E}_\Sigma) z_{\text{ref}}) = -(\mathcal{E}_\Sigma f, (\mathcal{I}_{\Omega_\oplus} + \mathcal{E}_\Sigma) z_{\text{ref}})_\Sigma \leq C_E \|\mathcal{E}_\Sigma f\|_{L^2(\Sigma)} \|z_{\text{ref}}\|_{H^1(\Omega_\oplus)} \\ &\leq C_E (S C_{\mathcal{D}})^{\frac{1}{3}} \epsilon^{\frac{2}{3}} \|\mathcal{E}_\Sigma f\|_{L^6(\Sigma)} \|z_{\text{ref}}\|_{H^1(\Omega_\oplus)} \leq C_E (S C_{\mathcal{D}})^{\frac{1}{3}} \epsilon^{\frac{2}{3}} \|(\mathcal{I}_{\Omega_\oplus} + \mathcal{E}_\Sigma) f\|_{L^6(\Omega)} \|z_{\text{ref}}\|_{H^1(\Omega_\oplus)} \\ &\qquad\qquad \leq C_E (1 + C_E) (S C_{\mathcal{D}})^{\frac{1}{3}} \epsilon^{\frac{2}{3}} C(1,6,\Omega) \|f\|_{H^1(\Omega_\oplus)} \|z_{\text{ref}}\|_{H^1(\Omega_\oplus)} \,, \end{aligned}$$

being $C(1,6,\Omega)$ the constant in the Sobolev embedding of $H^1(\Omega)$ in $L^6(\Omega)$. □

Lemma 15 (Property 3.2.2 for $u^{(2)}$)**.** *The solution of the reduced problem* $u^{(2)}$ *satisfies the Property 3.2.2 with the norm* $\|\cdot\|_\star = \|\cdot\|_{H^{\frac{3}{2}-\eta}(\Omega)}$*, for any* $\eta > 0$ *and the inequality* (3.27) *is satisfied with the constant*

$$\|a^{(2)}\|_\star = \frac{C_R \max\left(1 + C_E,\ \sqrt{C_T'(\Gamma, \Omega_\oplus)} \sqrt{C_{\partial\mathcal{D}} \epsilon} \|\kappa\|_{L^\infty}\right)}{1 - C_R \sqrt{C_T'(\Gamma, \Omega_\oplus)} \sqrt{C_T(\Gamma, \Omega_\oplus)} \|\kappa\|_{L^\infty}},$$

which is positive for ϵ *sufficiently small.*

Proof. We notice that (3.36a) in the strong form reads as

$$-\Delta u^{(2)} = \left(\mathcal{I}_{\Omega_\oplus} + \mathcal{E}_\Sigma\right) f - \kappa \left(u^{(2)} - U\right) \delta_\Gamma \ \text{ in } \Omega, \quad u^{(2)} = 0 \text{ on } \partial\Omega.$$

We can apply the same strategy and results of the previous section to prove that $u^{(2)} \in H^{\frac{3}{2}-\eta}(\Omega) \cap H_0^1(\Omega)\, \forall \eta > 0$. Moreover the following inequality holds

$$\|u^{(2)}\|_\star \leq \frac{C_R \max\left(1 + C_E,\ \sqrt{C_T'(\Omega_\oplus)} \sqrt{C_{\partial\mathcal{D}} \epsilon} \|\kappa\|_{L^\infty}\right)}{1 - C_R \sqrt{C_T'(\Gamma, \Omega_\oplus)} \sqrt{C_T(\Gamma, \Omega_\oplus)} \|\kappa\|_{L^\infty}} \left(\|f\|_{H^1(\Omega_\oplus)} + \|U\|_{L^2(\Lambda)}\right), \tag{3.38}$$

therefore

$$\|a^{(2)}\|_\star = \frac{C_R \max\left(1 + C_E,\ \sqrt{C_T'(\Omega_\oplus)} \sqrt{C_{\partial\mathcal{D}} \epsilon} \|\kappa\|_{L^\infty}\right)}{1 - C_R \sqrt{C_T'(\Gamma, \Omega_\oplus)} \sqrt{C_T(\Gamma, \Omega_\oplus)} \|\kappa\|_{L^\infty}}$$

and for Lemma 5, we can choose ϵ suffiently small such that

$$C_R \sqrt{C'{}_T(\Gamma, \Omega_\oplus)} \sqrt{C_T(\Gamma, \Omega_\oplus)} \|\kappa\|_{L^\infty} < 1.$$

□

We define the reference dual problem

$$\text{find } z^{(2)}_{\text{ref}} \in H^1_{\partial\Omega}(\Omega_\oplus) : (\nabla v, \nabla z^{(2)}_{\text{ref}})_{\Omega_\oplus} + (\kappa v, z^{(2)}_{\text{ref}})_\Gamma = j^{(2)}(v),\ \forall v \in H^1_{\partial\Omega}(\Omega_\oplus)\,. \tag{3.39}$$

There are different choices for the functional $j^{(2)}(\cdot) : H^1_0(\Omega) \to \mathbb{R}$. For example,

$$\begin{aligned} & j^{(2)}(v) = j^{(2)}_\Omega(v) = \int_\Omega (\mathcal{I}_{\Omega_\oplus} + \mathcal{E}_\Sigma) v\, d\Omega, \\ & \text{or} \\ & j^{(2)}(v) = j^{(2)}_\Gamma(v) = \int_\Gamma \nabla v \cdot \boldsymbol{n}\, d\gamma, \\ & \text{or} \\ & j^{(2)}(v) = j^{(2)}_e(v) = (e^{(2)}, (\mathcal{I}_{\Omega_\oplus} + \mathcal{E}_\Sigma) v)_\Omega. \end{aligned} \tag{3.40}$$

We now proceed to prove the stability of the dual solution in the particular case of $j^{(2)}(v) = j^{(2)}_e(v)$.

Lemma 16 (Property 3.2.2 for $z^{(2)}_{\text{ref}}$)**.** *The solution of the reference dual problem* (3.39) *with $j^{(2)}(v) = j^{(2)}_e(v)$ satisfies the following inequality,*

$$\begin{aligned} (1 + C_P(\Omega_\oplus))^{-1} \|z^{(2)}_{\text{ref}}\|^2_{\Omega_\oplus} &\le (\nabla z^{(2)}_{\text{ref}}, \nabla z^{(2)}_{\text{ref}})_{\Omega_\oplus} + (\kappa z^{(2)}_{\text{ref}}, z^{(2)}_{\text{ref}})_\Gamma \\ &= (e^{(2)}, (\mathcal{I}_{\Omega_\oplus} + \mathcal{E}_\Sigma) z^{(2)}_{\text{ref}})_\Omega \le (1 + C_E) \|e^{(2)}\|_{L^2(\Omega)} \|z^{(2)}_{\text{ref}}\|_{H^1(\Omega_\oplus)}\,. \end{aligned}$$

As a result, Property 3.2.2 is satisfied with the norm $\|\cdot\|_\circ = \|\cdot\|_{H^1(\Omega_\oplus)}$ and with the constant,

$$\|a^{(2)}_{\text{ref}}\|_\circ = (1 + C_P(\Omega_\oplus))(1 + C_E).$$

3.2.4 Analysis of modeling error relative to the transmission conditions (Assumption A3)

We want to characterize the modeling error of adapting the interface conditions between Σ and $\Omega_\oplus$ to the topological conditions. Let $U \in H^1(\Sigma)$ and $f \in H^1(\Omega_\oplus)$ be suitable functions; let us denote by $\mathcal{E}_\Sigma f$ the extension of f to $f \in H^1(\Sigma)$. We consider the reference problem on the domain $\Omega_\oplus$ and the reduced problem on the entire domain Ω, namely:

$$\begin{aligned} & \text{find } u^{(2)} \in H^1_0(\Omega) : \\ & (\nabla u^{(2)}, \nabla v)_\Omega + (\kappa u^{(2)}, v)_\Gamma = ((\mathcal{I}_{\Omega_\oplus} + \mathcal{E}_\Sigma) f, v)_\Omega + (\kappa U, v)_\Gamma\,,\ \forall v \in H^1_0(\Omega)\,, \end{aligned} \tag{3.41a}$$

$$\begin{aligned} & \text{find } u \in H^1_0(\Omega) : \\ & (\nabla u, \nabla v)_\Omega + (\kappa \overline{u}, \overline{v})_{\Lambda,|\partial\mathcal{D}|} = ((\mathcal{I}_{\Omega_\oplus} + \mathcal{E}_\Sigma) f, v)_\Omega + (\kappa U, \overline{v})_{\Lambda,|\partial\mathcal{D}|}\,,\ \forall v \in H^1_0(\Omega)\,. \end{aligned} \tag{3.41b}$$

Then, the reference solution relative to assumption A3 is achieved by averaging the solution $u_\oplus$ on cross sections of the interface $\partial\mathcal{D}(s)$ before enforcing the interface condition between $u_\oplus$ and U. The error that arises in this process corresponds to neglect the fluctuations of $u_\oplus$ at the interface, as stated in assumption A3. In this case, the reference problem is (3.41a), with solution $u^{(3)}_{\mathrm{ref}} = u^{(2)}$, while the reduced problem is (2.7) so that $u^{(3)} = u$, being u the solution of the final reduced model on Ω. The modeling error is easily defined as $e^{(3)} = u^{(3)}_{\mathrm{ref}} - u^{(3)} = u^{(2)} - u \in H^1_0(\Omega)$ for any $u, v \in H^1_0(\Omega)$. Let us derive the operators $d^{(3)}(u,v) = a^{(3)}_{\mathrm{ref}}(u,v) - a^{(3)}(u,v)$ and $l^{(3)}(v) = \mathcal{F}^{(3)}_{\mathrm{ref}}(v) - \mathcal{F}^{(3)}(v)$. The bilinear forms of the reference and reduced problems are

$$
\begin{aligned}
a^{(3)}_{\mathrm{ref}}(u,v) &= (\nabla u, \nabla v)_\Omega + (\kappa u, v)_\Gamma\,,\\
a^{(3)}(u,v) &= (\nabla u, \nabla v)_\Omega + (\kappa \overline{u}, \overline{v})_{\Lambda,|\partial\mathcal{D}|}\,,
\end{aligned}
$$

while the linear forms of the reference and reduced problems are

$$
\begin{aligned}
\mathcal{F}^{(3)}_{\mathrm{ref}}(v) &= ((\mathcal{I}_{\Omega_\oplus} + \mathcal{E}_\Sigma) f, v)_\Omega + (\kappa U, v)_\Gamma\,,\\
\mathcal{F}^{(3)}(v) &= ((\mathcal{I}_{\Omega_\oplus} + \mathcal{E}_\Sigma) f, v)_\Omega + (\kappa U, \overline{v})_{\Lambda,|\partial\mathcal{D}|}\,.
\end{aligned}
$$

Provided that U is uniformly extended from $H^1(\Lambda)$ to $H^1(\Sigma)$ the difference operators $d^{(3)}(u,v)$ and $l^{(3)}(v)$ between (3.41a) and (2.7) are

$$
d^{(3)}(u,v) = (\kappa u, v)_\Gamma - (\kappa \overline{u}, \overline{v})_{\Lambda,|\partial\mathcal{D}|} = (\kappa(\mathcal{I} - \overline{(\cdot)})u, v)_\Gamma\,, \tag{3.42a}
$$

$$
l^{(3)}(v) = (\kappa U, v)_\Gamma - (\kappa U, \overline{v})_{\Lambda,|\partial\mathcal{D}|} = 0\,. \tag{3.42b}
$$

We now aim to prove properties 3.2.1 and 3.2.2 for the operators d, l and a, a_{ref} respectively.

Lemma 17 (Property 3.2.1 for $d^{(3} l^{(3)}$)**.** *The operators $d^{(3)}(\cdot,\cdot)$ and $l^{(3)}(\cdot)$ satisfy Property 3.2.1 with the norms $\|\cdot\|_\star = \|\cdot\|_\circ = \|\cdot\|_{H^1(\Omega)}$ and with constants*

$$
\|d^{(3)}\|_{\star\circ} = \|\kappa\|_{L^\infty}\sqrt{C_T(\Gamma,\Omega_\oplus)}\sqrt{C_S\epsilon}\,, \quad \|l^{(3)}\|_\circ = 0\,.
$$

Proof. Using Cauchy-Schwarz, Stekloff and trace inequalities, we obtain that

$$
\begin{aligned}
d^{(3)}(u, z_{\mathrm{ref}}) &= (\kappa(\mathcal{I} - \overline{(\cdot)})u, z_{\mathrm{ref}})_\Gamma \le \|\kappa\|_{L^\infty}\sqrt{C_S\epsilon}\left(\int_\Lambda\int_{\mathcal{D}(s)} (\nabla_{\mathcal{D}} u)^2\, d\sigma\, ds\right)^{\frac{1}{2}} \|z_{\mathrm{ref}}\|_{L^2(\Gamma)}\\
&\le \|\kappa\|_{L^\infty}\sqrt{C_T(\Gamma,\Omega_\oplus)}\sqrt{C_S\epsilon}\|\nabla u\|_{L^2(\Sigma)}\|z_{\mathrm{ref}}\|_{L^2(\Omega)} \le \|\kappa\|_{L^\infty}\sqrt{C_T(\Gamma,\Omega_\oplus)}\sqrt{C_S\epsilon}\|u\|_\star\|z_{\mathrm{ref}}\|_\circ
\end{aligned}
$$

□

Lemma 18 (Property 3.2.2 for u)**.** *The solution $u^{(3)}$ of problem* (3.41b) *satisfies the following inequality*

$$\|u^{(3)}\|_{H^1(\Omega)} \leq (1+C_P(\Omega)) \max\left((1+C_E),\, \|\kappa\|_{L^\infty}\sqrt{C_T(\Gamma,\Omega_\oplus)}\sqrt{C_{\partial\mathcal{D}}\epsilon}\right)\left(\|f\|_{H^1(\Omega_\oplus)} + \|U\|_{L^2(\Lambda)}\right).$$

As result, Property 3.2.2 is satisfied with the norm $\|\cdot\|_\star = \|\cdot\|_{H^1(\Omega)}$ and with the constant

$$\|a^{(3)}\|_\star = (1+C_P(\Omega)) \max\left((1+C_E),\, \|\kappa\|_{L^\infty}\sqrt{C_T(\Gamma,\Omega_\oplus)}\sqrt{C_{\partial\mathcal{D}}\epsilon}\right).$$

Proof.

$$\begin{aligned}(1+C_P(\Omega))^{-1}\|u^{(3)}\|^2_{H^1(\Omega)} \leq& \|(\mathcal{I}_{\Omega_\oplus}+\mathcal{E}_\Sigma)f\|_{L^2(\Omega)}\|u^{(3)}\|_{L^2(\Omega)} + \|\kappa\|_{L^\infty}\|U\|_{L^2(\Lambda),|\partial\mathcal{D}|}\|\overline{u}\|_{L^2(\Lambda),|\partial\mathcal{D}|}\\ \leq& (1+C_E)\|f\|_{L^2(\Omega_\oplus)}\|u^{(3)}\|_{H^1(\Omega)}\\ &+ \|\kappa\|_{L^\infty}\sqrt{C_T(\Gamma,\Omega_\oplus)}\sqrt{C_{\partial\mathcal{D}}\epsilon}\|U\|_{L^2(\Lambda)}\|u^{(3)}\|_{H^1(\Omega)},\end{aligned}$$

from which it follows that

$$\|u^{(3)}\|_{H^1(\Omega)} \leq (1+C_P(\Omega)) \max\left(1+C_E,\, \|\kappa\|_{L^\infty}\sqrt{C_T(\Gamma,\Omega_\oplus)}\sqrt{C_{\partial\mathcal{D}}\epsilon}\right)\left(\|f\|_{H^1(\Omega_\oplus)} + \|U\|_{L^2(\Lambda)}\right).$$

Consequently,

$$\|a^{(3)}\|_\star = (1+C_P(\Omega)) \max\left(1+C_E,\, \|\kappa\|_{L^\infty}\sqrt{C_T(\Gamma,\Omega_\oplus)}\sqrt{C_{\partial\mathcal{D}}\epsilon}\right).$$

□

We define the reference dual problem

$$\text{find } z^{(3)}_{\text{ref}} \in H^1_0(\Omega) : (\nabla v, \nabla z^{(3)}_{\text{ref}})_\Omega + (\kappa v, z^{(3)}_{\text{ref}})_\Gamma = j^{(3)}(v),\ \forall v \in H^1(\Omega). \tag{3.43}$$

There are different choices for the functional $j^{(3)}(\cdot) : H^1_0(\Omega) \to \mathbb{R}$. For example,

$$\begin{aligned}&j^{(3)}(v) = j^{(3)}_\Omega(v) = \int_\Omega v\, d\Omega,\\ &\text{or}\\ &j^{(3)}(v) = j^{(3)}_\Gamma(v) = \int_\Gamma \nabla v \cdot \boldsymbol{n}\, d\gamma,\\ &\text{or}\\ &j^{(3)}(v) = j^{(3)}_e(v) = (e^{(3)}, v)_\Omega.\end{aligned} \tag{3.44}$$

We now proceed to prove the stability of the dual solution in the particular case of $j^{(3)}(v) = j^{(3)}_e(v)$.

Lemma 19 (Property 3.2.2 for $z^{(3)}_{\text{ref}}$)**.** *The solution of the reference dual problem* (3.43) *with* $j^{(3)}(v) = j^{(3)}_e(v)$ *satisfies the following inequality*

$$\|z^{(3)}_{\text{ref}}\|_{H^1(\Omega)} \leq (1 + C_P(\Omega))\|e^{(3)}\|_{L^2(\Omega)}.$$

As result, Property 3.2.2 is satisfied with the norm $\|\cdot\|_\circ = \|\cdot\|_{H^1(\Omega)}$. *and the constant*

$$\|a^{(3)}_{\text{ref}}\|_\circ = 1 + C_P(\Omega).$$

Proof. We observe that

$$(1 + C_P(\Omega))^{-1} \|z^{(3)}_{\text{ref}}\|^2_\circ \leq (\nabla z^{(3)}_{\text{ref}}, \nabla z^{(3)}_{\text{ref}})_\Omega + (\kappa z^{(3)}_{\text{ref}}, z^{(3)}_{\text{ref}})_\Gamma = (e^{(3)}, z^{(3)}_{\text{ref}})_\Omega \leq \|e^{(3)}\|_{L^2(\Omega)}\|z^{(3)}_{\text{ref}}\|_\circ,$$

from which it follows that the second inequality in (3.28) is satisfied with the constant

$$\|a^{(3)}_{\text{ref}}\|_\circ = 1 + C_P(\Omega).$$

□

3.2.5 Conclusions

We proved the Property 3.2.1 for operators $d^{(1)}(\cdot,\cdot)$, $d^{(2)}(\cdot,\cdot)$, $d^{(3)}(\cdot,\cdot)$, and $l^{(1)}(\cdot)$, $l^{(2)}(\cdot)$, $l^{(3)}(\cdot)$. This assures that we can use the theory of 3.1 when $\epsilon \to 0$. In Chapter 4 we will provide numerical tests which verifies this *a posteriori* technique.
We proved the Property 3.2.2 for operators $a^{(1)}(\cdot,\cdot)$, $a^{(2)}(\cdot,\cdot)$, $a^{(3)}(\cdot,\cdot)$ and $a^{(1)}_{\text{ref}}(\cdot,\cdot)$, $a^{(2)}_{\text{ref}}(\cdot,\cdot)$, $a^{(3)}_{\text{ref}}(\cdot,\cdot)$. Therefore, we can write an *a priori* estimate for the L^2 norm of the modeling error.
We recall that

$$\begin{aligned}
e^{(1)} &= u^{(1)}_{\text{ref}} - u^{(1)} = u_\ominus - U \in H^1(\Sigma)\\
e^{(2)} &= u^{(2)}_{\text{ref}} - u^{(2)} = (\mathcal{I}_{\Omega_\oplus} + \mathcal{E}_\Sigma)u_\oplus - u^{(2)} \in H^1_0(\Omega)\\
e^{(3)} &= u^{(3)}_{\text{ref}} - u^{(3)} = u^{(2)} - u \in H^1_0(\Omega)
\end{aligned}$$

As a result, the total modeling error, on Σ and Ω respectively can be straightforwardly decomposed as

$$e_\Sigma + e_\Omega = (u_\ominus - U) + ((\mathcal{I}_{\Omega_\oplus} + \mathcal{E}_\Sigma)u_\oplus - u) = e^{(1)} + e^{(2)} + e^{(3)},$$

with $e_\Sigma = e^{(1)} \in H^1(\Sigma)$ and $e_\Omega = e^{(2)} + e^{(3)} \in H^1_0(\Omega)$.
We remind that if Properties (3.2.1) and (3.2.2) are satisfied,

$$\|e^{(*)}\|_{L^2} \leq \left(\|l^{(*)}\|_\circ + \|d^{(*)}\|_{\star\circ}\|a^{(*)}\|_\star\|\mathcal{F}\|_{X'}\right) \|a^{(*)}_{\text{ref}}\|_\circ, \quad * = 1,\, 2,\, 3.$$

For e_Σ, from Lemmas 11, 12, 13 we have

$$\|e_\Sigma\|_{L^2} \le \|l^{(1)}\|_\circ \|a^{(1)}\|_\star \|a^{(1)}_{\mathrm{ref}}\|_\circ \tag{3.45}$$

which entails that $\|e_\Sigma\|_{L^2(\Sigma)} = \mathcal{O}(\epsilon^{\frac{1}{2}})$ as $\epsilon \to 0$. For e_Ω, from Lemmas 14, 15, 16

$$\|e^{(2)}\|_{L^2} \le \left(\|l^{(2)}\|_\circ + \|d^{(2)}\|_{\star\circ}\|a^{(2)}\|_\star \left(\|f\|_{H^1(\Omega_\oplus)} + \|U\|_{L^2(\Lambda)}\right)\right) \|a^{(2)}_{\mathrm{ref}}\|_\circ$$

and from Lemmas 17, 18, 19

$$\|e^{(3)}\|_{L^2} \le \|d^{(3)}\|_{\star\circ}\|a^{(3)}\|_\star \left(\|f\|_{H^1(\Omega_\oplus)} + \|U\|_{L^2(\Lambda)}\right) \|a^{(3)}_{\mathrm{ref}}\|_\circ.$$

We notice that $\|\mathcal{F}\|_{X'}$ has been bounded from above by a term proportional to $\left(\|f\|_{H^1(\Omega_\oplus)} + \|U\|_{L^2(\Lambda)}\right)$. Therefore

$$\begin{aligned}\|e_\Omega\|_{L^2} \le & \|l^{(2)}\|_\circ \|a^{(2)}_{\mathrm{ref}}\|_\circ \\ & + \left(\|d^{(2)}\|_{\star\circ}\|a^{(2)}\|_\star\|a^{(2)}_{\mathrm{ref}}\|_\circ + \|d^{(3)}\|_{\star\circ}\|a^{(3)}\|_\star\|a^{(3)}_{\mathrm{ref}}\|_\circ\right)\left(\|f\|_{H^1(\Omega_\oplus)} + \|U\|_{L^2(\Lambda)}\right)\end{aligned} \tag{3.46}$$

which entails that $\|e_\Omega\|_{L^2(\Omega)} = \mathcal{O}(\epsilon^{\frac{1}{3}})$ as $\epsilon \to 0$.

Chapter 4

Numerical tests

We address here the experimental results related to the modeling error analysis of Chapter 3. The aim of this chapter is to provide some numerical tests that show the magnitude of the modeling error and how is it distributed.
Starting from the definitions of the modeling operators $d^{(i)}(\cdot,\cdot)$ and $l^{(i)}(\cdot)$, defined in Sections 3.2.2, 3.2.3 and 3.2.4, we want to compute some functionals of the modeling error, through the *error representation formula* (3.8) and the *approximated* one (3.17).
In particular, we will localize this error in the elements of the triangulation $\mathcal{T}_t^h$ of the three-dimensional domain $\bar{\Omega}$; in order to achieve this result we must re-write the (3.8) as the sum of residuals, weighed with the dual solution. We address Section 4.1 the details of this localization.
Consequently, we show the results of the computational simulations, exploring the distribution of the modeling error in different test cases (see Table **??**). In Section 4.2 we show *Scenario* A, that is the problem (2.10) with $R = 0.25$, g and f constants, and the functional of the error defined as the integral on the reference domain; this will be our starting point for the following simulations. *Scenario* B in Section 4.3 employs a non-constant function for g. Similarly, in *Scenario* C the function f is variable in the cross section. In Section 4.5, we present *Scenario* D, in which the radius is set to $R = 0.1$. Finally, *Scenario* E employs the functional of the error defined as the flux through Γ. Finally, in 4.7 we discuss the numerical results.

4.1 Estimators

In this Section, we discuss how to compute the estimators based on the dual *a posteriori* modeling error presented in Section 3.1; the work in [7] will be the starting point.

Scenario	R	g	f	$j(\cdot)$	# el. in Ω	# el. in Σ	Time (s)
A	0.25	1	1	L^1-norm	354'753	17'198	1'621
B	0.25	$1+3y$	1	L^1-norm	354'753	17'198	1'628
C	0.25	1	$1+y$	L^1-norm	354'753	17'198	1'657
D	0.1	1	1	L^1-norm	347'870	47'523	1'730
E	0.25	1	1	flux through Γ	354'753	17'198	1'686

Table 4.1: Main parameters for the different Scenarios for estimators of modeling error. See Sections 4.2, 4.3, 4.4, 4.5 and 4.6

Afterwards, we will explicitly compute the estimators for our problem (2.10).

4.1.1 Localization of the estimator

Let us consider the generic reduced problem (3.4) and his dual (3.7). Let u, z be the correspondent solutions in X, and u_h, z_h their discrete solution in the finite element space X_h. Let $U, Z \in \mathbb{R}^N$ be the vector of nodal values of u_h and z_h respectively, where N is the number of nodes of the triangulation $\mathcal{T}_h$ for the finite element space X_h. Considering the Lagrangian nodal basis $\{\phi_i\} \subset X_h$, we can build the model residual vector ρ :

$$[\rho]_i = l(\phi_i) - d(u_h)(\phi_i),$$

The localized estimator are finally computed with the l_2 scalar product in $\mathbb{R}^N$, between this vector and the vector Z:

$$\begin{aligned} \eta &= \langle \rho, Z \rangle, \\ [\eta]_i &= \rho_i Z_i, \end{aligned} \tag{4.1}$$

where $\eta \in \mathbb{R}^N$ is our estimator for modeling error. Each nodal contribution of η represents the localization of the error in $\mathcal{T}_h$.
Finally, the steps of this technique are:

- computes some residuals ρ_i depending on the reduced solution u;
- compute some weights w_i using the dual solution z;
- compute the estimator η as $\eta = \sum_i \rho_i w_i$.

4.1.2 Derivation of $\eta^{(i)}$

Using the approach explained before, we explicitly derive the estimators η_1, η_2, η_3, regarding the three steps of the topological model reduction; in particular, we must compute the residuals $\rho^{(i)}$ and discuss the weights $w^{(i)}$ for $i = 1, 2, 3$.
We introduce $X^{(1)}_{h,k}$, $X^{(2)}_{h,k}$, $X^{(3)}_{h,k}$ the finite element spaces of order k over Σ, $\Omega_\oplus$, Ω, respectively. We introduce their degrees of freedom $N^{(1)}_h = dim\left(X^{(1)}_{h,k}\right)$, $N^{(2)}_h = dim\left(X^{(2)}_{h,k}\right)$, $N^{(3)}_h = dim\left(X^{(3)}_{h,k}\right)$, and their finite element basis $\left\{\phi^{(1)}_i\right\}_{i=1}^{N^{(1)}_h}$, $\left\{\phi^{(2)}_i\right\}_{i=1}^{N^{(2)}_h}$, $\left\{\phi^{(3)}_i\right\}_{i=1}^{N^{(3)}_h}$.
We recall that $z^{(1)}_{\text{ref}} \in H^1(\Sigma)$, $z^{(2)}_{\text{ref}} \in H^1_{\partial\Omega}(\Omega_\oplus)$, $z^{(3)}_{\text{ref}} \in H^1_0(\Omega)$; accordingly to the notation described above, the discrete reference dual solutions are $z^{(1)}_{h,\text{ref}} \in X^{(1)}_{h,k}$, $z^{(2)}_{h,\text{ref}} \in X^{(2)}_{h,k}$, $z^{(3)}_{h,\text{ref}} \in X^{(3)}_{h,k}$. These functions will be our weights: however, in order to simplify the notation and to clarify the meaning of these weights, we define $w^{(i)}$ to be in $X^{(3)}_{h,k}$ for $i = 1, 2, 3$. Therefore, all of our weights are defined on Ω, so that we can compare the different estimators on the same domain. For sake of clarity, from now on we dismiss the apex $(\cdot)^{(3)}$, and work on the finite element space $X_{h,k}$ defined on Ω, with degrees of freedom $N_h = dim\left(X_{h,k}\right)$, and basis $\{\phi_i\}_{i=1}^{N_h}$.
Although $z^{(3)}_{h,\text{ref}}$ already belongs to $X_{h,k}$, we must extend the functions $z^{(1)}_{h,\text{ref}}$ and $z^{(2)}_{h,\text{ref}}$:

$$w^{(1)} = \begin{cases} z^{(1)}_{h,\text{ref}} & \text{in } \Sigma \\ 0 & \text{in } \Omega_\oplus \end{cases} \qquad w^{(2)} = \begin{cases} 0 & \text{in } \Sigma \\ z^{(2)}_{h,\text{ref}} & \text{in } \Omega_\oplus \end{cases} \qquad w^{(3)} = z^{(3)}_{h,\text{ref}} \quad \text{in } \Omega \tag{4.2}$$

We now build the residuals $\rho^{(i)}$ for $i = 1, 2, 3$, depending on the reduced solutions u and U. Using the definitions of (3.33), (3.37), (3.42), the residuals are:

$$\rho^{(1)}_i = l^{(1)}(\phi_i) - d^{(1)}(U, \phi_i) = ((\mathcal{I} - \overline{\overline{(\cdot)}})g, \phi_i)_\Sigma + (\kappa(\mathcal{I} - \overline{(\cdot)})u, \phi_i)_\Gamma, \tag{4.3a}$$

$$\rho^{(2)}_i = l^{(2)}(\phi_i) - d^{(2)}(u, \phi_i) = (\nabla u, \nabla \phi_i)_\Sigma - (\mathcal{E}_\Sigma f, \phi_i)_\Sigma, \tag{4.3b}$$

$$\rho^{(3)}_i = l^{(3)}(\phi_i) - d^{(3)}(u, \phi_i) = -(\kappa(\mathcal{I} - \overline{(\cdot)})u, \phi_i)_\Gamma, \tag{4.3c}$$

for $i = 1 : N_h$.

Remark 4.1.1. One can notice an important result: although we derive the residuals from both the reduced solutions u and U, as a matter of fact all the terms containing the solution in the inclusion Λ vanish, namely:

$$\begin{aligned}
d^{(1)}(U,\phi_i) =& ((\mathcal{I}-\overline{\overline{(\cdot)}})d_sU, d_s\phi_i)_\Sigma + (\kappa(\mathcal{I}-\overline{(\cdot)})U,\phi_i)_\Gamma \\
&+ (\partial_r U, \partial_r\phi_i)_\Sigma + (r^{-1}\partial_\theta U, r^{-1}\partial_\theta\phi_i)_\Sigma \, , \\
l^{(3)}(\phi_i) =& (\kappa U, \left(\mathcal{I}-\overline{(\cdot)}\right)\phi_i)_\Gamma \, .
\end{aligned}$$

The term $d^{(1)}(U,\phi_i)$ vanishes because $U(s,r,\theta) = U(s) = \overline{U}(s) = \overline{\overline{U}}(s)$. On the other hand, $l^{(3)}(\phi_i)$ is equal to zero since every function in Σ dependent only on the position in the centerline Λ is L^2-orthogonal to the operator $\left(\mathcal{I}-\overline{(\cdot)}\right)$. In fact, for generic functions $F \in H^1_0(\Sigma)$, $F(s,r,\theta) = F(s)$, and $g \in H^1_0(\Omega)$:

$$\begin{aligned}
(F,g)_\Gamma =& \int_\Lambda \int_{\partial D(s)} (F\, g)\, d\gamma\, ds \\
=& \int_\Lambda F \int_{\partial D(s)} g\, d\gamma\, ds \\
=& \int_\Lambda F\, \overline{g}\, |\partial D|\, ds \\
=& (F,\overline{g})_{\Lambda,\partial\mathcal{D}},
\end{aligned}
\qquad
\begin{aligned}
(F,\overline{g})_\Gamma =& \int_\Lambda \int_{\partial D(s)} (F\, \overline{g})\, d\gamma\, ds \\
=& \int_\Lambda F\, \overline{g} \int_{\partial D(s)} d\gamma\, ds \\
=& \int_\Lambda F\, \overline{g}\, |\partial D|\, ds \\
=& (F,\overline{g})_{\Lambda,\partial\mathcal{D}}.
\end{aligned}$$

Therefore, our estimators will depends only on the reduced solution in tissue. This means that all the information about the error due to the topological reduction lays in the region of Σ; the reduced solution in Λ can't see the residuals in this region. We address the *Scenario* A, in the next Section, for further explanations.

Let us combine the weights and the residuals in order to compute the estimators:

$$\eta^{(1)} = \sum_{i=1}^{N_h} w_i^{(1)}\, \rho_i^{(1)} = \sum_{i=1}^{N_h} w_i^{(1)} \left[((\mathcal{I}-\overline{\overline{(\cdot)}})g,\phi_i)_\Sigma + (\kappa(\mathcal{I}-\overline{(\cdot)})u,\phi_i)_\Gamma\right], \tag{4.4a}$$

$$\eta^{(2)} = \sum_{i=1}^{N_h} w_i^{(2)}\, \rho_i^{(2)} = \sum_{i=1}^{N_h} w_i^{(2)} \left[(\nabla u, \nabla\phi_i)_\Sigma - (\mathcal{E}_\Sigma f, \phi_i)_\Sigma\right], \tag{4.4b}$$

$$\eta^{(3)} = \sum_{i=1}^{N_h} w_i^{(3)}\, \rho_i^{(3)} = \sum_{i=1}^{N_h} w_i^{(3)} \left[-(\kappa(\mathcal{I}-\overline{(\cdot)})u,\phi_i)_\Gamma\right]. \tag{4.4c}$$

We recall that at this stage, the weights are the reference dual solutions: this means that, when we compute these estimators, we are using the exact *representation formula* (3.8), that is $j^{(i)}(e^{(1)}) = l^{(i)}(z^{(i)}_{\text{ref}}) - d^{(i)}(u^{(i)}, z^{(i)}_{\text{ref}})$, for $i = 1,2,3$. Therefore, apart from the discretization error, the modeling error is completely described by $\eta^{(i)}$.

Luckily, $z_{\text{ref}}^{(1)}$, $z_{\text{ref}}^{(2)}$ and $z_{\text{ref}}^{(3)}$ present some interesting features: first of all, the dual reference problems (3.34), (3.39), (3.43) are uncoupled, therefore each dual algebraic system is less complex than its primal. Besides, once one has written the code for computing the modeling operators $d^{(i)}$ and $l^{(i)}$, it is straightforward to implement the terms for each reference dual problem. Therefore, as a first step, we will study these exact estimators.
Nevertheless, one may argue that the reference dual problems are too demanding, even if they are much less expensive than the primal ones; thanks to the considerations of Section 3.1, one may consider the radius ϵ small enough to replace the reference dual solutions with the reduced ones, using the *approximated representation formula* (3.17), that is $j^{(i)}(e^{(1)}) = l^{(i)}(z_{red}^{(i)}) - d^{(i)}(u^{(i)}, z_{red}^{(i)})$, for $i = 1, 2, 3$.
We now define the reduced dual problem of (2.10): it consists to find $z \in H_0^1(\Omega)$, $Z \in H^1(\Lambda)$ such that

$$a_\Omega(v, z) + b_\Lambda^\epsilon(\overline{v}, \overline{z}) = j^{red}(v) \qquad \forall v \in H_0^1(\Omega)\,, \tag{4.5a}$$

$$a_\Lambda(V, Z) + b_\Lambda^\epsilon(V, Z) = J^{red}(v) \qquad \forall V \in H^1(\Lambda)\,, \tag{4.5b}$$

where

$$\begin{aligned} a_\Omega(w, v) &= (\nabla w, \nabla v)_\Omega, \\ a_\Lambda(w, v) &= (d_s w, d_s v)_{\Lambda,|\mathcal{D}|}, \\ b_\Lambda^\epsilon(w, v) &= (\kappa w, v)_{\Lambda,|\partial\mathcal{D}|}. \end{aligned}$$

The functional $j^{red}(\cdot) \,:\, H_0^1(\Omega) \to \mathbb{R}$ can be:

$$\begin{aligned} & j^{red}(v) = j_\Omega^{red}(v) = \int_\Omega v \, d\Omega, \\ & \text{or} \\ & j^{red}(v) = j_\Gamma^{red}(v) = \int_\Gamma \nabla v \cdot \boldsymbol{n} \, d\gamma, \end{aligned} \tag{4.6}$$

while $J^{red}(\cdot) \,:\, H_0^1(\Lambda) \to \mathbb{R}$ can be:

$$\begin{aligned} & J^{red}(v) = J_\Lambda^{red}(v) = \int_\Lambda v \, d\Lambda, \\ & \text{or} \\ & J^{red}(v) = J_\Gamma^{red}(v) = \int_\Gamma \nabla v \cdot \boldsymbol{n} \, d\gamma. \end{aligned} \tag{4.7}$$

We now proceed to define the reduced weights $\tilde{w}^{(1)}$, $\tilde{w}^{(2)}$, $\tilde{w}^{(3)}$, using the reduced dual solution. As for the reference weights, the reduced ones are defined on the whole domain Ω through the finite element space $X_{h,k}$:

$$\tilde{w}^{(1)} = \begin{cases} Z_h & \text{in } \Sigma \\ 0 & \text{in } \Omega_{\oplus} \end{cases} \qquad \tilde{w}^{(2)} = z_h \quad \text{in } \Omega \qquad \tilde{w}^{(3)} = z_h \quad \text{in } \Omega. \tag{4.8}$$

Then, it is straightforward to define the approximated estimators based on the reduced weights:

$$\tilde{\eta}^{(1)} = \sum_{i=1}^{N_h} \tilde{w}_i^{(1)} \, \rho_i^{(1)}, \tag{4.9a}$$

$$\tilde{\eta}^{(2)} = \sum_{i=1}^{N_h} \tilde{w}_i^{(2)} \, \rho_i^{(2)}, \tag{4.9b}$$

$$\tilde{\eta}^{(3)} = \sum_{i=1}^{N_h} \tilde{w}_i^{(3)} \, \rho_i^{(3)}. \tag{4.9c}$$

$$\tag{4.9d}$$

4.2 Scenario A

We solve the primal reduced coupled problem (2.10) on a segment Λ from $(-0.51, 0, 0)$ to $(0.51, 0, 0)$, discretized with 1281 points, completely embedded in the parallelepiped $\Omega = (-1, 1)^2 \times (-0.51, 0.51)$; the tessellation of Ω is a quasi-uniform regular mesh, with characteristic length $h = 1/32 = 0.03125$, for a total of 354'753 tetrahedra. The other parameters are: $R = 0.25$, $k = 1$, $f = 1$ and $g = 1$.

We then solve the three reference dual problems (3.34), (3.39), (3.43), and the reduced dual problem (4.5), using as linear operators the L^1-norms, that are: $j^{(1)}(v) = j_{\Sigma}^{(1)}(v)$, $j^{(2)}(v) = j_{\Omega}^{(2)}(v)$, $j^{(3)}(v) = j_{\Omega}^{(3)}(v)$, $j^{red}(\cdot) = j_{\Omega}^{red}(\cdot)$ and $J^{red}(\cdot) = J_{\Lambda}^{red}(\cdot)$.

Finally, we can compute the residuals $\rho^{(i)}$ and the weights $w^{(i)}$ and $\tilde{w}^{(i)}$ for $i = 1:3$ with the definitions (4.3), (4.2) and (4.8).

We now present the results: as a first step, we validate our code by checking that the terms $d^{(1)}(U, \cdot)$ and $l^{(3)}(\cdot)$ actually vanish, as theoretically expected; this will be done only for this Scenario. Then, we will show the estimators, providing the weights and residuals related to each assumption.

Remark 4.2.1. All the following plots should be represented on Ω; unfortunately, the meaningful data are strictly inside the domain Ω, because of the homogeneous Dirichlet condition on his boundary. Therefore, in order to successfully represent the information of the plots, we will show only a 2D surface embedded in the 3D domain, i.e. the y-z plane in $x = 0$, crossing perpendicularly the centre of the inclusion Λ.

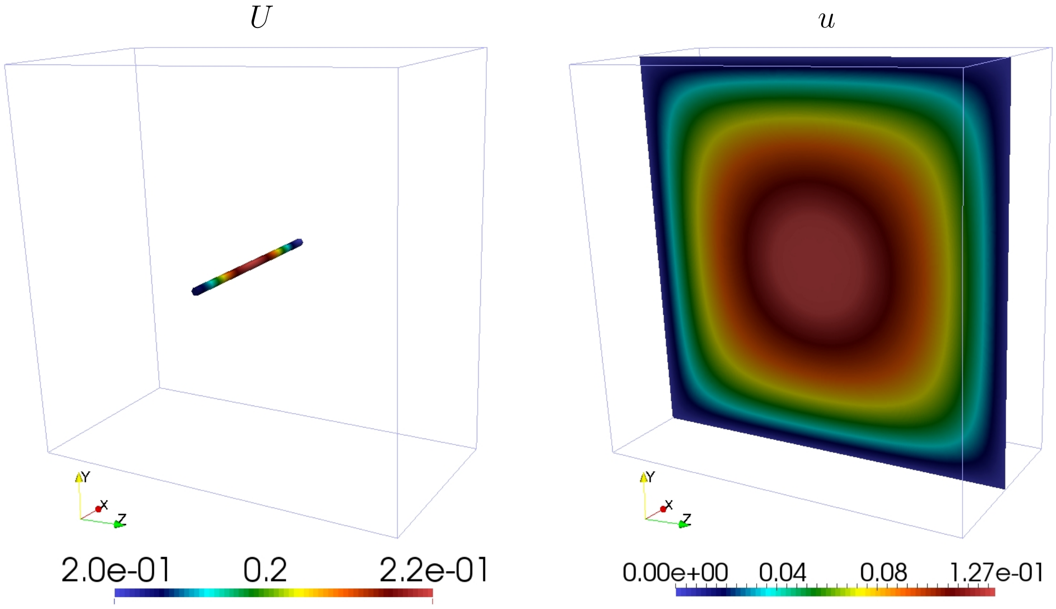

Figure 4.1: Reduced solutions in Scenario A. In the left, the reduced solution U on Λ, while on the right, the reduced solution u on Ω.

4.2.1 Validation: null terms

We want to check that the terms depending on U, namely $d^{(1)}(U, \phi_i)$ and $l^{(3)}(\phi_i)$, actually vanish for each base ϕ_i, as proved in 4.1.2. We recall their definition (3.33a),(3.42b), and analyze each term:

$$\begin{aligned} d^{(1)}(U, \phi_i) =& ((\mathcal{I} - \overline{\overline{(\cdot)}}) d_s U, d_s \phi_i)_\Sigma + (\kappa(\mathcal{I} - \overline{(\cdot)})U, \phi_i)_\Gamma \\ & + (\partial_r U, \partial_r \phi_i)_\Sigma + (r^{-1}\partial_\theta U, r^{-1}\partial_\theta \phi_i)_\Sigma \,, \\ l^{(3)}(\phi_i) =& (\kappa U, \phi_i)_\Gamma - (\kappa U, \overline{\phi_i})_{\Lambda, |\partial\mathcal{D}|} \,. \end{aligned}$$

For $d^{(1)}(U, \phi_i)$, we can separate the terms in Σ and those on Γ; in particular, we expect that $\sum_i (\nabla U, \nabla \phi_i)_\Sigma = \sum_i (d_s \overline{\overline{U}}, d_s \phi_i)_\Sigma$ and $\sum_i (\kappa U, \phi_i)_\Gamma = \sum_i (\kappa \overline{U}, \phi_i)_\Gamma$. Similarly, for $l^{(3)}(\phi_i)$ we expect $\sum_i (\kappa U, \phi_i)_\Gamma = \sum_i (\kappa U, \overline{\phi_i})_{\Lambda, |\partial\mathcal{D}|}$.
The results are shown in Figures 4.2,4.3, 4.4. One can observe that these terms are not exactly equal to zero: instead, they decrease of a factor around 10^{-2}. This is related to numerical errors that arise in the assembling the average discrete operators, $\overline{\overline{\Pi}}_{vt}$ and $\overline{\Pi}_{vt}$, corresponding to $\overline{\overline{(\cdot)}}$ (2.1a), and $\overline{(\cdot)}$ (2.1b), respectively. These errors can be reduced using more precise quadrature formulas. Nevertheless, the assembling of these matrices is already one of the most expensive tasks of the numerical procedure, therefore we couldn't afford better quadrature formulas.

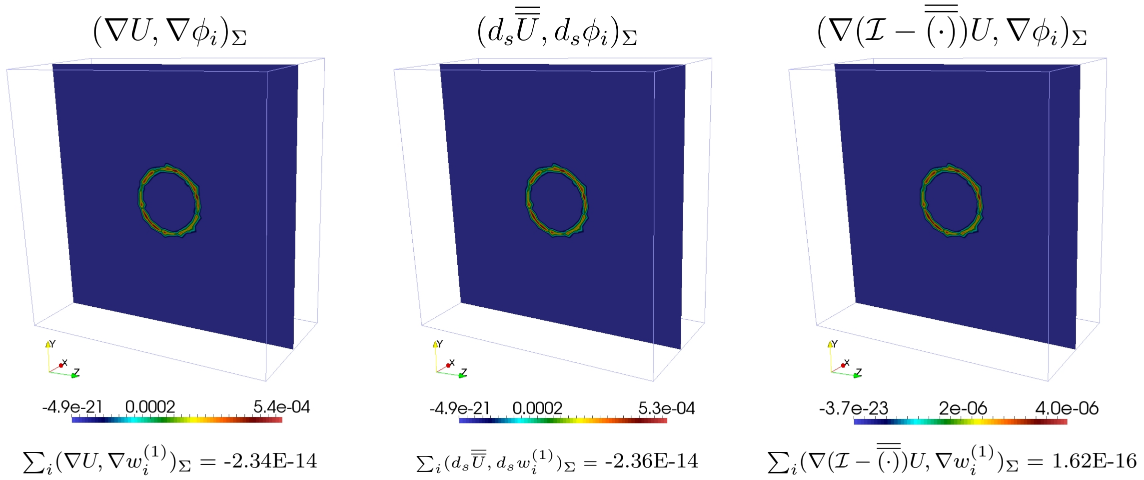
$(\nabla U, \nabla \phi_i)_\Sigma$ $\quad$ $(d_s\overline{\overline{U}}, d_s\phi_i)_\Sigma$ $\quad$ $(\nabla(\mathcal{I}-\overline{\overline{(\cdot)}})U, \nabla \phi_i)_\Sigma$

$\sum_i(\nabla U, \nabla w_i^{(1)})_\Sigma$ = -2.34E-14 $\quad$ $\sum_i(d_s\overline{\overline{U}}, d_s w_i^{(1)})_\Sigma$ = -2.36E-14 $\quad$ $\sum_i(\nabla(\mathcal{I}-\overline{\overline{(\cdot)}})U, \nabla w_i^{(1)})_\Sigma$ = 1.62E-16

Figure 4.2: Validation in Scenario A: discussion of term $(\nabla(\mathcal{I}-\overline{\overline{(\cdot)}})U, \nabla\phi_i)_\Sigma$. The plots refer to the residuals tested on generic functions ϕ_i. For every plot, it is shown the sum of all the weighted residuals.

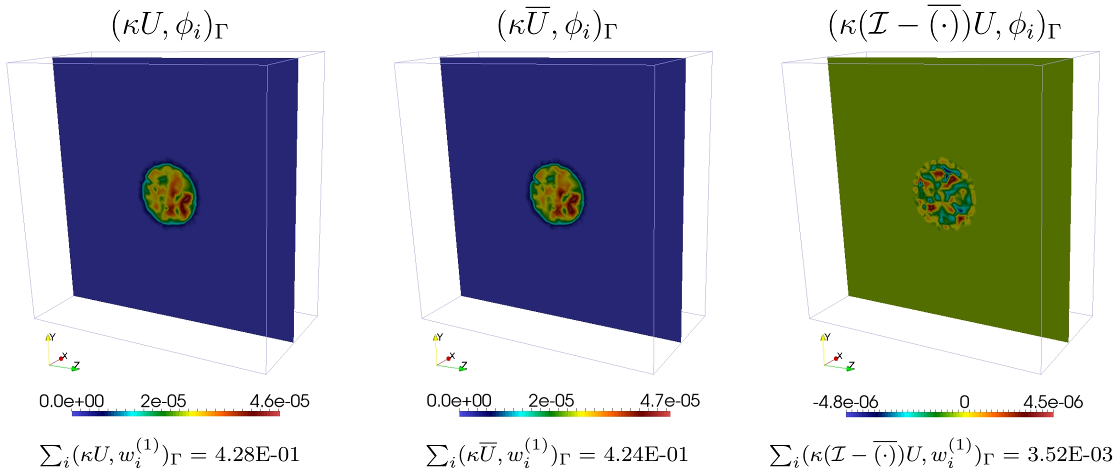
$(\kappa U, \phi_i)_\Gamma$ $\quad$ $(\kappa\overline{U}, \phi_i)_\Gamma$ $\quad$ $(\kappa(\mathcal{I}-\overline{(\cdot)})U, \phi_i)_\Gamma$

$\sum_i(\kappa U, w_i^{(1)})_\Gamma$ = 4.28E-01 $\quad$ $\sum_i(\kappa\overline{U}, w_i^{(1)})_\Gamma$ = 4.24E-01 $\quad$ $\sum_i(\kappa(\mathcal{I}-\overline{(\cdot)})U, w_i^{(1)})_\Gamma$ = 3.52E-03

Figure 4.3: Validation in Scenario A: discussion of term $(\kappa(\mathcal{I}-\overline{(\cdot)})U, \phi_i)_\Gamma$. The plots refer to the residuals tested on generic functions ϕ_i. For every plot, it is shown the sum of all the weighted residuals.

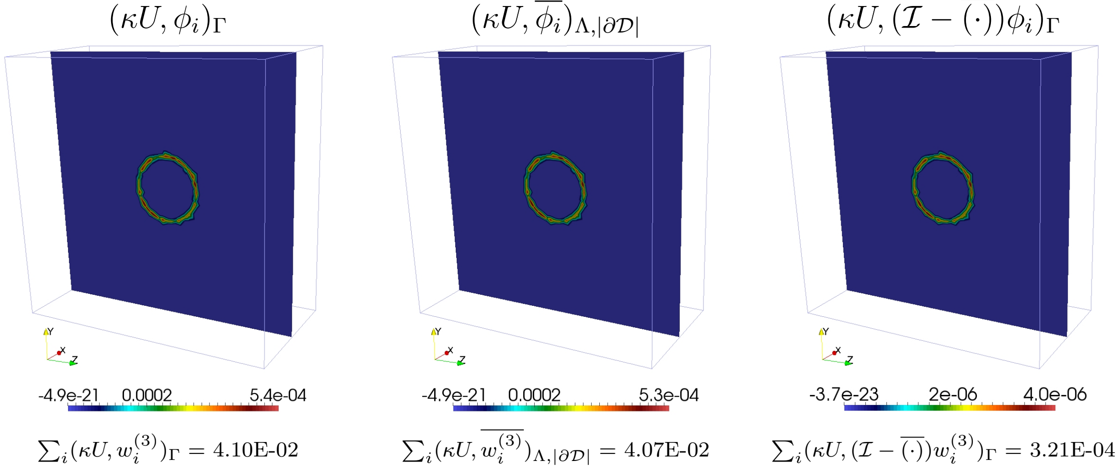

$(\kappa U, \phi_i)_\Gamma$ $\quad$ $(\kappa U, \overline{\phi_i})_{\Lambda,|\partial\mathcal{D}|}$ $\quad$ $(\kappa U, (\mathcal{I} - \overline{(\cdot)})\phi_i)_\Gamma$

$\sum_i (\kappa U, w_i^{(3)})_\Gamma = 4.10\text{E-}02$ $\quad$ $\sum_i (\kappa U, \overline{w_i^{(3)}})_{\Lambda,|\partial\mathcal{D}|} = 4.07\text{E-}02$ $\quad$ $\sum_i (\kappa U, (\mathcal{I} - \overline{(\cdot)})w_i^{(3)})_\Gamma = 3.21\text{E-}04$

Figure 4.4: Validation in Scenario A: discussion of term $(\kappa U, (\mathcal{I} - \overline{(\cdot)})\phi_i)_\Gamma$. The plots refer to the residuals tested on generic functions ϕ_i. For every plot, it is shown the sum of all the weighted residuals.

In addition, when going through the next Sections, one can notice that the magnitude of these residuals is comparable to the magnitude of the other residuals. Anyway, these residuals bring informations only about the discretization error, not about the modeling errors: it would be a mistake deciding to consider these terms in the estimator for the modeling error.
In conclusion, we will consider from now on $\eta^{(1)} \equiv l^{(1)}(w^{(1)})$ and $\eta^{(3)} \equiv -d^{(3)}(w^{(3)})$. On the other hand, in future works it will be interesting compute also estimators for the discretization error: those estimators should consider the effect of the terms $d^{(1)}(U, \phi_i)$ and $l^{(3)}(\phi_i)$.

4.3 Scenario B

We solve the primal reduced coupled problem (2.10) on a segment Λ from $(-0.51, 0, 0)$ to $(0.51, 0, 0)$, discretized with 1281 points, completely embedded in the parallelepiped $\Omega = (-1, 1)^2 \times (-0.51, 0.51)$; the tessellation of Ω is a quasi-uniform regular mesh, with characteristic length $h = 1/32 = 0.03125$, for a total of 354'753 tetrahedra. The other parameters are: $R = 0.25$, $k = 1$, $f = 1$ and $g = 1 + 3y$.
We then solve the three reference dual problems (3.34), (3.39), (3.43), and the reduced dual problem (4.5), using the following linear operators: $j^{(1)}(v) = j_\Sigma^{(1)}(v)$, $j^{(2)}(v) = j_\Omega^{(2)}(v)$, $j^{(3)}(v) = j_\Omega^{(3)}(v)$, $j^{red}(\cdot) = j_\Omega^{red}(\cdot)$ and $J^{red}(\cdot) = J_\Lambda^{red}(\cdot)$.
As one can observe, the only difference between Scenario A and Scenario B is the definition of g: in fact, Scenario B is designed to study the case $g(s) \neq \overline{\overline{g}}(s)$.

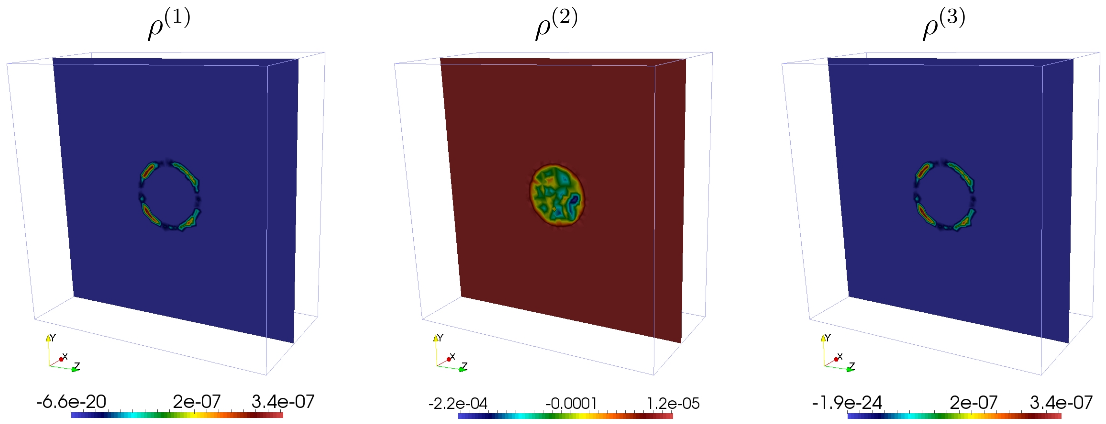
$\rho^{(1)}$ $\rho^{(2)}$ $\rho^{(3)}$

Figure 4.5: Residuals $\rho^{(1)}$, $\rho^{(2)}$, $\rho^{(3)}$ in Scenario A

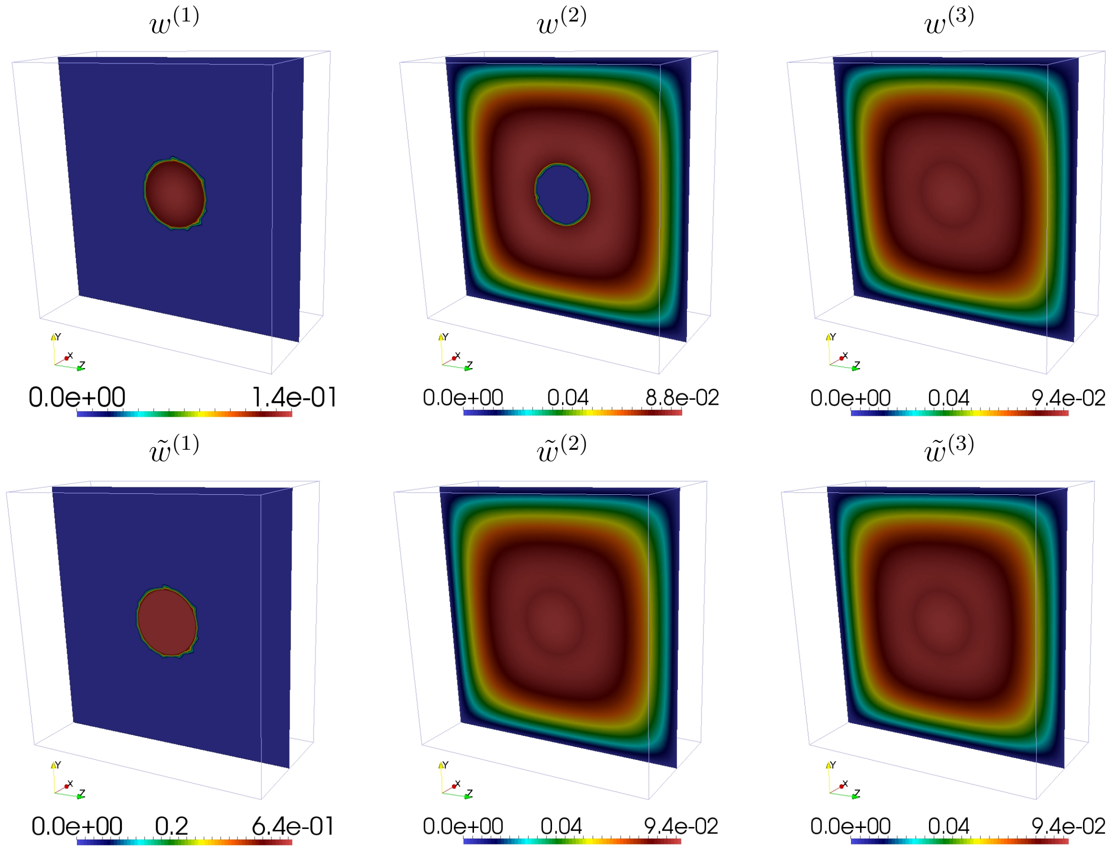
$w^{(1)}$ $w^{(2)}$ $w^{(3)}$

$\tilde{w}^{(1)}$ $\tilde{w}^{(2)}$ $\tilde{w}^{(3)}$

Figure 4.6: Weights in Scenario A. In the first row, the reference weights $w^{(1)}$, $w^{(2)}$, $w^{(3)}$; in the second row, the reduced weights $\tilde{w}^{(1)}$, $\tilde{w}^{(2)}$, $\tilde{w}^{(3)}$

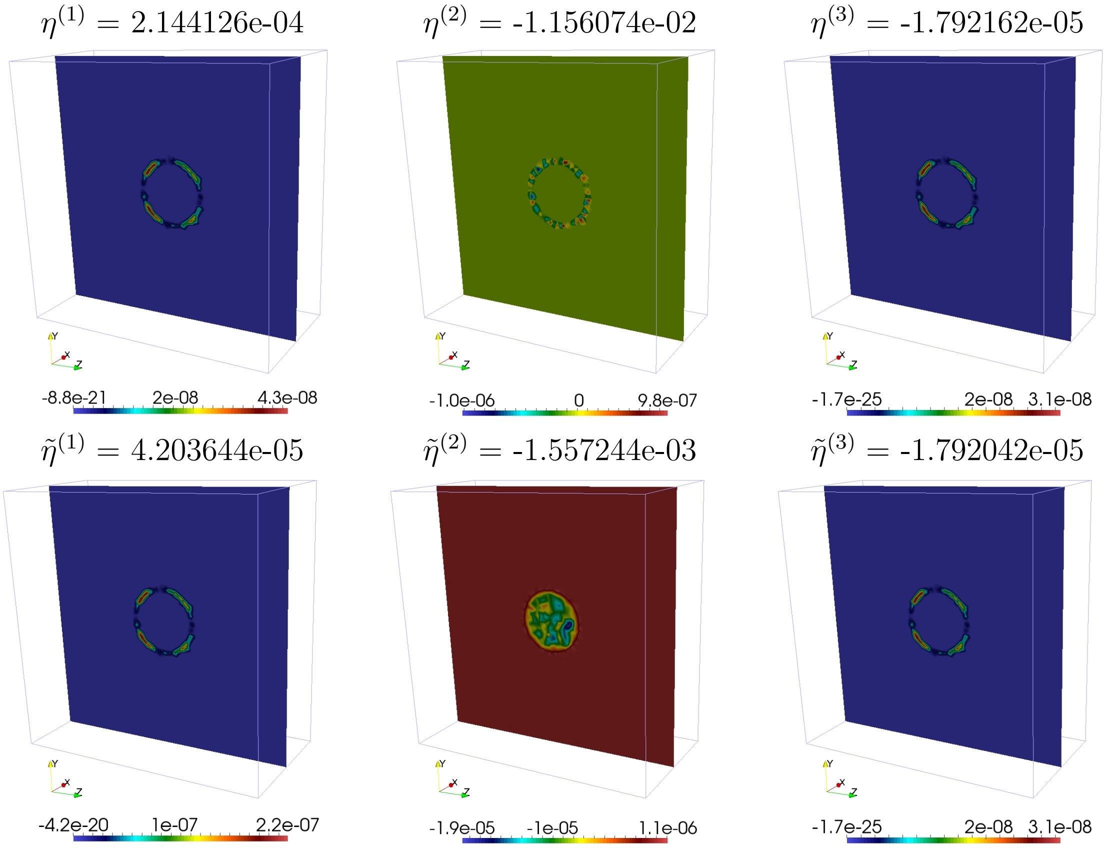

$\eta^{(1)} = 2.144126\text{e-}04$

$\eta^{(2)} = -1.156074\text{e-}02$

$\eta^{(3)} = -1.792162\text{e-}05$

$\tilde{\eta}^{(1)} = 4.203644\text{e-}05$

$\tilde{\eta}^{(2)} = -1.557244\text{e-}03$

$\tilde{\eta}^{(3)} = -1.792042\text{e-}05$

Figure 4.7: Estimators in Scenario A. In the first row, the reference estimators $\eta^{(1)}$, $\eta^{(2)}$, $\eta^{(3)}$; in the second row, the reduced estimators $\tilde{\eta}^{(1)}$, $\tilde{\eta}^{(2)}$, $\tilde{\eta}^{(3)}$

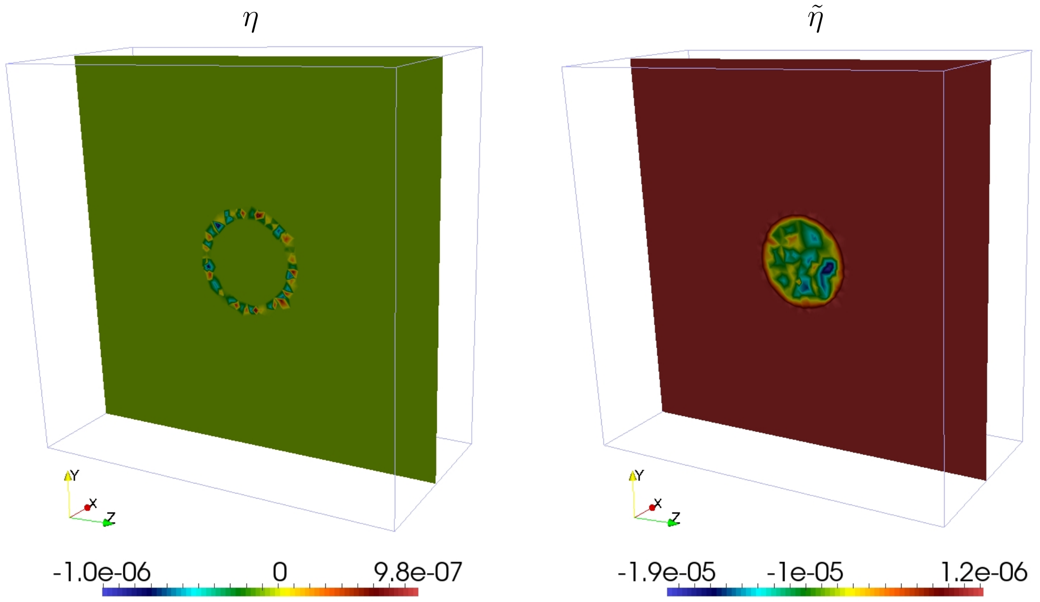

Figure 4.8: Global estimators in Scenario A. On the left, $\eta = \sum_i \eta^{(i)}$; on the right, $\tilde{\eta} = \sum_i \tilde{\eta}^{(i)}$.

Finally, we can compute the residuals $\rho^{(i)}$ and the weights $w^{(i)}$ and $\tilde{w}^{(i)}$ for $i = 1:3$ with the definitions (4.3), (4.2) and (4.8).

4.4 Scenario C

We solve the primal reduced coupled problem (2.10) on a segment Λ from $(-0.51, 0, 0)$ to $(0.51, 0, 0)$, discretized with 1281 points, completely embedded in the parallelepiped $\Omega = (-1, 1)^2 \times (-0.51, 0.51)$; the tessellation of Ω is a quasi-uniform regular mesh, with characteristic length $h = 1/32 = 0.03125$, for a total of 354'753 tetrahedra. The other parameters are: $R = 0.25$, $k = 1$, $f = 1 + y$ and $g = 1$.
We then solve the three reference dual problems (3.34), (3.39), (3.43), and the reduced dual problem (4.5), using the following linear operators: $j^{(1)}(v) = j_{\Sigma}^{(1)}(v)$, $j^{(2)}(v) = j_{\Omega}^{(2)}(v)$, $j^{(3)}(v) = j_{\Omega}^{(3)}(v)$, $j^{red}(\cdot) = j_{\Omega}^{red}(\cdot)$ and $J^{red}(\cdot) = J_{\Lambda}^{red}(\cdot)$.
As one can observe, the only difference between Scenario A and Scenario C is the definition of f: in fact, Scenario C is designed to study the case of $f(s, r, t) \neq f(s, r)$, that means it is not constant along Γ
Finally, we can compute the residuals $\rho^{(i)}$ and the weights $w^{(i)}$ and $\tilde{w}^{(i)}$ for $i = 1:3$ with the definitions (4.3), (4.2) and (4.8).

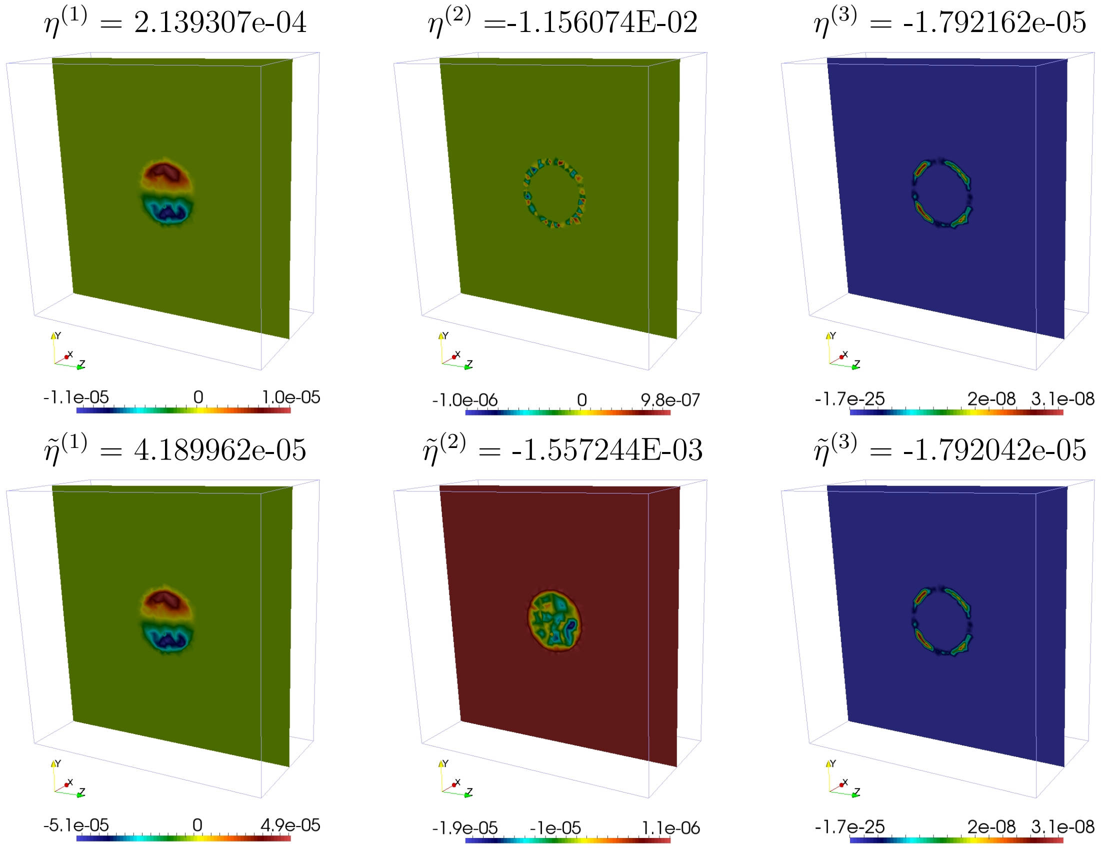

$\eta^{(1)} = 2.139307\text{e-}04$ $\eta^{(2)} = \text{-}1.156074\text{E-}02$ $\eta^{(3)} = \text{-}1.792162\text{e-}05$

$\tilde{\eta}^{(1)} = 4.189962\text{e-}05$ $\tilde{\eta}^{(2)} = \text{-}1.557244\text{E-}03$ $\tilde{\eta}^{(3)} = \text{-}1.792042\text{e-}05$

Figure 4.9: Estimators in Scenario B.In the first row, the reference estimators $\eta^{(1)}$, $\eta^{(2)}$, $\eta^{(3)}$; in the second row, the reduced estimators $\tilde{\eta}^{(1)}$, $\tilde{\eta}^{(2)}$, $\tilde{\eta}^{(3)}$

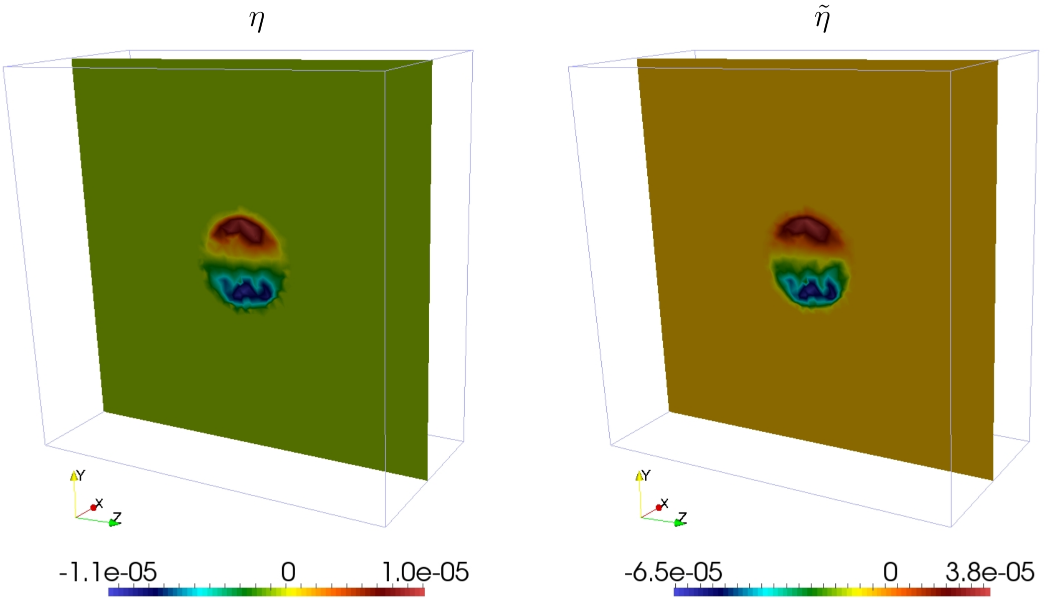

Figure 4.10: Global estimators in Scenario B. On the left, $\eta = \sum_i \eta^{(i)}$; on the right, $\tilde{\eta} = \sum_i \tilde{\eta}^{(i)}$.

4.5 Scenario D

We solve the primal reduced coupled problem (2.10) on a segment Λ from $(-0.51, 0, 0)$ to $(0.51, 0, 0)$, discretized with 1281 points, completely embedded in the parallelepiped $\Omega = (-1, 1)^2 \times (-0.51, 0.51)$; the tessellation of Ω is a quasi-uniform mesh, with characteristic length varying from $h = 1/16 = 0.0625$ on the boundary, to $h = 1/64 = 0.015625$, for a total of 347'870 tetrahedra. The other parameters are: $R = 0.1$, $k = 1$, $f = 1$ and $g = 1$.
We then solve the three reference dual problems (3.34), (3.39), (3.43), and the reduced dual problem (4.5), using the following linear operators: $j^{(1)}(v) = j^{(1)}_{\Sigma}(v)$, $j^{(2)}(v) = j^{(2)}_{\Omega}(v)$, $j^{(3)}(v) = j^{(3)}_{\Omega}(v)$, $j^{red}(\cdot) = j^{red}_{\Omega}(\cdot)$ and $J^{red}(\cdot) = J^{red}_{\Lambda}(\cdot)$.
As one can observe, the only difference between Scenario A and Scenario D is the dimension of radius, and consequently the mesh used. In this Scenario, we want to study the value of the estimators in a problem with a smaller radius, in order to discuss the theory of Section 3.1. The mesh of this Scenario (see Fig. 4.15) is designed to have a total number of elements close to the previous one, while simultaneously having a number of elements in Σ close to the previous one.
Finally, we can compute the residuals $\rho^{(i)}$ and the weights $w^{(i)}$ and $\tilde{w}^{(i)}$ for $i = 1:3$ with the definitions (4.3), (4.2) and (4.8).

Scenario A: $g = 1$

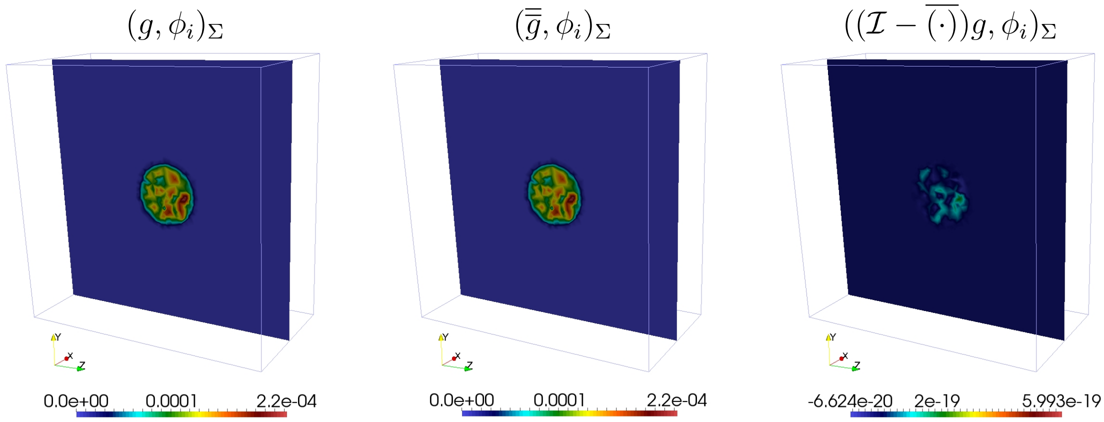

$\sum_i (g, w_i^{(1)})_\Sigma = 1.26\text{E-}01$ $\sum_i (\overline{\overline{g}}, w_i^{(1)})_\Sigma = 1.26\text{E-}01$ $\sum_i ((\mathcal{I} - \overline{\overline{(\cdot)}})g, w_i^{(1)})_\Sigma = 3.35\text{E-}17$

Scenario B: $g = 1 + 3y$

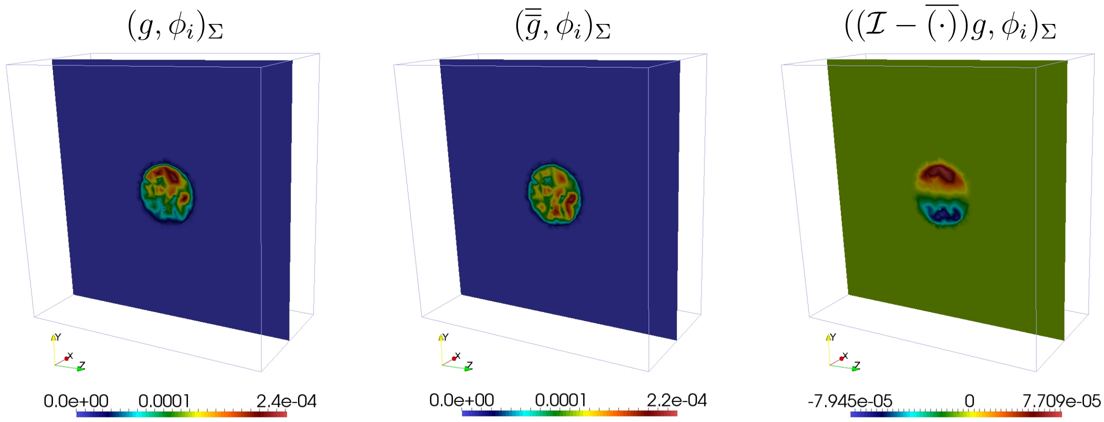

$\sum_i (g, w_i^{(1)})_\Sigma = 1.26\text{E-}01$ $\sum_i (\overline{\overline{g}}, w_i^{(1)})_\Sigma = 1.26\text{E-}01$ $\sum_i ((\mathcal{I} - \overline{\overline{(\cdot)}})g, w_i^{(1)})_\Sigma = \text{-}4.81\text{E-}07$

Figure 4.11: Terms depending on g: From left to right: $(g, \phi_i)_\Sigma$, $(\overline{\overline{g}}, \phi_i)_\Sigma$ and $((\mathcal{I} - \overline{\overline{(\cdot)}})g, \phi_i)_\Sigma$. In the first row, the plots are related to Scenario A, while the second row shows the simulations of Scenario B.

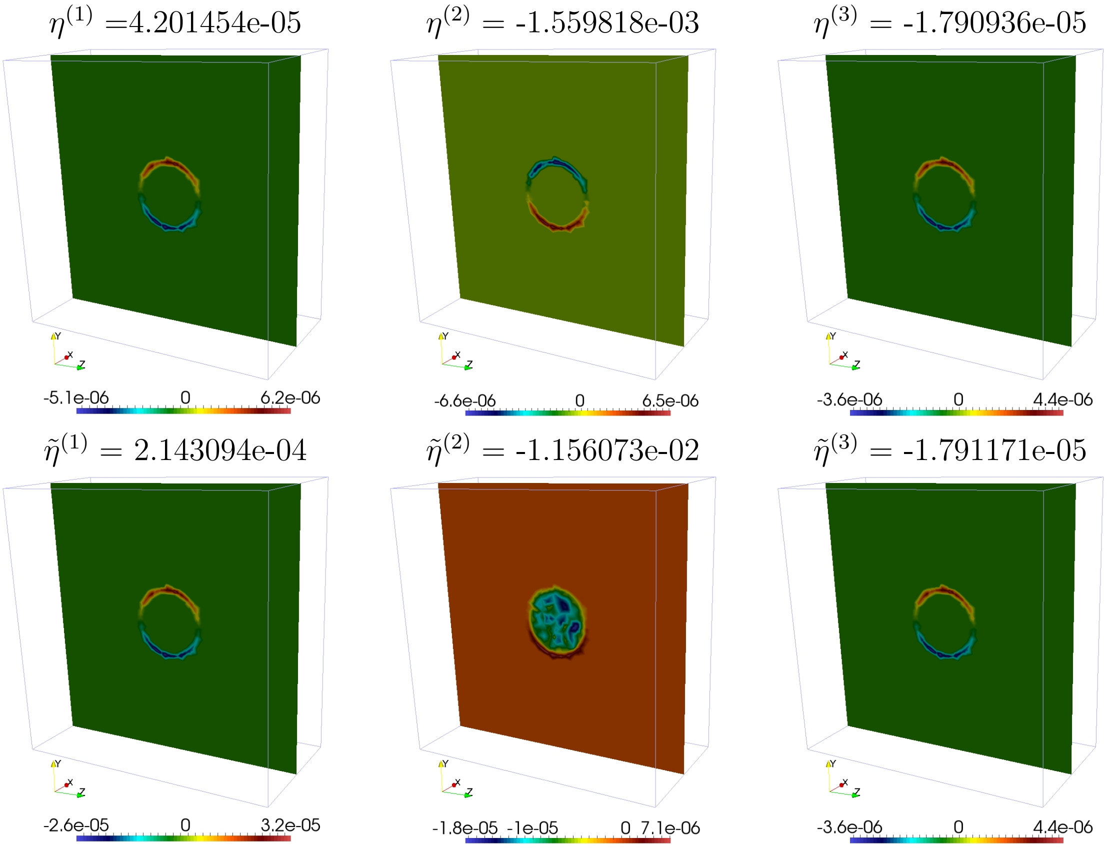

Figure 4.12: Estimators in Scenario C. In the first row, the reference estimators $\eta^{(1)}$, $\eta^{(2)}$, $\eta^{(3)}$; in the second row, the reduced estimators $\tilde{\eta}^{(1)}$, $\tilde{\eta}^{(2)}$, $\tilde{\eta}^{(3)}$

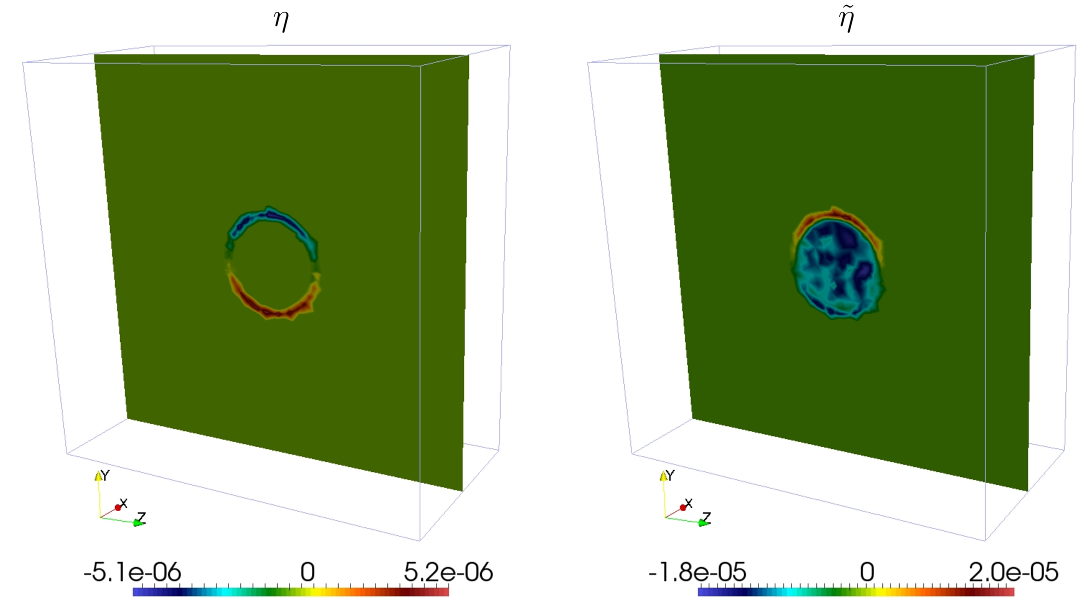

Figure 4.13: Global estimators in Scenario C. On the left, $\eta = \sum_i \eta^{(i)}$; on the right, $\tilde{\eta} = \sum_i \tilde{\eta}^{(i)}$.

4.6 Scenario E

We solve the primal reduced coupled problem (2.10) on a segment Λ from $(-0.51, 0, 0)$ to $(0.51, 0, 0)$, discretized with 1281 points, completely embedded in the parallelepiped $\Omega = (-1, 1)^2 \times (-0.51, 0.51)$; the tessellation of Ω is a quasi-uniform regular mesh, with characteristic length $h = 1/32 = 0.03125$, for a total of 354'753 tetrahedra. The other parameters are: $R = 0.25$, $k = 1$, $f = 1$ and $g = 1$.
We then solve the three reference dual problems (3.34), (3.39), (3.43), and the reduced dual problem (4.5), using the following linear operators: $j^{(1)}(v) = j_\Gamma^{(1)}(v)$, $j^{(2)}(v) = j_\Gamma^{(2)}(v)$, and $j^{(3)}(v) = j_\Gamma^{(3)}(v)$.
As one can observe, the only difference between Scenario A and Scenario E is the choice of the functionals in the dual problems: the theory holds for any linear operator, and depending on the application, one may want to use different definitions of the functionals. In this Scenario, we study the effect of operators the focus the attention to the interface Γ rather than the whole inclusion Σ.
In addition, we point out that, unlike the previous Scenarios, in Scenario D we don't provide the reduced weights and estimators: in fact, if we had to define the functional $J^{red}(\cdot)$ something like $J^{red}(\cdot) = J_\Lambda^{red}(\cdot)$, the solution of (4.5b) on Λ would be $Z \equiv 0$. As a result, $\tilde{w}^{(1)} \equiv 0$ and therefore $\tilde{eta}^{(1)} equiv0$. For this reason, in this case the reduced weights are not meaningful, and we do not provide them.

Scenario A: $f = 1$

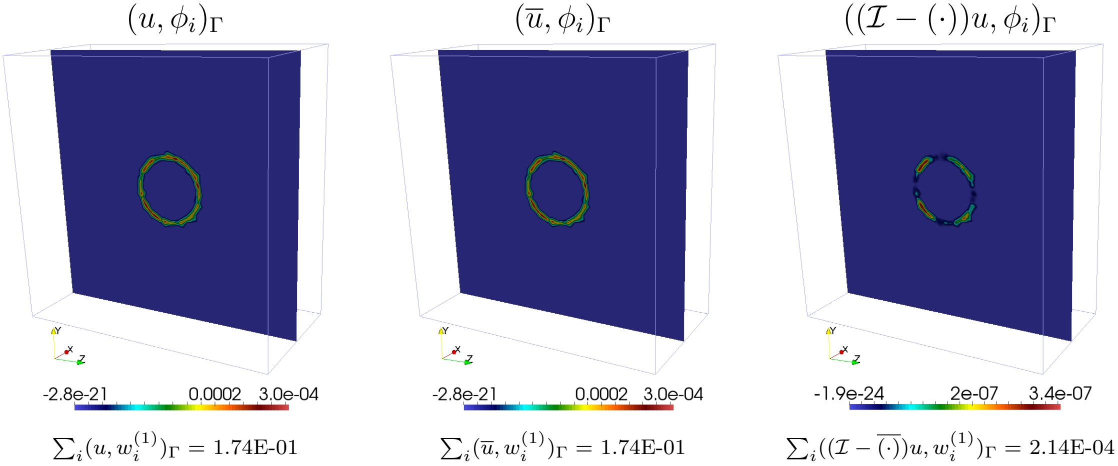

Scenario C: $f = 1 + y$

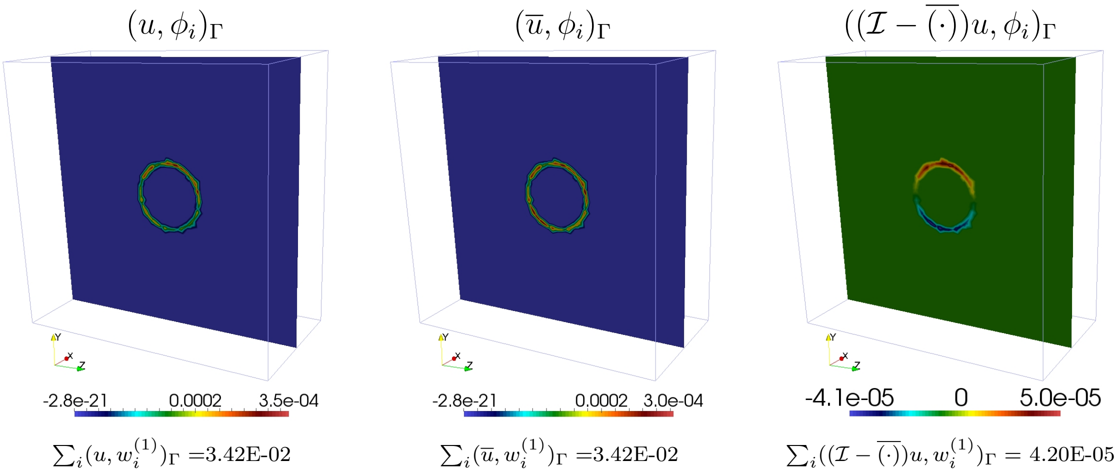

Figure 4.14: Terms depending on f: From left to right: $(u, \phi_i)_\Gamma$, $(\overline{u}, \phi_i)_\Gamma$ and $((\mathcal{I} - \overline{(\cdot)})u, \phi_i)_\Gamma$. In the first row, the plots are related to Scenario A, while the second row shows the simulations of Scenario C.

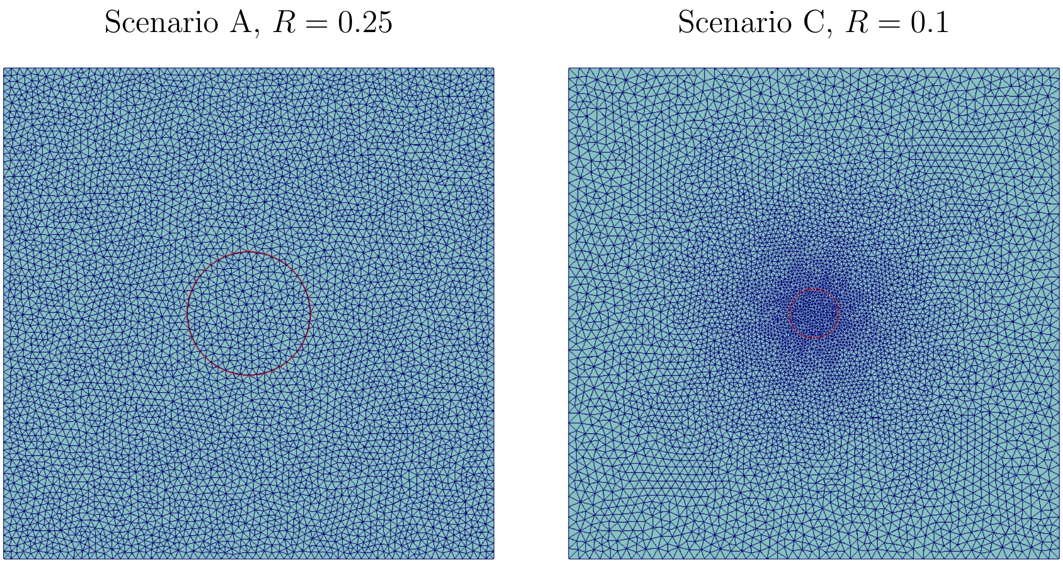
Scenario A, $R = 0.25$

Scenario C, $R = 0.1$

Figure 4.15: Different grids between Scenario A and Scenario D. On the left, the grid with $R = 0.25$ and 354’753 elements, of which 17’198 in Σ; on the right the grid with $R = 0.1$ and 347’870 elements, of which 47’523 in Σ

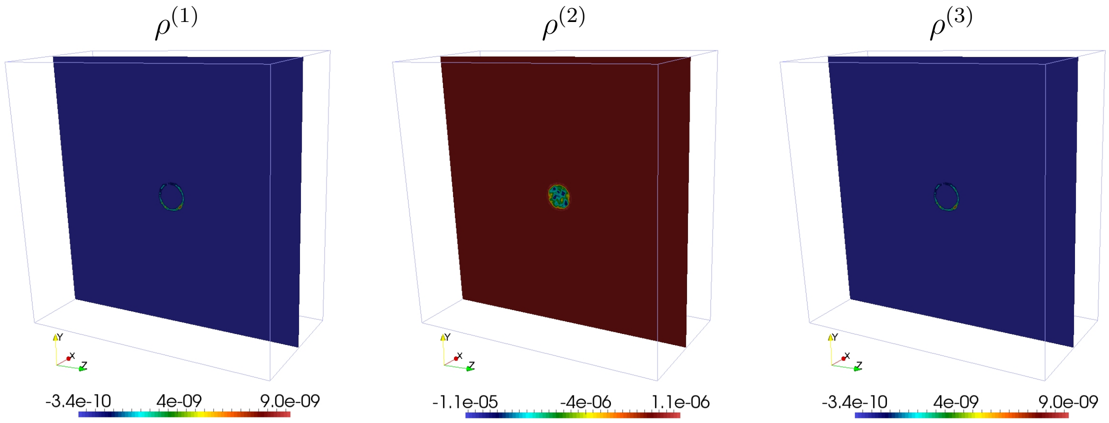
$\rho^{(1)}$

$\rho^{(2)}$

$\rho^{(3)}$

Figure 4.16: Residuals $\rho^{(1)}$, $\rho^{(2)}$, $\rho^{(3)}$ in Scenario D

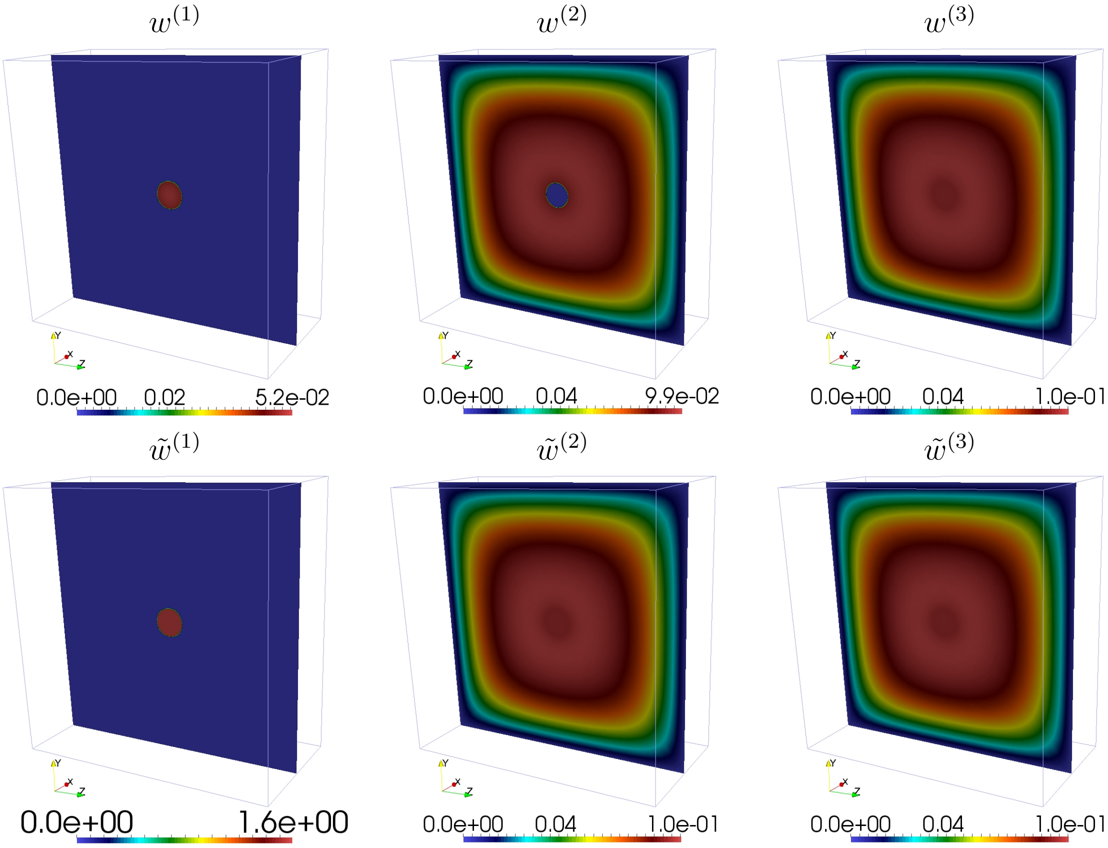

Figure 4.17: Weights in Scenario D. In the first row, the reference weights $w^{(1)}$, $w^{(2)}$, $w^{(3)}$; in the second row, the reduced weights $\tilde{w}^{(1)}$, $\tilde{w}^{(2)}$, $\tilde{w}^{(3)}$

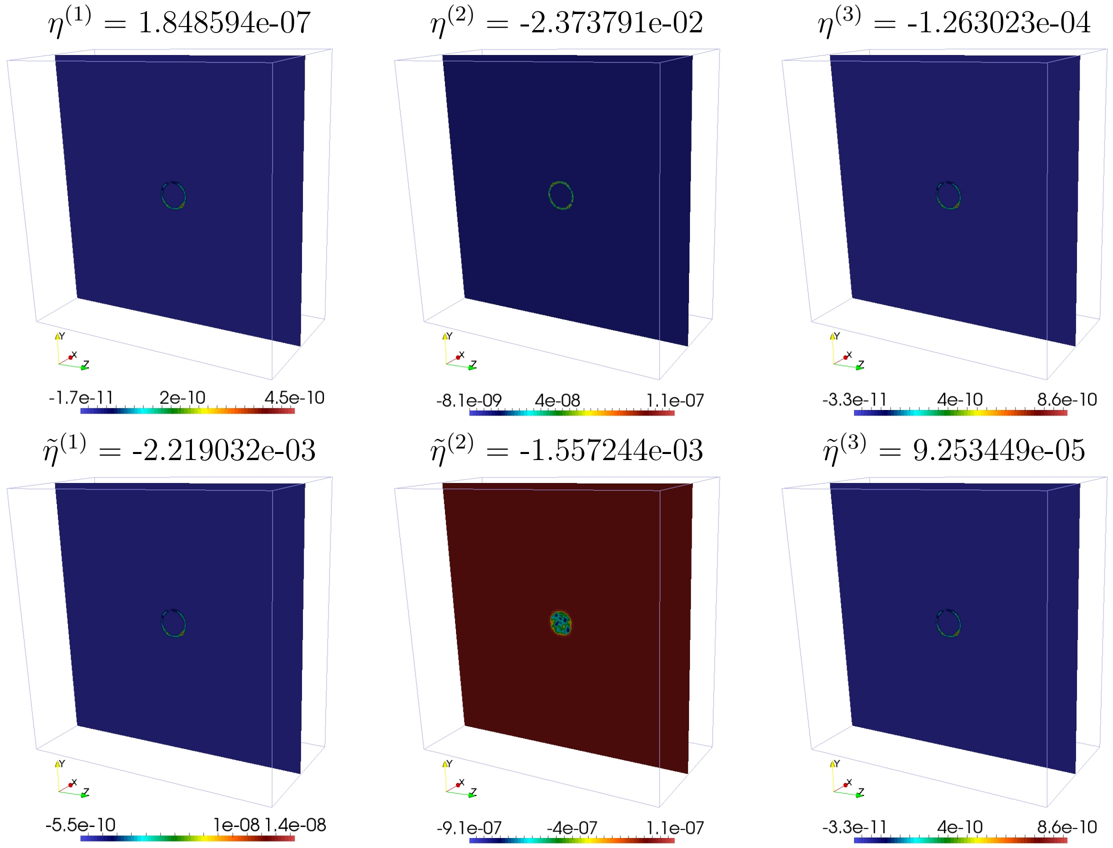
$\eta^{(1)}$ = 1.848594e-07 $\quad$ $\eta^{(2)}$ = -2.373791e-02 $\quad$ $\eta^{(3)}$ = -1.263023e-04

$\tilde{\eta}^{(1)}$ = -2.219032e-03 $\quad$ $\tilde{\eta}^{(2)}$ = -1.557244e-03 $\quad$ $\tilde{\eta}^{(3)}$ = 9.253449e-05

Figure 4.18: Estimators in Scenario D. In the first row, the reference estimators $\eta^{(1)}$, $\eta^{(2)}$, $\eta^{(3)}$; in the second row, the reduced estimators $\tilde{\eta}^{(1)}$, $\tilde{\eta}^{(2)}$, $\tilde{\eta}^{(3)}$

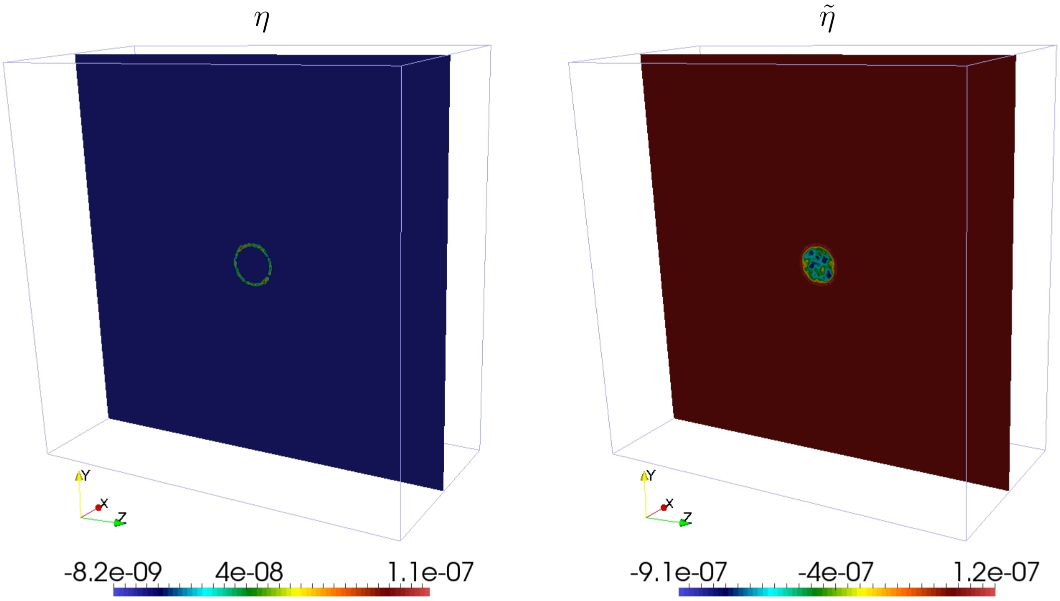

Figure 4.19: Global estimators in Scenario D. On the left, $\eta = \sum_i \eta^{(i)}$; on the right, $\tilde{\eta} = \sum_i \tilde{\eta}^{(i)}$.

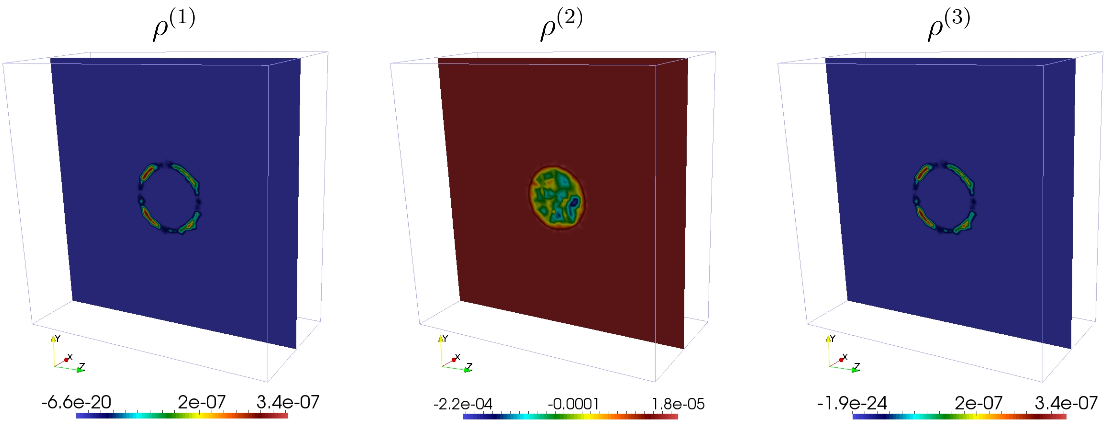

Figure 4.20: Residuals $\rho^{(1)}$, $\rho^{(2)}$, $\rho^{(3)}$ in Scenario E

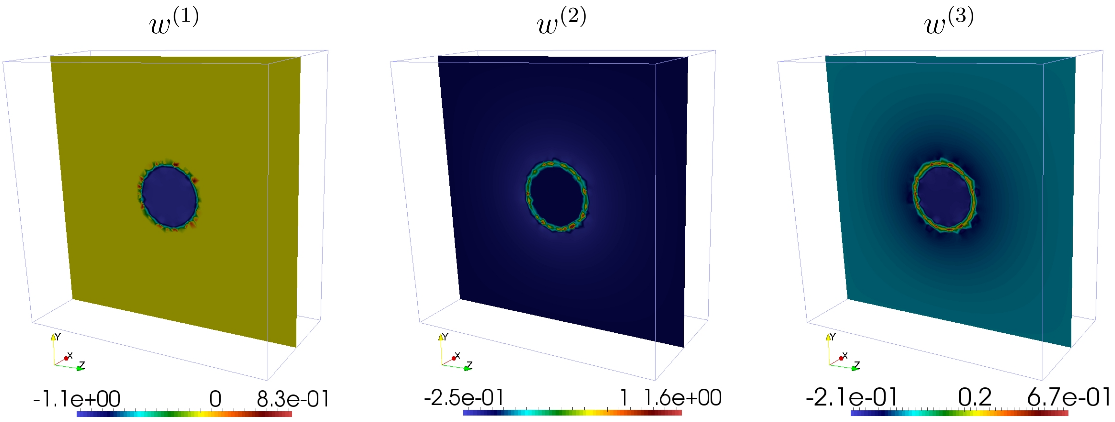

Figure 4.21: Reference weights $w^{(1)}$, $w^{(2)}$, $w^{(3)}$ in Scenario E.

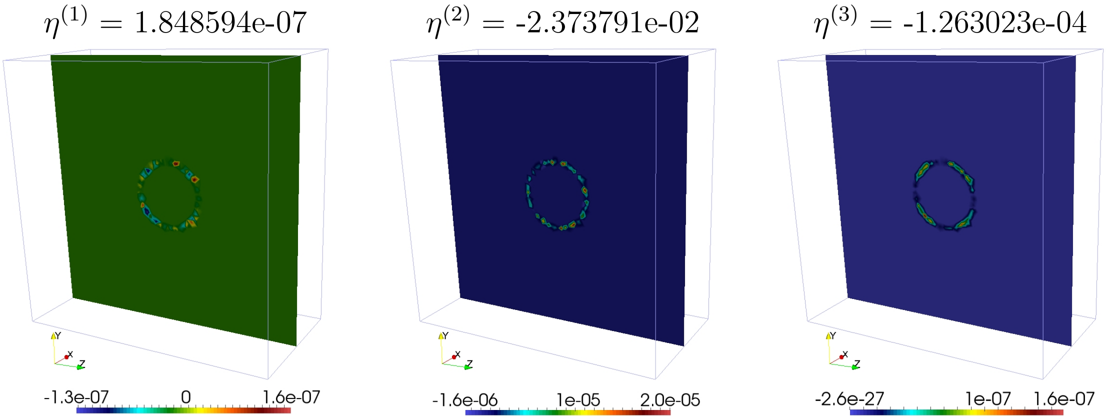

Figure 4.22: Reference estimators $\eta^{(1)}$, $\eta^{(2)}$, $\eta^{(3)}$ in Scenario E.

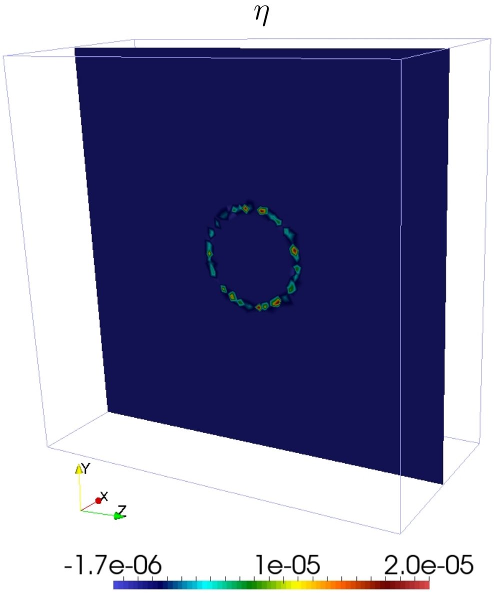

Figure 4.23: Global estimator $\eta = \sum_i \eta^{(i)}$ in Scenario E.

Finally, we can compute the residuals $\rho^{(i)}$ and the weights $w^{(i)}$ for $i = 1 : 3$ with the definitions (4.3), (4.2).

4.7 Discussion of the results

We now discuss the results of Sections 4.2, 4.3, 4.4, 4.5 and 4.6. We aim to understand where the modeling error is localized in the discrete mesh, what is its magnitude, which assumption brings the largest modeling error, how the radius and the choice of the functionals affect the estimators. We will point out different considerations on the results in order to answer these questions.

Scenario		$\eta^{(1)}$	$\eta^{(2)}$	$\eta^{(3)}$
A	w	2e-04	-1e-02	-1e-05
	$\tilde{w}$	4e-05	-1e-03	-1e-05
B	w	2e-04	-1e-02	-1e-05
	$\tilde{w}$	4e-05	-1e-03	-1e-05
C	w	4e-05	-1e-03	1e-05
	$\tilde{w}$	2e-04	-1e-02	1e-05
D	w	9e-07	-3e-05	-1e-06
	w	3e-05	-1e-03	-1e-06
E	w	1e-07	-2e-02	-1e.04

		$\eta^{(1)}$		$\eta^{(2)}$		$\eta^{(3)}$	
		$\min_i$	$\max_i$	$\min_i$	$\max_i$	$\min_i$	$\max_i$
A	w	-8e-21	4e-08	-1e-05	9e-07	-1e-25	3e-08
	$\tilde{w}$	-4e-20	2e-07	-1e-05	1e-06	-1e-25	3e-08
B	w	-1e-05	1e-05	-1e-06	9e-07	-1e-25	3e-08
	$\tilde{w}$	-5e-05	4e-05	-1e-05	1e-06	-1e-25	3e-08
C	w	-5e-06	6e-06	-6e-06	6e-06	-3e-06	4e-06
	$\tilde{w}$	-2e-05	3e-05	-2e-05	7e-06	-3e-06	4e-06
D	w	-1e-11	4e-10	-8e-09	1e-07	-3e-11	8e-10
	$\tilde{w}$	-6e-10	1e-08	-9e-07	1e-07	-3e-11	8e-10
E	w	-1e-07	1e-07	-1e-06	2e-05	-2e-27	1e-07

Table 4.2: Estimators in different Scenarios. In the first table, the values of $\eta^{(1)} = \sum_i \eta_i^{(1)}$, $\eta^{(2)} = \sum_i \eta_i^{(2)}$, and $\eta^{(3)} = \sum_i \eta_i^{(3)}$ in each Scenario. In the second table, the range of the localized estimator, that is their minimum and maximum value. For each Scenario, we provide the complete estimator $\eta^{(\cdot)} = \sum_i \rho_i^{(\cdot)} w_i^{(\cdot)}$ and the approximated estimator $\tilde{\eta}^{(\cdot)} = \sum_i \rho_i^{(\cdot)} \tilde{w}_i^{(\cdot)}$

Before we start the analysis, it's essential to recall the definitions of our estimators:

$$\begin{aligned}
\eta^{(1)} &= \sum_{i=1}^{N_h} w_i^{(1)}\, \rho_i^{(1)} = \sum_{i=1}^{N_h} w_i^{(1)}\, \left[((\mathcal{I} - \overline{\overline{(\cdot)}})g, \phi_i)_\Sigma + (\kappa(\mathcal{I} - \overline{(\cdot)})u, \phi_i)_\Gamma \right], \\
\eta^{(2)} &= \sum_{i=1}^{N_h} w_i^{(2)}\, \rho_i^{(2)} = \sum_{i=1}^{N_h} w_i^{(2)}\, \left[(\nabla u, \nabla \phi_i)_\Sigma - (\mathcal{E}_\Sigma f, \phi_i)_\Sigma \right], \\
\eta^{(3)} &= \sum_{i=1}^{N_h} w_i^{(3)}\, \rho_i^{(3)} = \sum_{i=1}^{N_h} w_i^{(3)}\, \left[-(\kappa(\mathcal{I} - \overline{(\cdot)})u, \phi_i)_\Gamma \right].
\end{aligned}$$

These estimators represents the modeling error, being $\eta^{(i)} = j(e^{(i)})$, where $e^{(i)}$ is the error due to the i-th assumption. Besides that, we define the reduced estimators $\tilde{\eta}^{(i)}$ using the reduced weights $\tilde{w}^{(i)}$, connected to the modeling error through the relationship $\tilde{\eta}^{(i)} = j(e^{(i)}) + o(w^{(i)} - \tilde{w}^{(i)}) \approx j(e^{(i)})$

The firs step of this discussion is the residual $\rho^{(1)}$, in particular $((\mathcal{I} - \overline{\overline{(\cdot)}})g, \phi_i)_\Sigma$. This integral on Σ represents the error due to the average $\overline{(\cdot)}$ on the quantities in the cross section $\mathcal{D}$. The Figure 4.11 highlights the fact that, when $g(s, r, t) = g(s)$ is constant in the cross section, the residual is equal to zero in all the inclusion. On the other hand, when g is variable in $\mathcal{D}$, the residual represents the variation of g. This is an interesting result, because if the source term in Σ is constant in our model, then the modeling error inside the inclusion depends only on $\eta^{(2)}$. All the remaining terms are integrals localized on the interface Γ.

The terms on the interface are $\sum_{i=1}^{N_h} w_i^{(1)}\, (\kappa(\mathcal{I} - \overline{(\cdot)})u, \phi_i)_\Gamma$ in $\eta^{(1)}$ and $\sum_{i=1}^{N_h} w_i^{(3)}\, (\kappa(\mathcal{I} - \overline{(\cdot)})u, \phi_i)_\Gamma$ in $\eta^{(3)}$. These terms are strictly connected with the function f, as shown in the Figure 4.14 in Scenario C. If f is constant around Γ, then the solution u is dependent only on the distance from the centerline Λ ($u(s, r, t) \equiv u(s, r)$). In such a case, $u(s) \approx \overline{u}(s)$. Therefore, the integrals on Γ becomes relevant especially when f is not constant around the inclusion.

In addition, one should notice that $l^{(1)}$ and $d^{(3)}$ actually are the same residual, $(\kappa(\mathcal{I} - \overline{(\cdot)})u, \phi_i)_\Gamma$, and they differ only by the weight that multiplies them. Therefore, when we sum the three estimators, one obtains:

$$\begin{aligned}
\eta =& \eta^{(1)} + \eta^{(2)} + \eta^{(3)} \\
=& + \sum_{i=1}^{N_h} w_i^{(1)}\, \left[((\mathcal{I} - \overline{\overline{(\cdot)}})g, \phi_i)_\Sigma \right] + \sum_{i=1}^{N_h} w_i^{(2)}\, \left[(\nabla u, \nabla \phi_i)_\Sigma - (\mathcal{E}_\Sigma f, \phi_i)_\Sigma \right] \\
& + \sum_{i=1}^{N_h} \left[w_i^{(1)} - w_i^{(3)} \right] \left[(\kappa(\mathcal{I} - \overline{(\cdot)})u, \phi_i)_\Gamma \right].
\end{aligned} \tag{4.10}$$

Then, the terms on Γ are weighted by the difference between $w_i^{(1)} \in \Sigma$ and $w_i^{(3)} \in \Omega$ at their interface. One can expect this difference to be smaller than the individual

weights.
It remains to discuss the estimator $\eta^{(2)}$: it represents how well the reduced elliptic problem is solved in the inclusion. Therefore, whereas the other terms depend on the computation of the averages of certain functions, this estimator depends on the discretization method in Σ. For this reason, we expect this error to be larger than the others and to affect the distribution of the global estimator η (see Table 4.2). In addition, one should be careful using the values of $\eta^{(2)}$ strictly inside Σ. In fact, $z_{\text{ref}}^{(2)}$ has no value in the inclusion, and the definition of the estimator holds for any extension of the reference dual solution. The safest extensions are $z_{\text{ref}}^{(2)} = 0$ (reference case) and $z_{\text{ref}}^{(2)}$ constant (reduced case) in the inclusion. Depending on the objectives (whether it's better to evaluate the functions only on Γ or if it's needed to analyze the function also in the inclusion) one can decide for one or the other extension.
We now compare Scenario A and Scenario D, which have different dimensions of the radius. According to the results on the L^2-norm of the modeling error, (3.45) and (3.46), the modeling error decreases when the radius is smaller. The results on Table 4.2 confirm this trend for what regards the L^1-norm of the modeling error. In fact, the estimators $\eta^{(i)}$ are considerably smaller in scenario D with respect to the other Scenarios. Anyway, Figures 4.7 and 4.18 show a similar pattern of the distribution of the modeling error. Therefore we can infer that the dimension of the radius affects only the magnitude of the error, but not its localization.
The theory employed holds for every definition of the linear operators j. Using, for example, functionals that evaluate the flux on the interface Γ allow us to focus on this region, instead of computing the error in the whole Σ. We can see that the estimators in Scenario E are larger with respect to the other Scenarios, because the functionals are localized in a smaller region, and the residuals are more weighed on Γ.
We now discuss the use of the reduced weights instead of the reference ones. The theory of Section 3.1 tells us that using the approximated representation formula of the modeling error we neglect higher-order terms, depending on the reference dual solution. These terms have a sign, since there is no absolute value, therefore we cannot *a priori* infer that the reduced estimators are smaller than the reference ones. Nevertheless, Table 4.2 confirms this trend: we can experimentally see that $\eta^{(i)} > \tilde{\eta}^{(i)}$. However, in $\eta^{(3)}$ it's not so evident what is the difference between complete and approximated estimators. One can argue that $z_{\text{ref}}^{(3)}$ is the closest reference dual solution to the reduced one, so it's not hard to think that $z_{\text{ref}}^{(3)} \approx z$. The larger difference between the reference and residual estimators lays in $\eta^{(2)}$. In fact, this reference estimator depends on the extension in Σ of the dual solution $z^{(2)}$. The choice of $w^{(2)} = 0$ in Σ results in an estimator with value only on Γ, while the reduced dual solution has non-zero values in the inclusion too, as highlighted just

above. With these considerations in mind, one can notice that, even though in the various Scenarios the values of $\eta^{(i)}$ can be different from the values of $\tilde{\eta}^{(i)}$, their localization is almost the same (see Figures 4.7, 4.9, 4.12,4.18).

In conclusion, we analyzed the different contributions of the modeling error in (4.10). The term $\sum_{i=1}^{N_h} w_i^{(1)} \left[((\mathcal{I} - \overline{\overline{(\cdot)}})g, \phi_i)_\Sigma\right]$ represents the variation of the solution in each cross section of the inclusion. It mainly depends on the function g. The term $\sum_{i=1}^{N_h} \left[w_i^{(1)} - w_i^{(3)}\right] \left[(\kappa(\mathcal{I} - \overline{(\cdot)})u, \phi_i)_\Gamma\right]$ represents the variation of the solution around the inclusion. It mainly depends on the function f and on the difference $w^{(1)} - w^{(3)}$. The term $\sum_{i=1}^{N_h} w_i^{(2)} \left[(\nabla u, \nabla \phi_i)_\Sigma - (\mathcal{E}_\Sigma f, \phi_i)_\Sigma\right]$ is linked to the resolution of the elliptic problem inside the inclusion. It mainly depends on the numerical solver and on the definition of the weight $w^{(2)}$ or $\tilde{w}^{(2)}$. We observed that the dimension of the radius is proportional to the magnitude of the modeling error. Besides, the reduced weights return a good approximation of the reference weights. Finally, we remark that our estimate of this error depends on the choice of the functional j.

Conclusion and future perspectives

The objective of this work was to propose an *a posteriori* estimate of the modeling error in coupled problems with topological reduction. To this purpose, we started in Chapter 1 with the derivation of a coupled model applied to microcirculation. This model was a time-dependent advection-diffusion-reaction PDE with source term depending on the solution $f = f(c_t, c_v)$ and concentrated on a manifold with different dimensionality, $f\delta_\Gamma$. We analyzed the weak formulation and the discrete approximation of the problem in order to use a finite element scheme. We implemented a C++ solver in order to simulate the particles transport in an arbitrarily complex network perfused in a generic biological tissue with known physical properties.

The next step is a rigorous analysis of the well-posedness of this problem. The complete formulation is not the right framework on which perform this analysis, so we moved to an elliptic formulation in Chapter 2. We explicitly derived the reduced formulation from the reference one, describing the essential three assumptions involved in the topological reduction. We proved the well-posedness of the reduced model and described the discretization of the differential problem.

The numerical results in Chapter 1 and the analysis in Chapter 2 persuade us that the model reduction is meaningful and reliable, especially if dimension of the inclusion is much smaller than the surrounding domain. Nevertheless, we need to further investigate the modeling error due to the topological reduction. Therefore, in Chapter 3 we laid the foundations for the *a posteriori* analysis of the modeling error, by introducing the Dual-Based Residual estimators. We derive the theory for a generic PDE and afterwards we applied to our specific problem. We identified the operators involved in the modeling reduction and we proved that their contribution depends on the radial dimension of the inclusions.

Finally, in Chapter 4 we explicitly wrote the discrete localized estimators, with the corresponding residuals and weights. We used our solver to simulate the coupled elliptic problem in different test cases and compute the DWR estimators.

Let us draw the conclusion of the present project and discuss the future perspective. The DWR estimators represent a simple but effective way to quantify the modeling error in topological reduction. The work proposed represents a first step on the *a posteriori* analysis of coupled 3D/1D problems, but certainly not the last. The results of Scenario D suggest that our estimator depends on the size of the inclusion, as expected from theory. Nevertheless, it's worth studying accurately the rate of convergence of the modeling error with respect to the radius. Furthermore, open questions remain on the discretization error. The general DWR theory provides for suitable *a posteriori* estimators for the numerical error. Future works will build a more general *a posteriori* framework able to distinguish the contribution related to the model reduction and to the discretization scheme. In this context it will be possible to deepen the considerations on the vanishing terms $d^{(1)}$, $l^{(3)}$, and on the estimator $\eta^{(2)}$. In fact, as shown in Chapter 4, this last term contains the greatest contribution of the modeling error,due to the discretization of the elliptic problem inside the inclusion. In addition, we have not collected enough evidence for choosing, for the simple test case considered here, between reference and reduced weights yet. The computational time of the dual reference and reduced problems are comparable, and the spatial distribution of the error is similar. Once an *a posteriori* error estimator will be developed for the numerical error, it will be possible to weigh up the benefits between the accuracy of the reference dual solution and the lower computational cost of the reduced dual solution. Finally, the DWR can be used for an adaptive scheme, in order to optimize the ratio between accuracy and computational cost of the simulation. As a final step, it can be applied to different contexts with few adjustment.

Appendices

Appendix A

C++ Code

We developed a C++ code that exhibits one-to-one correspondence with respect to the mathematical and numerical models derived in Chapters 1, 2, 3, 4. The code has been developed in the context of the MANworks project. The purpose is to develop a C++ library based on Getfem++ [47] for the solution of PDEs on networks coupled with the surrounding environment. The starting point of this project was the code by Domenico Notaro [39], that solve the equations of fluid dynamics 1.4. Our work was to implement a new solver for the transport equations 1.1, that could read the advection and pressure fields from the previous solver.

The latest stable release of the code is available on request. Please contact us via mail at stefano14.brambilla@mail.polimi.it or paolo.zunino@polimi.it.

A.1 Design of the code

Before starting to write the new solver, we decided to follow three main rules: separation, consistency and synthesis.
First, the solver for fluid problem is continuously being improved, in the whole context of the MANwork project. Therefore, we needed something that could use the different features of the first solver, but that was able to easily integrate the new versions of the code: we decided to keep the two solver as separated as possible.
Second, in order to make the code more readable, we decided to unify the terminology between the two solvers. Also, the whole structure of the library has been maintained as far as possible.
Third, we recognized that, apart from the structure of the monolithic matrix, the structure of the code was quite similar. We tried to not duplicate parts of code or objects used in both the solvers.

Since the fluid solver was written following the two main design principles of OOP, namely *encapsulation* and *information hiding*, it has been easy to achieve our goals. The fluid equations solver contains a main class, `problem3d1d`, containing all the attributes and methods which are needed to solve the fluid problems. We buildt a new class, `transport3d1d`, that inherits from the class `problem3d1d`. As a good programming practise, the declaration of the class `transport3d1d` was exported to an appropriate header file (`transport3d1d.hpp`), while its definition was moved to a source file (`transport3d1d.cpp`).
In the class `transport3d1d` we added all the new attributes for the transport problem, only when needed: for example, the header files `descr3d1d.hpp`, `dof3d1d.hpp` and `param3d1d.hpp` contained the definitions of the descriptors of the algorithm, the dimensions of the problem and the physical parameters, respectively, used in the fluid problem. We added the header files `descr3d1d_transp.hpp`, `dof3d1d_transp.hpp` and `param3d1d_transp.hpp` that contained the definitions of the descriptors of the algorithm, the dimensions of the problem and the physical parameters, respectively, that are used only in the transport problem. Furthermore, other attributes that are shared between the two problems, like the meshes, are not declared again.

```
//! Main class defining the coupled 3D/1D transport problem.
class transport3d1d: public problem3d1d {

public:
transport3d1d(void) :
mf_Ct(mesht), mf_Cv(meshv){}

///// Main methods for transport problem
//! Initialize the transport problem
void init_transp (int argc, char *argv[]);
//! Assemble the transport problem
void assembly_transp (void);
//! Solve the transport problem
bool solve_transp (void);
//! Export the transport solution
void export_vtk_transp (const string & time_suff = "",const string
    & suff = "");

///// Aux methods for interface with problem3d1d class
//! Initialize the fluid problem
void init_fluid (int argc, char *argv[]);
//! Assemble the fluid problem
void assembly_fluid (void);
//! Solve the fluid problem
bool solve_fluid (void);
//! Export the fluid solution
void export_vtk_fluid (const string & suff = "");
```

```
///// Methods for processing the solution
//! Compute residuals for mass balance at each junction
void mass_balance (void);
//! Compute the test for convergence error
void convergence_error(void);
//! Compute the dual problems and estimators for modeling error
void model_error(void)

protected:

//! Finite Element Method for the tissue concentration @f$c_t@f$
mesh_fem mf_Ct;
//! Finite Element Method for the vessel concentration @f$c_v@f$
mesh_fem mf_Cv;


//! Algorithm description strings (mesh files, FEM types, solver
    info, ...)
descr3d1d_transp descr_transp;
//! Physical parameters
param3d1d_transp param_transp;
//! Number of degrees of freedom
dof3d1d_transp dof_transp;


//! List of BC nodes of the network
vector< node > BCv_transp;
//! List of BC nodes of the tissue
vector< node > BCt_transp;
//! List of junction nodes of the network
vector< node_transp > Jv_transp;

//! Monolithic matrix for the coupled problem
sparse_matrix_type AM_transp;
//! Monolithic array of unknowns for the coupled problem
vector_type        UM_transp;
//! Monolithic right hand side for the coupled problem
vector_type        FM_transp;

//Monolithic temporary matrix for update
sparse_matrix_type AM_temp;
//Monolithic temporary right hand side for update
vector_type        FM_temp;


// Aux methods for init
//! Import algorithm specifications
void import_data_transp(void);
//! Import mesh for tissue (3D) and vessel (1D)
```

```
void build_mesh_transp(void);
//! Set finite elements methods and integration methods
void set_im_and_fem_transp(void);
//! Build problem parameters
void build_param_transp(void);
//! Build the list of tissue boundary data
/*! Face numbering:
0 : {x = 0 }  "back"
1 : {x = Lx}  "front"
2 : {y = 0 }  "left"
3 : {y = Ly}  "right"
4 : {z = 0 }  "bottom"
5 : {z = Lz}  "top"
*/
void build_tissue_boundary_transp(void);
//! Build the list of vessel boundary (and junctions) data
void build_vessel_boundary_transp(void);

//Aux method for assembly
//! Build the monolithic matrix AM_transp by blocks
void assembly_mat_transp(void);
//! Build the monolithic rhs FM_transp by blocks
void assembly_rhs_transp(void);

//Aux method for solve
//! Aux function for update of rhs at each time step
void update_transp(void);



}; //end of class trasport3d1d
```

The structure of the user-interface is preserved: the code is divided in four main steps: (*i*) initializing of the problem, (*ii*) assembling of the linear system, (*iii*) solving it and (*iv*) saving the solution for post-processing. These phases are the only methods that remain **public**.

Remark A.1.1. In order to have only this methods in the user-interface, we choosed to run the time loop inside the function `solve_transp`(); therefore, in order to save the solution at each time step, we decided to insert the method `export_vtk_transp` directly in the solver. Anyway, one can call the export method at the end of the `main.cpp`.

```

// Declare a new problem
getfem::transport3d1d p;

//////// fluid problem: velocity field and pressure
```

```
// Initialize the problem
p.init_fluid(argc, argv);
// Build the monolithic system
p.assembly_fluid();
// Solve the problem
if (!p.solve_fluid()) GMM_ASSERT1(false, "solve procedure has
   failed");
// Save results in .vtk format
p.export_vtk_fluid();

//////// transport problem: concentration

//initialize
p.init_transp(argc, argv);
//assemble
p.assembly_transp();
//solve
if (!p.solve_transp()) GMM_ASSERT1(false, "solve procedure has
   failed");  // the export is in the solve at each time step
```

The package MANworks contains:

`fluid`/ : A stable version of the code for fluid problem

`transport`/ : The code for transport problem

`Makefile` : Instruction to install the whole project

The folder `fluid`/ can be replaced with any new release of the code. The folder `transport`/ has the following structure:

`doc`/ : Code documentation (to be generated).

`include`/ : General header files

`lib`/ : Main library (to be generated)

`src`/ : Example sources

- `1_uncoupled_branch`/ : solve the uncoupled 1d and 3d problems
- `2_coupled_branch`/ : solve the coupling with single-vessel network
- `3_bifurcation`/ : solve the problem with Y-shaped network
- `4_network`/ : simulate the transport of particles in a network with physiological parameters

`config.mk` : Instruction to find the GetFEM++ and the problem3d1d libraries in the system

`Doxyfile` : Instruction to build the code documentation

`Makefile` : Instruction to install the whole project

`vtk/` : Output in vtk format

`input.param` : List of user-defined parameters

`main.cpp` : Main program

`Makefile` : Instruction to install the example

`mesh1d/` : One-dimensional meshes in pts format

- `network.pts` : File of points of the vessel network, with boundary conditions for fluid problem
- `network_transp.pts` : File of points of the vessel network, with boundary conditions for transport problem

A.2 Assembling routines

After the design of the main class, we assemble the different terms arising from 1.18. The buildt-in functions of Getfem++, and the tool `generic_assembly` for non-standard terms, are the basis for the assembling phase.

In `assembling1d_transp.hpp` we build the matrixes $\mathcal{M}_v$ and $\mathcal{A}_v$. The function `asm_network_transp` builds in particolar the mass matrix for time derivative and the stiffness matrix for the diffusion term; the function `asm_advection_network` builds the two advection terms 1.14.

```
template<typename MAT, typename VEC, typename VEC2>
void
asm_network_transp
(MAT & M, MAT & D,
const mesh_im & mim,
const mesh_fem & mf_c,
const mesh_fem & mf_data,
const VEC & diff,
const VEC2 & R,
const mesh_region & rg = mesh_region::all_convexes()
)
{
```

```
GMM_ASSERT1(mf_c.get_qdim() == 1 ,
"invalid data mesh fem (Qdim=1 required)");
//build mass matrix Mv for time derivative
VEC param(mf_data.nb_dof()); gmm::clear(param);
gmm::add(R, param);
gmm::vscale(R, param);
gmm::scale(param, pi); //param = pi*R^2
getfem::asm_mass_matrix_param(M, mim, mf_c, mf_data, param, rg);
// Build the diffusion matrix Dv
gmm::vscale(diff, param); //param= 2pi*R^2*Av
getfem::asm_stiffness_matrix_for_laplacian(D,mim,mf_c,mf_data,
    param, rg);

} //end of asm_network_transp
```

```
template<typename MAT, typename VEC>
void
asm_advection_network
(MAT & B,
const mesh_im & mim,
const mesh_fem & mf_c,
const mesh_fem & mf_data,
const mesh_fem & mf_u,
const mesh_fem & mf_R,
const VEC & U,
const VEC & lambdax, const VEC & lambday, const VEC & lambdaz,
const VEC & R,
const mesh_region & rg = mesh_region::all_convexes()
)
{
generic_assembly
assem1("l1=data$1(#2); l2=data$2(#2); l3=data$3(#2);  u=data$4(#3)
    ; R=data$5(#4);"
"t=comp(Base(#1).Grad(#1).Base(#2).Base(#3).Base(#4).Base(#4));"
"M$1(#1,#1)+=t(:,:,1,i,p,m,n).l1(i).u(p).R(m).R(n)+t(:,:,2,i,p,m,n
    ).l2(i).u(p).R(m).R(n)+t(:,:,3,i,p,m,n).l3(i).u(p).R(m).R(n);")
    ;
assem1.push_mi(mim);
assem1.push_mf(mf_c);
assem1.push_mf(mf_data);
assem1.push_mf(mf_u);
assem1.push_mf(mf_R);
assem1.push_data(lambdax);
assem1.push_data(lambday);
assem1.push_data(lambdaz);
assem1.push_data(U);
assem1.push_data(R);
assem1.push_mat(B);
assem1.assembly(rg);
```

```
generic_assembly
assem2("l1=data$1(#2); l2=data$2(#2); l3=data$3(#2);  u=data$4(#3)
   ;  R=data$5(#4);"
"t=comp(Base(#1).Base(#1).Base(#2).Grad(#3).Base(#4).Base(#4));"
"M$1(#1,#1)+=t(:,:,i,p,1,m,n).l1(i).u(p).R(m).R(n)+t(:,:,i,p,2,m,n
   ).l2(i).u(p).R(m).R(n)+t(:,:,i,p,3,m,n).l3(i).u(p).R(m).R(n);")
   ;
assem2.push_mi(mim);
assem2.push_mf(mf_c);
assem2.push_mf(mf_data);
assem2.push_mf(mf_u);
assem2.push_mf(mf_R);
assem2.push_data(lambdax);
assem2.push_data(lambday);
assem2.push_data(lambdaz);
assem2.push_data(U);
assem2.push_data(R);
assem2.push_mat(B);
assem2.assembly(rg);

} //end of asm_advection_network
```

In `assembling3d_transp.hpp` we build the matrixes $\mathcal{M}_t$ and $\mathcal{A}_t$. The function `asm_tissue_transp` builds in particolar the mass matrix for time derivative, the stiffness matrix for the diffusion term and the reaction terms; the function `asm_advection_tissue` builds the two advection terms 1.9.

```
template<typename MAT, typename VEC>
void
asm_tissue_transp
(MAT & M, MAT & D,MAT & R,
const mesh_im & mim,
const mesh_fem & mf_c,
const mesh_fem & mf_coef,
const VEC & diff_data,
const VEC & reac_data,
const mesh_region & rg = mesh_region::all_convexes()
)
{
GMM_ASSERT1(mf_c.get_qdim() == 1,
"invalid data mesh fem for pressure (Qdim=1 required)");
// Build the mass matrix Mt (consumption)
getfem::asm_mass_matrix_param(R, mim, mf_c, mf_coef, reac_data, rg
   );
// Build the mass matrix Tt for time derivative
getfem::asm_mass_matrix(M, mim, mf_c, rg);
// Build the divergence matrix Dtt
getfem::asm_stiffness_matrix_for_laplacian(D,mim,mf_c, mf_coef,
```

```
    diff_data, rg);

} /* end of asm_tissue_transp*/
```

```
template<typename MAT, typename VECT>
void asm_advection_tissue(MAT &B, const getfem::mesh_im &mim,
const getfem::mesh_fem &mf,
const getfem::mesh_fem &mfvel,
const VECT &vel,
const mesh_region & rg = mesh_region::all_convexes()
) {
getfem::generic_assembly
assem1("vel=data(#2);"
"M$1(#1,#1) += comp(Base(#1).Grad(#1).vBase(#2)) (:, :,i, k,i).vel
    (k);");
assem1.push_mi(mim);
assem1.push_mf(mf);
assem1.push_mf(mfvel);
assem1.push_data(vel);
assem1.push_mat(B);
assem1.assembly(rg);


getfem::generic_assembly
assem2("vel=data(#2);"
"M$1(#1,#1) += comp( Base(#1).Base(#1).vGrad(#2) )(:, :,k, p,p).
    vel(k);");
assem2.push_mi(mim);
assem2.push_mf(mf);
assem2.push_mf(mfvel);
assem2.push_data(vel);
assem2.push_mat(B);
assem2.assembly(rg);
}  /* end of asm_advection_tissue*/
```

The coupling terms B_{tt}, B_{tv}, B_{vt} and B_{vv} are easily assembled by the routines in `assembling3d1d_transp.hpp`, that essentially exploits the corresponding functions in `assembling3d1d.hpp` paying attention at the parameter for permeability.

The boundary conditions are assembled by the functions `asm_network_bc_transp`, `asm_tissue_bc_transp` and `asm_coupled_bc_transp`. As for the fluid equations, the user can choose between Dirichlet and Robin conditions for every face of the tissue Ω and every inlet or outlet point of the network Λ.

```
template<typename MAT, typename VEC>
void
asm_network_bc_transp
(VEC & F, MAT & M,
```

```
const mesh_im & mim,
const mesh_fem & mf_c,
const mesh_fem & mf_data,
const std::vector<getfem::node> & BC,
const scalar_type beta,
const VEC & R)
{
GMM_ASSERT1(mf_c.get_qdim()==1,  "invalid data mesh fem (Qdim=1
    required)");
GMM_ASSERT1(mf_data.get_qdim()==1, "invalid data mesh fem (Qdim=1
    required)");


for (size_type bc=0; bc < BC.size(); bc++) {
GMM_ASSERT1(mf_c.linked_mesh().has_region(bc), "missed mesh region
    " << bc);
if (BC[bc].label=="DIR") { // Dirichlet BC
VEC BC_temp(mf_c.nb_dof(), BC[bc].value);
getfem::assembling_Dirichlet_condition(M, F, mf_c, BC[bc].rg,
    BC_temp);
gmm::clear(BC_temp);
}
else if (BC[bc].label=="MIX") { // Robin BC
VEC BETA(mf_data.nb_dof(), beta*pi);
gmm::vscale(R, BETA); gmm::vscale(R, BETA);
getfem::asm_mass_matrix_param(M, mim, mf_c, mf_data, BETA,mf_c.
    linked_mesh().region(BC[bc].rg) ); //int(beta*cv*bv)

VEC BETA_C0(mf_data.nb_dof(), pi*beta*BC[bc].value);
gmm::vscale(R, BETA_C0); gmm::vscale(R, BETA_C0);
asm_source_term(F,mim, mf_c, mf_data,BETA_C0); //int(beta*c0*bv)
}
else if (BC[bc].label=="INT") { // Internal Node
GMM_WARNING1("internal node passed as boundary.");
}
else if (BC[bc].label=="JUN") { // Junction Node
GMM_WARNING1("junction node passed as boundary.");
}
else {
GMM_ASSERT1(0, "Unknown Boundary Condition"<< BC[bc].label << endl
    );
}
}

}
```

```
template<typename MAT, typename VEC>
void
asm_tissue_bc_transp
```

```
(VEC & F,
MAT & M,
const mesh_im & mim,
const mesh_fem & mf_c,
const mesh_fem & mf_data,
const std::vector<getfem::node> & BC,
const scalar_type beta
)
{



GMM_ASSERT1(mf_c.get_qdim()==1,  "invalid data mesh fem (Qdim=1
   required)");
GMM_ASSERT1(mf_data.get_qdim()==1, "invalid data mesh fem (Qdim=1
   required)");


for (size_type bc=0; bc < BC.size(); ++bc) {
GMM_ASSERT1(mf_c.linked_mesh().has_region(bc), "missed mesh region
   " << bc);
if (BC[bc].label=="DIR") { // Dirichlet BC
VEC BC_temp(mf_c.nb_dof(), BC[bc].value);
getfem::assembling_Dirichlet_condition(M, F, mf_c, BC[bc].rg,
   BC_temp);
gmm::clear(BC_temp);
}
else if (BC[bc].label=="MIX") { // Robin BC
VEC BETA(mf_data.nb_dof(), beta);
getfem::asm_mass_matrix_param(M, mim, mf_c, mf_data, BETA,mf_c.
   linked_mesh().region(BC[bc].rg) );

VEC BETA_C0(mf_data.nb_dof(), beta*BC[bc].value);
asm_source_term(F,mim, mf_c, mf_data,BETA_C0);

}
else if (BC[bc].label=="INT") { // Internal Node
GMM_WARNING1("internal node passed as boundary.");
}
else if (BC[bc].label=="JUN") { // Junction Node
GMM_WARNING1("junction node passed as boundary.");
}
else {
GMM_ASSERT1(0, "Unknown Boundary Condition " << BC[bc].label <<
   endl);
}
}

} /* end of asm_tissue_bc */
```

```
template<typename MATRM, typename VECT1, typename VECT2>
void assembling_Dirichlet_condition_coupled_tissue
(MATRM &B, VECT1 &F, const mesh_fem &mf1, const mesh_fem &mf2,
    size_type boundary,
const VECT2 &DIR) {

size_type Q1=mf1.get_qdim();
size_type Q2=mf2.get_qdim();

size_type nb_dof1=mf1.nb_dof();
size_type nb_dof2=mf2.nb_dof();

GMM_ASSERT1(!(mf1.is_reduced()), "This function is not adapted to
    "
"reduced finite element methods");
GMM_ASSERT1(!(mf2.is_reduced()), "This function is not adapted to
    "
"reduced finite element methods");

dal::bit_vector nndof = mf1.basic_dof_on_region(boundary);
pfem pf1;

for (dal::bv_visitor cv(mf1.convex_index()); !cv.finished(); ++cv)
     {    //per tutti i convessi cv della mesh 1

pf1 = mf1.fem_of_element(cv);
pdof_description ldof = lagrange_dof(pf1->dim());
size_type nbd = pf1->nb_dof(cv);
for (size_type i = 0; i < nbd; i++) {         //per tutti i dof i
    del convesso cv
size_type dof1 = mf1.ind_basic_dof_of_element(cv)[i*Q1];         //
    trova l'indice delle colonne riferite all
if (nndof.is_in(dof1) && pf1->dof_types()[i] == ldof) {     //se
    il dof i del convesso cv    in "boundary"

for (size_type j = nb_dof1; j < nb_dof1+ nb_dof2; j++) {         //
    allora per tutti i dof j della mesh 2
for (size_type l = 0; l < Q1; ++l) {
F[j] -= B(j, dof1+l) * DIR[dof1+l];
B(j, dof1+l) =  0;
B(dof1+l, j) =  0;
}
}
}
}
}
} /* end of assembling_Dirichlet_condition_coupled_tissue*/
```

```
template<typename MATRM, typename VECT1, typename VECT2>
void assembling_Dirichlet_condition_coupled_vessel
(MATRM &B, VECT1 &F, const mesh_fem &mf1, const mesh_fem &mf2,
   size_type boundary,
const VECT2 &DIR) {

size_type Q1=mf1.get_qdim();
size_type Q2=mf2.get_qdim();

size_type nb_dof1=mf1.nb_dof();
size_type nb_dof2=mf2.nb_dof();

GMM_ASSERT1(!(mf1.is_reduced()), "This function is not adapted to
   "
"reduced finite element methods");
GMM_ASSERT1(!(mf2.is_reduced()), "This function is not adapted to
   "
"reduced finite element methods");

dal::bit_vector nndof = mf2.basic_dof_on_region(boundary);
pfem pf2;

for (dal::bv_visitor cv(mf2.convex_index()); !cv.finished(); ++cv)
    {    //per tutti i convessi cv della mesh 1

pf2 = mf2.fem_of_element(cv);
pdof_description ldof = lagrange_dof(pf2->dim());
size_type nbd = pf2->nb_dof(cv);
for (size_type i = 0; i < nbd; i++) {          //per tutti i dof i
   del convesso cv
size_type dof2 = mf2.ind_basic_dof_of_element(cv)[i*Q2];         //
   trova l'indice delle colonne riferite all
if (nndof.is_in(dof2) && pf2->dof_types()[i] == ldof) {      //se
   il dof i del convesso cv    in "boundary"

for (size_type j = 0; j < nb_dof1; j++) {       //allora per tutti
    i dof j della mesh 2
for (size_type l = 0; l < Q2; ++l) {
F[j] -= B(j, nb_dof1 + dof2+l) * DIR[nb_dof1 + dof2+l];
B(j, nb_dof1 + dof2+l) =  0;
B(nb_dof1 + dof2+l, j) =  0;
}
}
}
}
}
```

```
} /* end of assembling_Dirichlet_condition_coupled_vessel*/



template<typename MAT, typename VEC>
void
asm_coupled_bc_transp
(MAT & M,
VEC & F,
const mesh_fem & mf_ct,
const mesh_fem & mf_cv,
const std::vector<getfem::node> & BC_tissue,
const std::vector<getfem::node> & BC_vessel
)
{

GMM_ASSERT1(mf_ct.get_qdim()==1,  "invalid data mesh fem (Qdim=1
   required)");
GMM_ASSERT1(mf_cv.get_qdim()==1,  "invalid data mesh fem (Qdim=1
   required)");

//cycle over the tissue boundary nodes
for (size_type bc=0; bc < BC_tissue.size(); ++bc) {
GMM_ASSERT1(mf_ct.linked_mesh().has_region(bc), "missed mesh
   region" << bc);
if (BC_tissue[bc].label=="DIR") { // Dirichlet BC
VEC BC_temp(mf_ct.nb_dof(), BC_tissue[bc].value);
getfem::assembling_Dirichlet_condition_coupled_tissue(M, F, mf_ct,
    mf_cv, BC_tissue[bc].rg, BC_temp);
gmm::clear(BC_temp);
}
}

//cycle over the vessels boundary nodes
for (size_type bc=0; bc < BC_vessel.size(); ++bc) {
GMM_ASSERT1(mf_cv.linked_mesh().has_region(bc), "missed mesh
   region" << bc);
if (BC_vessel[bc].label=="DIR") { // Dirichlet BC
VEC BC_temp(mf_cv.nb_dof(), BC_vessel[bc].value);
getfem::assembling_Dirichlet_condition_coupled_vessel(M, F, mf_ct,
    mf_cv, BC_vessel[bc].rg, BC_temp);
gmm::clear(BC_temp);
}
}

} /* end of asm_coupled_bc_transp */
```

A.3 The library `transport3d1d`

With the code above described, we build a dynamic library collecting all the routines, external functions and variables defining our coupled 3D-1D transport problem.
There are many pros and cons to take in considerations when choosing between a static and a dynamic library. For example, the library of the fluid problem, `libproblem3d1d.a`, was buildt statically: the size of the executable with the static linking is comparable to the total size of the executable with the dynamic linking and the files of the library; therefore, there were no need to build the library dynamically, preferring a stand-alone executable. On the other hand, for the transport problem we opted for dynamic linking: the MANwork project is fastly getting wider, with different versions of the code. In this context, we prefer to have more flexible executable, that can quickly load different libraries when necessary, without the need of recompilation.
Anyway, we finally decided to let the user choose between static and dynamic linking: the Makefile in `MANworks/transport/include` contains both the instructions. The default `make` will install the library `libtransport3d1d.so` dynamically, while a `make static` will install the library `libtransport3d1d.a` statically. The library for transport problem is buildt from the following headers:

`assembling1d_transp.hpp` :	Miscellaneous assembly routines for the 1D network problem
`assembling3d_transp.hpp` :	Miscellaneous assembly routines for the 3D tissue problem
`assembling3d1d_transp.hpp` :	Miscellaneous assembly routines for the 3D-1D coupling
`descr3d1d_transp.hpp` :	Definition of the aux class for algorithm description strings
`dof3d1d_transp.hpp` :	Definition of the aux class for the number of degrees of freedom
`node_transp.hpp` :	Definition of the class *node_transp*
`param3d1d_transp.hpp` :	Definition of the aux class for physical parameters
`transport3d1d.cpp`:	Definition of the main class for the 3D-1D coupled transport problem

`transport3d1d.hpp` : Declaration of the main class for the 3D-1D coupled transport problem

`model_error.cpp`: Definition of the methods for computing the modeling error

`convercenge_error.cpp`: Definition of the methods for computing the convergence error

`utilities_transp.hpp` : Miscellaneous aux functions for the 3D-1D coupled transport problem

See the README file for installation instructions.

A.4 Doxygen documentation

The whole code has been extensively commented and documented. The last release of the code provides the possibility to automatically generate a detailed code documentation using Doxygen . See the README file for installation instructions.

Bibliography

[1] Mark Ainsworth and J.Tinsley Oden. A posteriori error estimation in finite element analysis. *Computer Methods in Applied Mechanics and Engineering*, 142(1):1 – 88, 1997.

[2] Serge Alinhac and Patrick Gérard. *Pseudo-differential operators and the Nash-Moser theorem*, volume 82 of *Graduate Studies in Mathematics*. American Mathematical Society, Providence, RI, 2007. Translated from the 1991 French original by Stephen S. Wilson.

[3] Roland Becker and Rolf Rannacher. An optimal control approach to a posteriori error estimation in finite element methods. *Acta Numerica*, 10:1102, 2001.

[4] Gregory Berkolaiko, Robert Carlson, Stephen A. Fulling, and Peter Kuchment. *Quantum graphs and their applications*, volume 415 of *Contemporary Mathematics*. American Mathematical Society, Providence, RI, 2006.

[5] S. Bertoluzza, A. Decoene, L. Lacouture, and S. Martin. Local error estimates of the finite element method for an elliptic problem with a dirac source term. *Numerical Methods for Partial Differential Equations*, 34(1):97–120, 2018.

[6] Wietse Boon, Jan Nordbotten, and Jon Vatne. Mixed-dimensional elliptic partial differential equations. Technical report, arXiv, Cornell University Library, 2017. arXiv:1710.00556v2.

[7] M. Braack and A. Ern. A posteriori control of modeling errors and discretization errors. *Multiscale Modeling & Simulation*, 1(2):221–238, 2003.

[8] Susanne C. Brenner. Poincar–friedrichs inequalities for piecewise h1 functions. *SIAM Journal on Numerical Analysis*, 41(1):306–324, 2003.

[9] L. Cattaneo. *FEM for PDEs with unfitted interfaces: application to flow through heterogeneous media and microcirculation, PhD Thesis*. Politecnico di Milano, 2014.

[10] L. Cattaneo and P. Zunino. A computational model of drug delivery through microcirculation to compare different tumor treatments. *International Journal for Numerical Methods in Biomedical Engineering*, 30(11):1347–1371, 2014.

[11] L. Cattaneo and P. Zunino. Computational models for fluid exchange between microcirculation and tissue interstitium. *Networks and Heterogeneous Media*, 9(1):135–159, 2014.

[12] C. D'Angelo. *Multi scale modelling of metabolism and transport phenomena in living tissues, PhD Thesis.* EPFL, Lausanne, 2007.

[13] C. D'Angelo. Finite element approximation of elliptic problems with dirac measure terms in weighted spaces: Applications to one- and three-dimensional coupled problems. *SIAM Journal on Numerical Analysis*, 50(1):194–215, 2012.

[14] C. D'Angelo and A. Quarteroni. On the coupling of 1d and 3d diffusion-reaction equations. application to tissue perfusion problems. *Mathematical Models and Methods in Applied Sciences*, 18(8):1481–1504, 2008.

[15] A. Ern and J.L. Guermond. *Theory and Practice of Finite Elements.* Applied Mathematical Sciences. Springer New York, 2004.

[16] Alexandre Ern and Jean-Luc Guermond. *Theory and practice of finite elements*, volume 159 of *Applied Mathematical Sciences.* Springer-Verlag, New York, 2004.

[17] J. Fernndez Bonder and J. Rossi. Asymptotic behavior of the best sobolev trace constant in expanding and contracting domains. 1:359–378, 2002.

[18] L. Formaggia, A. Fumagalli, A. Scotti, and P. Ruffo. A reduced model for darcys problem in networks of fractures. *ESAIM: Mathematical Modelling and Numerical Analysis*, 48(4):1089–1116, 2014.

[19] L. Formaggia, Gerbeau J.F., F. Nobile, and A. Quarteroni. One the coupling of 3d and 1d navier-stokes equations for flows in compliant vessels. *Computer Methods in Applied Mechanics and Engineering*, 191(6-7):561–582, 2001.

[20] L. Formaggia, D. Lamponi, and A. Quarteroni. One-dimensional models for blood flow in arteries. *Journal of Engineering Mathematics*, 47(3-4):251–276, 2003.

[21] L. Formaggia, A. Quarteroni, and A. Veneziani. Cardiovascular mathematics: Modeling and simulation of the circulatory system. *Modeling, Simulation and Applications*, 1:1–512, 2009.

[22] D. Gilbarg and N. Trudinger. *Elliptic Partial Differential Equations of Second Order*, volume 224. Springer Science & Business Media, 2001.

[23] Daniel Goldman and Aleksander S Popel. A Computational Study of the Effect of Capillary Network Anastomoses and Tortuosity on Oxygen Transport. *Journal of Theoretical Biology*, 206(2):181–194, 2000.

[24] W. Gong, G. Wang, and N. Yan. Approximations of elliptic optimal control problems with controls acting on a lower dimensional manifold. *SIAM Journal on Control and Optimization*, 52(3):2008–2035, 2014.

[25] D. Hanahan and R.A. Weinberg. The hallmarks of cancer. *Cell*, 100(1):57–70, 2000.

[26] T. Köppl, E. Vidotto, and B. Wohlmuth. A local error estimate for the poisson equation with a line source term. In *Numerical Mathematics and Advanced Applications ENUMATH 2015*, pages 421–429. Springer, 2016.

[27] T. Köppl and B. Wohlmuth. Optimal a priori error estimates for an elliptic problem with dirac right-hand side. *SIAM Journal on Numerical Analysis*, 52(4):1753–1769, 2014.

[28] Tobias Köppl, Ettore Vidotto, Barbara Wohlmuth, and Paolo Zunino. Mathematical modeling, analysis and numerical approximation of second-order elliptic problems with inclusions. *Mathematical Models and Methods in Applied Sciences*, 28(05):953–978, 2018.

[29] T. Kppl, R. Helmig, and B. Wohlmuth. A multi-scale model for mass transport in arteries and tissue. *Lecture Notes in Computational Science and Engineering*, 105:197–213, 2015.

[30] M. Kuchta, M. Nordaas, J. Verschaeve, M. Mortensen, and K. Mardal. Preconditioners for saddle point systems with trace constraints coupling 2d and 1d domains. *SIAM Journal on Scientific Computing*, 38(6):B962–B987, 2016.

[31] Miroslav Kuchta, Kent-Andre Mardal, and Mikael Mortensen. Preconditioning trace coupled 3d-1d systems using fractional laplacian. *Numerical Methods for Partial Differential Equations*, 0(0).

[32] J. R. Kuttler and V. G. Sigillito. An inequality of a Stekloff eigenvalue by the method of defect. *Proc. Amer. Math. Soc.*, 20:357–360, 1969.

[33] F. Laurino and P. Zunino. Derivation and analysis of coupled pdes on manifolds with high dimensionality gap arising from topological model reduction, *submitted.*

[34] M. Lesinigo, C. D'Angelo, and A. Quarteroni. A multiscale darcy-brinkman model for fluid flow in fractured porous media. *Numerische Mathematik*, 117(4):717–752, 2011.

[35] E.K. Lindstrom, J. Schreiner, G.A. Ringstad, V. Haughton, P.K. Eide, and K.-A. Mardal. Comparison of phase-contrast mr and flow simulations for the study of csf dynamics in the cervical spine. *Neuroradiology Journal*, 2018.

[36] M. F. Mehler and S. Gokhan. Mechanisms underlying neural cell death in neurodegenerative diseases: alterations of a developmentally-mediated cellular rheostat. *Trends in Neurosciences*, 23(12):599605, 2000.

[37] M. Nabil, P. Decuzzi, and P. Zunino. Modelling mass and heat transfer in nano-based cancer hyperthermia. *Royal Society Open Science*, 2(10), 2015.

[38] M. Nabil and P. Zunino. A computational study of cancer hyperthermia based on vascular magnetic nanoconstructs. *Royal Society Open Science*, 3(9), 2016.

[39] D. Notaro. Mixed finite element methods for coupled 3d/1d fluid problem, *Master Thesis.*

[40] D. Notaro, L. Cattaneo, L. Formaggia, A. Scotti, and P. Zunino. *A Mixed Finite Element Method for Modeling the Fluid Exchange Between Microcirculation and Tissue Interstitium*, pages 3–25. Springer International Publishing, 2016.

[41] L. E. Payne and H. F. Weinberger. An optimal Poincaré inequality for convex domains. *Arch. Rational Mech. Anal.*, 5:286–292 (1960), 1960.

[42] R. Penta and D. Ambrosi. The role of the microvascular tortuosity in tumor transport phenomena. *Journal of Theoretical Biology*, 364:80 – 97, 2015.

[43] L. Possenti, G. Casagrande, S. Di Gregorio, M.L. Costantino, and P. Zunino. A finite element model of vascular fluid balance at the microscale: influence of a non-linear model of lymphatics. Technical report, Politecnico di Milano, 2018.

[44] Luca Possenti, Simone Gregorio, Fannie Maria Gerosa, Giorgio Raimondi, Giustina Casagrande, Maria Laura Costantino, and Paolo Zunino. A computational model for microcirculation including fahraeus-lindqvist effect, plasma skimming and fluid exchange with the tissue interstitium. *International Journal for Numerical Methods in Biomedical Engineering*, 0(0):e3165.

[45] A. Quarteroni, A. Veneziani, and C. Vergara. Geometric multiscale modeling of the cardiovascular system, between theory and practice. *Comput. Methods Appl. Mech.Engrg.*, 302:193–252, 2016.

[46] R. Rannacher. *Error control in finite element computations*, volume 536.

[47] Y. Renard and J. Pommier. Getfem++. `https://home.gna.org/getfem`.

[48] S. A. Sauter and R. Warnke. Extension operators and approximation on domains containing small geometric details. *East-West J. Numer. Math.*, 7(1):61–77, 1999.

[49] R. J. Shipley and S. J. Chapman. Multiscale modelling of fluid and drug transport in vascular tumours. *Bulletin of Mathematical Biology*, 72(6):1464–1491, 2010.

[50] Michael Solomyak. On approximation of functions from Sobolev spaces on metric graphs. *J. Approx. Theory*, 121(2):199–219, 2003.

[51] P.W. Sweeney, S. Walker-Samuel, and R.J. Shipley. Insights into cerebral haemodynamics and oxygenation utilising in vivo mural cell imaging and mathematical modelling. *Scientific Reports*, 8(1), 2018.

[52] A.-K. Tornberg and B. Engquist. Numerical approximations of singular source terms in differential equations. *Journal of Computational Physics*, 200(2):462–488, 2004.

[53] A. Veneziani. The future of coronary stenting, a mathematical view. *volume Coronary Stents, Innovations*, 2015.

[54] C. Vergara and P. Zunino. Multiscale modeling and simulation of drug release from cardiovascular stents. *Multiscale Modeling and Simulation*, 7(2):565–588, 2008.

Acknowledgements

Desidero ringraziare innanzitutto il Prof. Paolo Zunino per avermi dato la possibilità di lavorare con lui a questo progetto. Mi ha costantemente aiutato nello sviluppo di questa impegnativa ma stimolante tesi, incoraggiandomi a puntare a obiettivi sempre più alti.

Un sincero ringraziamento va a Federica Laurino, per i suoi preziosi consigli durante lo sviluppo della tesi. È inoltre doveroso ringraziare tutti i ragazzi del Tender, che in questi mesi mi hanno accolto così calorosamente. Franz, Francesco, Fracco, Daniele C., Daniele R., Stefano, Luigi, Mattia, Laura, Anna, Ludovica, Davide, Abele: i pranzi alle 11.59, i discorsi impegnati e quelli meno, i suggerimenti sulle simulazioni, i progetti con la stampa 3D, hanno contribuito a superare questo difficile traguardo.

Ringrazio Riccardo, Mattia, Daniele, Camilla, Matteo, Pietro, Luca, Elisa, Romario, Francesca, Chiara, Paolo, Teme, e tutti gli altri con cui ho condiviso le gioie e le difficoltà di questi anni al Politecnico. Anche se ormai siamo sparpagliati in giro per il mondo, il legame formatosi in questi anni non si spezzerà mai.

Voglio inoltre ringraziare gli amici da una vita, i veri eroi: Davide, Angelo, Matteo, Luca, Elia, Federica, Elena, Arianna, Giulia. Non esistono parole per esprimere il vostro supporto in tutti questi anni, e la gratitudine che provo per voi.

Un ringraziamento speciale va alla mia famiglia, che ha sempre creduto in me. I miei genitori mi hanno insegnato a dare sempre il massimo, e mio fratello è sempre stato un modello a cui aspirare. Nonostante i contrattempi lungo la strada, questo traguardo è anche e soprattutto merito vostro.

Infine, voglio ringraziare la persona più importante, Eleonora. Il tuo supporto è stato fondamentale nei momenti più difficili, sei la parte più preziosa della mia vita. Questo lavoro rappresenta un primo grande passo verso il nostro futuro, e per questo è dedicato a te.